Chemical Genetic Analysis of Echinochrome A Isolated from *Evechinus chloroticus* (Sea Urchin, Kina) in New Zealand

By

Joseph Hammond

A thesis submitted to Victoria University of Wellington in fulfilment of the requirements for the degree of Master of Science

Victoria University of Wellington

2021

Abstract

Using unbiased genome-wide proteomic and genomic analyses available to *Saccharomyces cerevisiae*, this thesis aims to provide further insight into the mode of action of Echinochrome A (Ech A) extracted from the shells of New Zealand kina (*Evechinus chloroticus*). Abundance was measured for 4,100 proteins every 30 minutes for four hours using fluorescent microscopy, which resulted in the identification of 92 proteins with significant alterations in protein abundance caused by Ech A treatment that were over-represented with specific changes in DNA replication, repair and RNA binding at 30 minutes, followed by metabolism of metal ions (specifically iron and copper) from 60-240 minutes. Further analysis indicated that Ech A chelated iron, and that iron supplementation negated the growth inhibition caused by Ech A. Likewise, copper supplementation negated the growth inhibition caused by Ech A. Via a genome-wide analysis of 4,800 gene deletion strains that measured sensitivity of growth of these deletion strains, it was identified that 20 gene deletion strains were sensitive to Ech A and these genes were over-represented in the cellular response to oxidative stress. To directly evaluate the potential antioxidant properties of Ech A suggested by the proteomic and genomic analyses, yeast growth was measured in the presence and absence of oxidative stress induced by hydrogen peroxide, whereby Ech A suppressed growth inhibition caused by the oxidative stress. Building off publications investigating Ech A in mammalian models, there were a number of mitochondrial gene deletions with significantly altered growth and mitochondrial proteins with significantly altered abundance. Overall, my thesis identified the iron chelation mechanism of Ech A as a key causative factor in Ech A bioactivity via the identification of novel genes and proteins that are essential to the iron chelation and antioxidant molecular mechanisms of Ech A.

Acknowledgments

Thank you to everyone who has helped me through my journey in completing my Masters, I am so grateful for all the support and encouragement I received from you all.

Firstly, to my supervisor Andrew, thank you for giving me this opportunity to work with everyone in the Chemical Genetics Lab. I appreciate all your guidance, help and support over the past few years. I have enjoyed all our discussions, whether that was on my research or discussing the latest developments in the NBA on our way to Krishna.

I would like to thank Hikurangi Bioactives Limited Partnership for allowing me to be a part of the Ech A collaboration team and allowing me to be the student that leads the investigation of Ech A in the yeast model. To Matt Miller at Cawthron Institute, I would like to thank you for performing all of the extractions and providing me with more compound whenever I ran out. Your guidance in handling of the compound and the chemical properties contributed to my overall knowledge of Ech A.

Thank you to everyone in the Chemical Genetics Lab. I have enjoyed my time with you all and am thankful for all the support and critiques along the way - I wish you all the best in your current/future research. Lab Mums (Cintya and Dr Woolner), thank you for your words of encouragement; Buddy's favourite babysitter (Tamin) thank you for always making me laugh, and Storm, thank you for always being so quick with the 9-letter word – one day I will get it before you! Buddy's second favourite babysitter (Jeff), your guidance and support over the past few years has taught me so many new skills which were essential in producing a thesis that I am proud of.

To my family, I love you all and thank you for all your love and support during this journey. Natalie, thank you so much for giving me the courage to take this next step in my studies. I appreciate all your support in and out of the lab and thank you listening to all of my

struggles and helping to come up with solutions. Love you and I wish you luck with finishing your PhD. Mum and Dad, you have supported me in every way possible, your support has allowed me to achieve all my goals and I cannot thank you enough.

Contents

List of figures

List of tables

Chapter One

Literature review

1.1 Drug discovery

Historically, natural products have played a key role in the treatment of human diseases and illness and were key ingredient of medicines. From 1981 to 2019, around 64% of approved drugs were natural products, derived from natural products or mimics of natural products (Newman & Cragg, 2020). Drug discovery is the approach where novel compounds and druggable targets are identified (Hughes et al., 2011). It is known that nature is enriched with compounds that have bioactivity with the potential for human pharmaceutical use (Malve, 2016). Numerous examples of using medicinal plants to treat various conditions have been documented from traditional medicine in ancient civilizations (Petrovska, 2012). These traditional medicines have since been exploited to produce many drugs that modern society relies on today. Some of the most well-known include morphine isolated from *Papaver somniferum* (opium poppy) extract that the ancient Greeks used medicinally and also the discovery of the antibiotic penicillin from the fungus *Penicillium notatum* (Dias et al., 2012).

The use of natural products in drug discovery declined in the 1990's. This is partly due to the cost and time period (10-15 years) it takes to go from the compound being isolated to a marketable product available for public consumption (Harrison, 2016). This lengthy delay means that agents reaching the market today may have been discovered over decade ago. But also, the developments in high-throughput screening against specific molecular targets prompted companies to move away from natural products to synthetic compounds (Koehn & Carter, 2005). However natural products differentiate themselves from the synthetic compounds as they have evolutionary unique chemical structures, a diverse range of bioactivities and other molecular properties that make them favourable and successful starting

points for drug discovery (Dias et al., 2012; Koehn & Carter, 2005). With the recent increase in antibiotic resistance, there is currently high demand for discovery of drugs with novel mechanisms (Ventola, 2015).

1.2 Marine natural products

The ocean covers approximately 70% of the earth's surface and contains extraordinary organisms that are unique to those ecosystems (Haefner, 2003). This diversity of organisms provides the opportunity to discover bioactive compounds with unique chemical features that are generally not found in terrestrial natural products, resulting in the marine environment being a top spot for the identification of new drug leads (Malve, 2016; Martins et al., 2014). Indeed, there has been an increase in new marine natural products in recent years with approximately 1490 new marine natural products in 2017 and 1277 new marine natural products in 2016, both considerably greater than 332 new marine natural products in 1984 (Blunt et al., 2016; Carroll et al., 2019). Overall, there are more than 30,000 structurally diverse marine natural products (El-Demerdash et al., 2019).

Marine organisms have evolved to adapt to their extreme environments of the oceanic zones, meaning there could be greater novelty in chemical features of marine natural products. Companies are thus investing in this field as the marine natural products are now considered high-value drug leads in the pharmaceutical industry. For example, approximately 1% of marine natural products exhibited anti-tumour potential in a National Cancer Institute preclinical cytotoxicity screen compared to only 0.1% of terrestrial natural products (Munro et al., 1999). The marine natural products are also desirable in that there is minimal manipulation needed to make them safe for human use (Vignesh et al., 2011). Improvements in the collection of marine organisms (*e.g.*, remotely operated vehicles to collect samples in extreme

environments such as deep sea and hydrothermal vents) as well as methodological improvements in the isolation and identification of compounds both contribute to the increased number of publications of new marine natural products (Dias et al., 2012).

Marine sponges (phylum Porifera) are mini-factories of bioactive natural products, with multiple approved drugs on the market being either natural products of sponges or a derivative; these include anticancer drugs such as cytarabine, vidarabine, and eribulin mesylate (El-Demerdash et al., 2019; Patridge et al., 2016; Rangel & Falkenberg, 2015). With such an abundance of unique natural products, it is understanding why there has been an increase in demand for marine natural products. The investment in marine bioactives could be highly beneficial considering there is a high demand of new drugs with unique mechanism to combat global health issues.

1.3 Yeast as a model organism

Saccharomyces cerevisiae (Baker's yeast) is a simple eukaryote with a wide range of characteristics that has led to it becoming a powerful model organism, notably for chemical genetic analysis (Botstein & Fink, 2011). It is less expensive than other model organisms as it can grow on simple media (liquid or agar) and has a very short generation time of only 90 minutes. Yeast are unicellular organisms with a simple and compact genome consisting of approximately 6,000 genes, with it being the first eukaryote to have its genome fully sequenced and mapped in 1996 (Goffeau et al., 1996). This has resulted in yeast having one of the most characterised genomes, as it has been altered in many ways to study the functions of genes, proteins and pathways on a genome-wide scale creating informative data bases specific to the yeast model.

Cellular processes are conserved from yeast to human, with thousands of yeast genes having similar functions to human genes, meaning it is an attractive model organism to study bioactive compounds being developed to treat human diseases (Foury, 1997; Nijman, 2011). Due to the ease of genetic manipulation in yeast, genome-wide libraries and high-throughput screening methods have provided extensive understanding of chemical-genetic interactions (Giaever et al., 2002, 2004). There have been many elegant examples of using yeast to study the mode of action of novel compounds (Lopez et al., 2008). In fact, the yeast model has been used to identify the fungal-specific mode of action of the marine antifungal compound, turbinmicin isolated from a sea squirt microbiome (Zhang et al., 2020). The chemical-genetic tools available and the characteristics of yeast make *S. cerevisiae* a powerful model to begin my study of novel drug candidates.

1.4 Chemical-genetic analysis via gene deletion libraries

The ease of genetic manipulation has allowed the creation of mutant libraries using homologous recombination (Giaever et al., 2002). Every genome has essential genes that are required for the survival of the organism. Using homologous recombination to delete genes, it was identified that approximately 1,000 of the 6,000 genes in the yeast genome are identified as essential genes. This was performed by systematically knocking out each gene and viewing if the mutant strain will survive. Death of the cells meant that the knocked-out gene was an essential gene for survival (Boone et al., 2007; Winzeler et al., 1999). A deletion mutant library consisting of single gene deletion strains of non-essential genes was created with each gene being replaced by a deletion cassette, containing a kanamycin resistance marker with unique barcodes for each strain on either side. The unique barcodes allow for easier identification via PCR of each gene deletion without the need of sequencing the whole genome (Boone et al., 2007; Giaever et al., 2002; Winzeler et al., 1999). Alternatively and more simply, sensitivity

of gene deletion strains can be evaluated by growth on agar, via assessing colony size using image analysis tools, such as SGAtools (Wagih et al., 2013).

Synthetic lethality arises when the combination of two or more gene deletions results in cell death. Compounds can also act as a "surrogate gene deletion" in chemical-genetics by inhibiting a target protein (Parsons et al., 2004, 2006). By measuring the colony size of each of the treated strains compared to the untreated strains, it is possible to identify strains sensitive to drug treatment and in turn identify chemical-genetic interactions. If strains exhibit sensitivity to a drug treatment, this may suggest that these genes are essential for the metabolism of the drug (Hillenmeyer et al., 2010). Screening the homozygous deletion collection with novel compounds thus provides insights into the stress response upon treatment at a genetic level and provides insight into what genes are essential to buffer the toxic effect of drug treatments. Hence with this methodology, it becomes possible to identify the drug target, and the associated pathway, but also identify the compound's mode of action (Lum et al., 2004).

1.5 Chemical-genetic analysis via the GFP-tagged protein library

Studies at the genomic level provide insight into the mode of action of compounds; however, this does not give the full picture as to what occurs within individual cells under these conditions. Cells detect and respond to environmental changes in many ways such as through regulating protein abundance or altering protein localization (Kraus et al., 2017; Tkach et al., 2012). A change in protein abundance or protein localisation may cause drastic changes in cellular physiology and thus also give insight into the molecular mode of action of a drug (Chong et al., 2015; Tkach et al., 2012).

Currently *S. cerevisiae* is the only model organism that has a comprehensive library of C-terminally GFP-tagged proteins covering over two thirds of the yeast proteome (Huh et al.,

2003; Kraus et al., 2017). High-throughput fluorescent imaging of this library has made it possible to systematically identify both protein abundance and protein localization (Huh et al., 2003). Furthermore, the GFP protein in this library does not require external cofactors to produce a fluorescent signal (Huh et al., 2003). The inclusion of cell markers for nuclei and cytoplasm integrated into the genome made it possible to use automated image analysis software to identify and segment individual cells for single cell analysis of protein abundance (Bircham et al., 2011; Kraus et al., 2017). Together, the cell markers and GFP-tagged proteins allow for researchers to monitor proteomic changes over time in live cells, which is an ideal tool to study the changes to the proteome caused by drug treatment. Furthermore, machine learning can be used to segment cells with known localisations as training sets, which will allow for an automated localisation assignment of proteins in cells (Xiao et al., 2019). Utilising the yeast GFP collection therefore allows for protein abundance and localization to be measured over time under different conditions to provide insight into the mode of action of bioactive compounds.

1.6 Echinochrome A

Echinochrome A (Ech A), 6-ethyl-2,3,5,7,8,-pentahydroxy-1,4-naphthoquinone, is a marine bioactive compound extracted from the shells and spines of sea urchins (Lebedev et al., 2005). Ech A is a water insoluble compound that has exhibited antioxidant, antimicrobial, anti-inflammatory, chelating, and cardio-protective activities (Jeong, Kim, Song, Lee, et al., 2014; Lebedev et al., 2005). Studies of Ech A have been performed in multiple cell and animal models including rats, rat cardiomyocytes, and H9c2 rat cells. Most research has investigated the antioxidant properties of Ech A isolated from sea urchins in Asia and Europe and how this alters cellular mitochondrial function (Jeong, Kim, Song, Lee, et al., 2014; Jeong, Kim, Song, Noh, et al., 2014), and notably has not investigated Ech A isolated from kina in New Zealand.

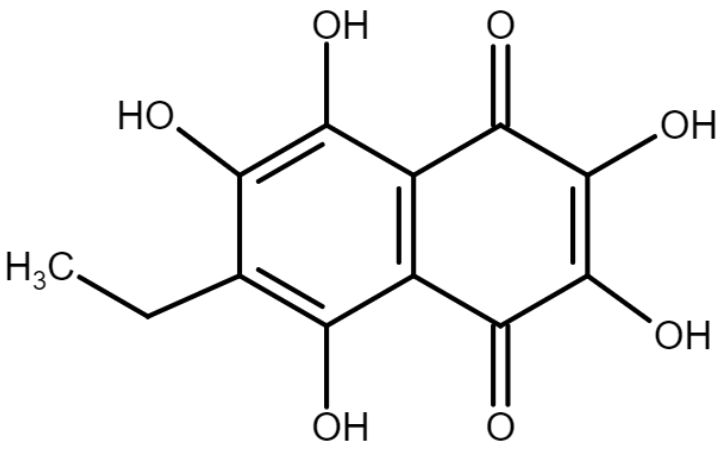

Figure 1.1: **Chemical structure of Echinochrome A.** Adapted from PubChem (Kim et al., 2021).

Free radical scavenging, iron chelation and copper chelation properties of Ech A have been identified through several chemical assays (Lebedev et al., 2005, 2008), albeit in most cases the genes, proteins and overall molecular basis of these bioactivities are not known. Ech A was found to be a stronger DPPH (2,2-diphenyl-1-picrylhydrazyl) scavenger than established antioxidants such as α-tocopherol using the free radical scavenging colorimetric assay (Lebedev et al., 2005, 2008). The UV-visible spectrum of Ech A is altered when ferrous iron is added, indicating that formation of an iron-Ech A complex is possible (Lebedev et al., 2005, 2008). An Ech A-copper complex has also been suggested as the addition of copper ions altered the spectrophotometric spectrum of Ech A (Kuzuya et al., 1973). Compared to the radical scavenging and antioxidant properties of Ech A, iron chelation and copper chelation have only been reported in four and one publications, respectively.

Gastric ulcers are a deep wound in the stomach wall that involve tissue damage caused by the increase of reactive oxygen species at the wound site. Antioxidants have been used for healing these wounds as they are able to deduce tissue damaged by reactive oxygen species and inflammation (Sayed et al., 2018). Rats with gastric ulcers treated with Ech A displayed a

significant decrease in the volume of gastric juices and acidity compared to the control group. Interestingly, there was an observed increase in SOD (superoxide dismutase) activity with Ech A treatment, whereas the control group showed decreased SOD activity (Sayed et al., 2018). The lipid peroxidation marker malondialdhyde also increased in the control group and resulted in the highest amount of tissue damage. With Ech A treatment, there was a reduction in malondialdhyde, thus suggesting that Ech A treatment protected the tissue from lipid peroxidation (Sayed et al., 2018). These results emphasized the *in vivo* protective effects of Ech A against oxidative stress and lipid peroxidation.

Cardiotoxic agents reduce the viability of rat cardio myoblast H9c2 cells via increased oxidative stress (Jeong, Kim, Song, Lee, et al., 2014). Co-treatment with Ech A protected H9c2 cells from oxidative stress by preventing the increase in reactive oxygen species (ROS) levels, and thus increased cell viability (Jeong, Kim, Song, Lee, et al., 2014). Ech A acts as an antioxidant agent and reduces the levels of ROS, therefore protecting mitochondrial membrane potential, mitochondrial oxygen consumption and mitochondrial ATP levels. Mitogen-activated protein kinases (MAPK) are activated by cardiotoxic drugs and involved in numerous cellular functions such as cell growth and cell death (Jeong, Kim, Song, Lee, et al., 2014). Downstream of the MAPK pathway includes transcription factors whose activity is enhanced via phosphorylation, which can result in cell death. Ech A prevents mitochondrial dysfunction and the activation of MAPKs caused by cardiotoxic drugs (Jeong, Kim, Song, Lee, et al., 2014).

The treatment of Ech A on rat cardio myoblast H9c2 cells increased mitochondrial mass, resulting in an increase of mitochondrial contents in the cell and therefore an increase in cell viability (Jeong, Kim, Song, Noh, et al., 2014). This increased mitochondrial function was due to increased expression levels of the transcription factors NRF-1 and PGC-1α that regulate mitochondrial biogenesis. Since there was an increase in mitochondrial mass, there were morphological changes observed in the mitochondria, suggesting that Ech A upregulated

mitochondrial biogenesis transcription genes (Jeong, Kim, Song, Noh, et al., 2014). This proposed Ech A function could be clinically beneficial for the treatment of various mitochondrial dysfunctions caused by metabolic diseases. Ech A also has been shown to exhibit potential benefits in physical exercise. For example, Ech A treatment resulted in a significant improvement in short-term endurance capacity in rats wherein the mitochondrial abundance increased within the skeletal muscles of rats treated with Ech A (Seo et al., 2015), suggesting that Ech A increases mitochondria in the skeletal muscle cells.

Overall, these studies highlight the antioxidant properties of Ech A in mammalian cells and establish an interaction between mitochondria and Ech A. However, whilst these studies provide a foundation regarding the activity of Ech A, in most cases they do not elucidate the molecular basis of the activity. Moreover, there have not been any publications on the bioactivity or molecular mechanism of Ech A extracted from New Zealand kina (*Evechinus chloroticus*).

1.7 Histochrome®

Ech A is an active parent component for the water-soluble antioxidant drug Histochrome® that was developed and approved in Russia for the treatment of ischemic heart disease and myocardial infarction (Mishchenko et al., 2003; Park et al., 2019). Cardiac progenitor cells (CPCs) are stem cells in portions of ischemic heart tissue that function in repairing the damage. Histochrome® treatment scavenges ROS in human CPCs and protects cells from oxidative stress (Park et al., 2019). By scavenging ROS, Histochrome® in turn downregulates pro-apoptotic signals (Bcl-2 associated X (Bax)), upregulates anti-apoptotic signals (Bcl-2 and Bcl-xL), and protects the cells from DNA damage (Park et al., 2019).

Patients suffering from ischemic heart disease or myocardial infarction have an increased concentration of reactive oxygen species, which in turn can cause lipid peroxidation resulting in cell and tissue death. Ischemic heart disease patients treated with Histochrome® showed a decrease in levels of the lipid peroxidation product, malonic dialdehyde, in blood serum by 47% compared to the control group, suggesting that Histochrome® scavenged the free radicals and protected the cells from lipid peroxidation (Mishchenko et al., 2003). Patients treated with Histochrome® after suffering a heart attack showed a 55% reduction in damaged tissue compared to the control group. The clinical trial also demonstrated that the administration of Histochrome® to heart muscles under ischemic stress had an additional cardioprotective mechanism with an ATP saving effect (Mishchenko et al., 2003).

1.8 Aims and hypothesis

This thesis will be centred on the further characterization of the bioactivity of echinochrome A (Ech A) extracted from the shells New Zealand East Coast kina (*Evechinus chloroticus*) using unbiased genome wide genomic and proteomic screens in *S. cerevisiae.* Based on previous findings in mammalian cells, I hypothesise unbiased genomic and proteomic analyses in yeast will identify the genes and proteins involved in the antioxidant properties of Ech A and highlight the importance of mitochondria in the metabolism of Ech A. Specifically, my thesis aims are the following:

Aim 1: To identify the protein abundance changes in response to Ech A at multiple time points.

Aim 2: To identify the genes required to buffer the metabolism of Ech A.

Chapter Two

2.1 Introduction

The ocean covers approximately 70% of the earth's surface and is a source of diverse organisms that contain unique bioactive compounds (Haefner, 2003). The investigation of marine natural products has increased in recent years, with 1490 new marine natural products being reported in 2017 compared to only 332 in 1984 (Blunt et al., 2016; Carroll et al., 2019). The discovery of new natural products is essential for drug discovery and development to treat human diseases.

Evechinus chloroticus (commonly known as kina) is a species of sea urchin indigenous to New Zealand. The edible roe of the kina is considered a delicacy in the Māori culture, resulting in the commercial harvesting of kina in New Zealand (Miller & Abraham, 2011). However, the shell of the kina is not edible and considered a waste product. Echinochrome A (Ech A) is a bioactive compound extracted from the shells of sea urchins and has been extracted from the shells of New Zealand kina (Hou et al., 2019). Previous literature on Ech A extracted from other species of sea urchins, such as *Scaphechinus mirabilis* (commonly known as Sand dollar) and *Strongylocentrotus intermedius*, has established Ech A to have chelation and antioxidant properties via increased mitochondrial mass, mitochondrial function and mitochondrial membrane potential that protect mammalian cells from reactive oxygen species and cardiotoxic agents (Jeong, Kim, Song, Lee, et al., 2014; Jeong, Kim, Song, Noh, et al., 2014; Seo et al., 2015). Whilst these studies provide a foundation regarding the activity of Ech A, in most cases these studies did not determine the molecular basis of bioactivity.

There has not yet been any research into the mode of action of Ech A in the yeast model organism, *S. cerevisiae*. Yeast is a powerful simple model organism to determine the mode of action of bioactive drug candidates (Lopez et al., 2008). High-throughput methodology exists

in yeast to identify genes and proteins sensitive to compounds (Chong et al., 2015; Lopez et al., 2008; Tkach et al., 2012). The major aim of this thesis is to identify the genes and proteins involved in the metabolism of Ech A in yeast in order to provide further insight into the mechanisms of Ech A, to relate the molecular mechanisms to human diseases, and to determine if Ech A extracted from New Zealand kina has the same bioactivity as Ech A extracted from other species of sea urchins.

2.2 Materials and methods

2.2.1 Strains

The *Saccharomyces cerevisiae* strains used throughout my thesis were derived from the S288C genetic background (Table 2.1).

Strain/Library	Genotype	Reference
BY4741	MAT**a** *ura3Δ0 leu2Δ0 his3Δ1 met15Δ0*	Open Biosystems
pdr1Δpdr3Δ	MAT**a** *ura3Δ0 leu2Δ0 his3Δ1 met15Δ0 pdr1Δ::URA3 pdr3Δ*::NatR	Coorey et al., 2015
xxxΔ (Deletion library)	MAT**a** *xxxΔ*::kanR; *his3Δ1 leu2Δ0 ura3Δ0 met15Δ0*	Tong et al., 2001
xxx-GFP (GFP Library)	MAT**a** xxx-GFP::*HIS5 can1Δ*::STE2pr-Sp_*LEU2*; *lyp1Δ*::HPH::NLS-RS2::TEF2pr_mCherry; *his3Δ1 leu2Δ0 ura3Δ0 met15Δ0 LYS2*	Bircham et al., 2011

Table 2.1: **Genotypes of strains and libraries used in this thesis.**

2.2.2 Media

All media reagents were purchased from Formedium unless stated otherwise.

Synthetic Complete (SC) amino acid mixture:

3g adenine, 2g alanine, 2g asparagine, 2g aspartic acid, 2g cysteine, 2g glutamic acid, 2g glutamine, 2g glycine, 2g histidine, 2g inositol, 2g isoleucine, 10g leucine, 2g lysine, 2g methionine, 0.2g para-aminobenzoic acid, 2g phenylalanine, 2g proline, 2g serine, 2g threonine, 2g tryptophan, 2g tyrosine, 2g uracil and 2 g valine.

SC broth:

0.1% (w/v) L-Glutamic acid monosodium salt hydrate (Sigma-Aldrich), 0.17% (w/v) Yeast Nitrogen Base W/O acids or ammonium sulphate, 0.2% (w/v) amino acid mixture to suit, 2% (w/v) glucose (Sigma-Aldrich) added to autoclaved media.

SC agar:

Same preparation as SC broth, with the addition of 2% (w/v) agar granulated bacteriological grade.

Synthetic dropout (SD) broth:

Same preparation as SC broth but without appropriate amino acid(s).

Yeast extract peptone dextrose (YPD) broth:

2% (w/v) yeast extract, 2% (w/v) peptone, 0.012% (w/v) adenine, 2% (w/v) glucose (Sigma-Aldrich) added to autoclaved media.

Yeast extract peptone dextrose (YPD) agar:

Same preparation as YPD broth, with the addition of 2% (w/v) agar granulated bacteriological grade.

2.2.3 Echinochrome A (Ech A) isolation

Ech A was extracted from kina (*Evechinus chloroticus*) shells collected by Hikurangi Bioactives Limited Partnership on the East Coast of New Zealand. The extraction was conducted by Dr Matt Miller at Cawthron Institute in the dark with minimal UV exposure, and sent to Victoria University of Wellington. The harvested kina shells were freeze dried and crushed into a very fine powder. In a 5 L conical flask containing 1 L of 6 M HCl (1:1 concentrated HCl and water), the kina shell powder was added into the flask in 30 g stages (up to 400 g). Once the bubbling had finished the solution was then filtered, followed by the addition of 800 mL of ethyl acetate and 200 mL of brine. This was then separated using a separation funnel, washed twice with water to remove any acid, washed with sodium sulphate, transferred into a large round bottom flask, and dried in 20°C *in vacuo*. The powder was then suspended in dichloromethane, washed with water, dried in 20°C *in vacuo*, resuspended in absolute ethanol (vehicle), and stored in aluminium foil-wrapped tubes at -20˚C. A nitrogen blanket was applied after each use and before storage at -20˚C to minimise any degradation of the compound due to oxidation and minimise any evaporation of the ethanol.

2.2.4 Liquid-based bioactivity assay

Bioactivity was assessed by quantifying the growth of yeast in the presence and absence of Ech A as previously described (Amberg et al., 2005). Single colonies of BY4741 and *pdr1*Δ*pdr3*Δ were incubated overnight in 2 mL of SC broth at 30°C with rotation, and subcultured to generate 1 mL of each strain at 0.128 x 10^7 cells/mL. The desired Ech A concentrations were prepared in SC broth with a final concentration of ethanol being 1% across all concentrations. In a 96-well plate (JET BIOFIL®), 95 µL of the Ech A + SC stocks were added to the wells in triplicate, to which 5 µL of the subcultured cells were added to the wells to give a final volume

of 100 µL in each well. The control media contained only SC broth with 1% ethanol. Plates were incubated in the dark at 30°C, and absorbance (OD_{590}) readings were recorded at the start of the experiment (t0) as well as at mid-log growth for the untreated cells. The absorbance measurements were normalised by subtracting the initial t0 absorbance. Growth percentage (the ratio of growth in treated and untreated cells) was calculated using the following formula:

Growth Percentage (%) = (Absorbance (Treated)/Absorbance (Control)) x 100

2.2.5 High-throughput confocal time-lapse microscopy

The abundance of GFP-tagged proteins was measured using high-throughput microscopy as previously described (Tkach et al., 2012) with the addition of a time-lapse component. For each of the strains in the GFP library (4,100 strains), cells were pinned from agar in a 384 colony format into 96-well plates (JET BIOFIL®), containing 200 µL SC broth, grown overnight at 30˚C, shaken and diluted to approximately $5x10^5$ cells/mL. Then 30 µL of each strain was aliquoted into two wells of a 384-well Cell Carrier Ultra optical clear plate (Perkin Elmer), accounting for control and treated wells on the same plate. The optical plate was incubated for 2 hours at 30˚C, followed by the addition of 20 µL of SC + 2.5% Ethanol (Pure Science)/Tyloxapol (Sigma) (4:1) with and without Ech A to achieve a final concentration of 1% Ethanol/Tyloxapol and a final Ech A concentration of 2 µg/mL that elicited 50% growth inhibition. The optical plate was then shaken, left to settle for 10 minutes, incubated at 30˚C in the InCell Analyzer 6500 HS (General Electric) using the environmental control unit, and imaged every 30 minutes over 4 hours (9 timepoints) using the following settings at 100 % laser power. The RFP channel had an exposure time of 2000 ms, with the excitation at 561 nm and the emission filter of 605 nm. The GFP channel had an exposure time of 800 ms, with the excitation at 488 nm and an emission filter of 524 nm.

2.2.6 Analysis of high-throughput microscopy

Images captured using high-throughput microscopy were analysed for fluorescent abundance. The captured RFP images had a Gaussian blur and exposure contrast correction applied to them and converted to 8-bit images using Fiji (Figure 2.1) (Schindelin et al., 2012). This was performed to decrease the signal to noise ratio between the cells and the background and increase the accuracy of cell segmentation. The corrected images and the original images were inputted and run through a custom CellProfiler pipeline (McQuin et al., 2018) for segmentation and analysis. Using the corrected images fluorescence cells were segmented from a bright nuclear red fluorescent protein Redstar2 and the dimmer cytoplasmic mCherry (Figure 2.1). Only cells with a single nucleus and cytoplasm were used for analysis. These cells were masked and cropped for analysis. The GFP fluorescence intensity was measured for each cell and normalised to the RFP intensity. Z-scores were calculated using relative fluorescence for each strain, treatment and timepoint by the population average. Z-scores were used to determine changes in protein abundance.

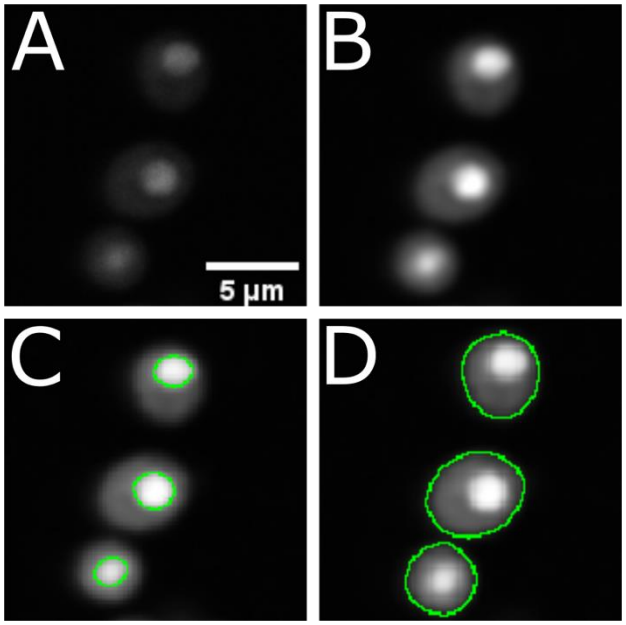

Figure 2.1: **Image contrast correction and segmentation for analysis of high-throughput microscopy images**. **(A)** RFP image taken with the confocal fluorescent microscope. **(B)** RFP image with Gaussian blur and exposure contrast correction performed with Fiji (Schindelin et al., 2012). **(C)** segmentation of cells by cell nucleus. **(D)** segmentation of cells by cytoplasm. Segmentation of cells performed with CellProfiler (McQuin et al., 2018).

2.2.7 Iron rescue assay

Iron treatment was used to evaluate intracellular iron levels as previously described (Shakoury-Elizeh et al., 2010). BY4741 was incubated overnight at 30°C in 2 mL of SC broth, and then diluted to a 1 mL subculture with a concentration of approximately 0.128 x 10^7 cells/mL. A range of Ech A concentrations were prepared in 500 µL of SC broth, SC broth + 100 µM $FeCl_3$ (Sigma), SC broth + 100 µM $FeSO_4$ (Sigma), and iron-free SC broth with a final concentration of 1% ethanol across all treatments. In a 96-well plate (JET BIOFIL®), 95 µL of each treatment were added to the wells in triplicate, followed by the addition of 5 µL of the subculture to give a final volume of 100 µL in each well. The plate was incubated in the dark at 30°C. Absorbance readings were recorded at a wavelength of 590 nm at the start of the experiment as well as the timepoint where the untreated cells were at mid-log. Absorbance was normalised by subtracting

the initial t0 and growth percentage was calculated for each treatment compared to the control in the same media with or without iron.

2.2.8 Iron chelation analysis

The colorimetric chrome azurol S (CAS) assay was used to assess if Ech A chelates iron (Alexander & Zuberer, 1991). The CAS assay solution was prepared by mixing 750 µL of 1 mM $FeCl_3$ in 10mM HCl with 3.75 mL 2 mM CAS in a 50 mL volumetric flask, followed by the addition of 25 mL 0.92 M MES monohydrate (2-(N-morpholino) ethane sulfonic acid) buffer (pH 5.6) (Sigma) that was added dropwise to the volumetric flask. Then 10.95 mg of HDTMA (hexa-decyl-trimethyl-ammonium bromide) (Sigma) dissolved in 12.5 mL of ddH_20 was added and made up to 50 mL with ddH_2O. Next 95 µL of the prepared CAS assay solution was aliquoted to each well in a 96-well plate (JET BIOFIL®), followed by the addition of 5 µL of varying concentrations of Ech A or the well-established iron chelator EDTA (ethylenediaminetetraacetic acid) (Thermo Fisher). A concentration of 500 mM EDTA was used as a positive control. Images and absorbance readings (630 nm) were taken at the start of the experiment and after 2 hours of incubation in the dark at room temperature.

2.2.9 Agar-based bioactivity assay

Bioactivity in agar was determined by measuring growth in treated cells compared to untreated cells. Using a 24-well plate (JET BIOFIL®), 1 mL of molten SC agar was added to each well containing Ech A for the desired concentrations and slowly resuspended with a pipette. The control and treatments all contained a vehicle control of 1% ethanol. The plates were then covered and left to set for 1 hour and then dried for 15 minutes in a laminar flow hood (Holten HB2460 LaminAir). An overnight culture of BY4741 was diluted to three different

concentrations of cells: $1x10^8$, $1x10^6$ and $1x10^4$ cells/mL. Then 2 µL of each yeast concentration was spotted into each well (three spots per well), incubated at 30˚C for 24 hours in the dark, and imaged using a digital camera (Canon EOS 600D).

2.2.10 Optimisation for genome-wide analysis

A single plate of the yeast deletion mutant array (DMA) was chosen at random to identify a concentration that conferred 10-20% growth inhibition in a 1536 colony format (4x colonies of each deletion). The ROTOR HDA (Singer Instruments) was used to replicate the sample plate from the DMA library on SC agar onto Singer plates (Singer Instruments) that contained 40 mL of SC agar with either a specific concentration of Ech A or the 1% ethanol vehicle control. Plates were then incubated at 30°C for 24 hours in the dark and imaged with a digital camera (Canon EOS 600D). The images were then processed using SGA Tools where colony size was normalized for growth across the plate and growth inhibition was calculated for each strain via the ratio of growth on treated and control plates (Wagih et al., 2013).

2.2.11 Genome-wide analysis of bioactivity

From the optimization in 1536 format, the concentration 7.5 µg/ml of Ech A was used for the genome-wide analysis (Lopez et al., 2008; Parsons et al., 2004). The Singer ROTOR HDA (Singer Instruments) was used to replicate the plates DMA plates from SC agar onto the treated and control plates, in a 1536 format. The control and treated plates contained 1% ethanol. The plates were then incubated at 30˚C for 24 hours in the dark, imaged using a digital camera (Canon EOS 600D), and analysed with SGA Tools (Wagih et al., 2013). The treated colonies in quadruplicate were compared to the quadruplicate control colonies in order to calculate the z-scores representing the growth inhibition for each strain. Deletion strains that were resistant

(negative z-score) or sensitive (positive z-score) with a *P*-value less than 0.05 were selected for validation. Validation was conducted via growth comparisons of serial dilutions of each strain that were grown in the same conditions as the genome-wide analysis and imaged using a digital camera (Canon EOS 600D) after 12, 24 and 48 hours of incubation at 30˚C in the dark.

2.2.12 Genomic DNA extraction

To confirm the gene deletion strains used were the correct genotype, the genomic DNA (gDNA) was extracted from each strain to be assessed via PCR analysis. The gDNA extraction method was previously described by (Hoffman & Winston, 1987). Single colonies of each strain were inoculated in 2 mL of SC broth and incubated overnight at 30°C with rotation. 1 mL of the overnight culture was harvested via centrifugation at 13000 rpm for 30 sec and supernatant discarded. 100 µL scoop of glass beads (DNature), 200 µL of DNA breaking buffer (2% (w/v) triton (Sigma-Aldrich), 1% (w/v) SDS (Sigma-Aldrich), 100 mM NaCl (Sigma-Aldrich), 10 mM Tris (Sigma-Aldrich) (pH 8) and 1 mM EDTA (Sigma-Aldrich) (pH 8)) and 200 µL of phenol;chloroform;isoamyl alcohol (25:24:1) was added to the cell pellet and vortexed for 6 minutes on high. The tubes were then centrifuged at 13000 rpm for 10 minutes and 100 µL of the aqueous phase was added to 1 mL of 95% ethanol. Tubes were briefly shaken by hand and centrifuged at 13000 rpm for 10 minutes. The supernatant was discarded, and the pellets were air dried in the laminar flow hood (Holten HB2460 LaminAir). The pellets were then resuspended in 40 µL 1X TE and stored at -20°C.

2.2.13 Molecular confirmation of gene deletion strains

To confirm gene deletion strains used were the correct strains, PCR analysis using confirmation primers (Table 2.2) was performed on the previously extracted gDNA, as previously described (Reid et al., 2002). 1 µL of the extracted gDNA was added to PCR tubes containing 2.5 µL 10XExTaq buffer, 2 µL dNTPs, 1 µL 10 µM forward primer, 1 µL 10 µM reverse primer, and 0.125 µL Takara ExTaq which was filled to a total volume of 25 µL with ddH_2O water. PCR (BioRad 5000) cycle conditions used were as follows: initial denature step at 94°C for 10 minutes, followed by 36 cycles of 94°C for 30 seconds, 58°C for 1 minute, 68°C for 3 minutes and a final extension step at 72°C for 10 minutes. PCR products were electrophoresed on a 1% agarose gel containing ethidium bromide to stain DNA and visualised under UV light (Alpha/Mager Mini, Cell Biosciences). Band sizes were confirmed against a $1Kb^+$ DNA ladder (Thermo Fisher).

Primer Name	Primer Sequence
AIM26_Confirmation_A	GCTGGTATTGACAGGTAACTATGCT
AIM26_Confirmation_D	GAATCCAGTTCGTTCTCAAACTTAG
CRD1_Confirmation_A	ACGAAGGGAGAAGGAAAGTAAAATA
CRD1_Confirmation_D	ACGAACACCTATGAAGAACACATCT
DBP7_Confirmation_A	GCCTGAAAAATGAACAGAGTTTTTA
DBP7_Confirmation_D	CAACAGAATAGAAAAACGGAAGAAA
DUG2_Confirmation_A	TCCTCTGATTTCGATGTTTTGTTAT
DUG2_Confirmation_D	ATCATCACTGCTTAAAAATGGTAGC

ERG2_Confirmation_A	TATGGAAGAATTTGGATAGATCTGC
ERG2_Confirmation_D	ATATATCCGTCGTCGTAGGTGATAA
HSP12_Confirmation_A	GTATACGCAAGCATTAATACAACCC
HSP12_Confirmation_D	AGTGAAATAGAACAATACGCACACA
HUR1_Confirmation_A	TTTTTCTTCGAAAACTTTCATCATC
HUR1_Confirmation_D	GTAATGAAACGTTTACTAACCACCG
IPK1_Confirmation_A	ATGTAAAAGATAATGATCGCCTTTG
IPK1_Confirmation_D	CATCTGTTTCTTCCTCCTCATAAAA
RPS27b_Confirmation_A	AAAATTTAATAAAAATCTGCCGGG
RPS27b_Confirmation_D	TACAATTCAAATGACAAAACCTCCT
SHE4_Confirmation_A	ATAACTCTGCAGCAACCTCTTCTT
SHE4_Confirmation_D	TAAAGAAGCGAAAAAGAGAAGATCA
SKA1_Confirmation_A	ATCTCAGTATAAACCTGTAGCGTGG
SKA1_Confirmation_D	ACAGCAAAACTGGAAGTAATAATGC
SLT2_Confirmation_A	GCGGCGATTTTTATATTATCTTTTT
SLT2_Confirmation_D	TAAAGGGCTTCTCAGTGAATACATC
SOD2_Confirmation_A	CTAATTGCTATTATCATTGTTGGCG
SOD2_Confirmation_D	ATTATCGGTTGGAACAATAACAAGA
SRB8_Confirmation_A	AGAGAAACCAAACTAATGAATGCAC
SRB8_Confirmation_D	TTCGTTAATAAGCGTCTCTAGCTGT
TUS1_Confirmation_A	GAAAATTAACTGAGCTTCGGTCATA

TUS1_Confirmation_D	TGTTTCTAACCTCATGCCTATTTTC
UME6_Confirmation_A	ATTGCTACAAGTAGTAGAGCGCAGT
UME6_Confirmation_D	GAAATTTGGCTTATCAGTACGAATG
VPS24_Confirmation_A	CTTAATGAATATCGCTTTTGACGAT
VPS24_Confirmation_D	TATGTGGATGAAGTGAAAGAAGTGA
YLR124W_Confirmation_A	GCAAACATCTGTGTAGACGTAGAGA
YLR124W_Confirmation_D	TTTTCTACTGGCTCTCCTCACTAAA
YMR031W-A_Confirmation_A	ACCCCGTACTTCAACTTCGCCTTATAT
YMR031W-A_Confirmation_D	ACACTTTCCAAGTCTCACACGAGG
YRR1_Confirmation_A	TCATACTGGCAGAAATCATAGTGAA
YRR1_Confirmation_D	GTGGTGTACGGGTGTAAAAGTAGTC
kanMX_Confirmation_B	GTTCGCATGTGATGTGAG

Table 2.2: **List of primers used during my thesis.**

2.2.14 Antioxidant activity

To determine if Ech A acts as an antioxidant in yeast, cells were exposed to Reactive Oxygen Species (ROS) via treatment with hydrogen peroxide (H_2O_2) (Thermofisher). Hydrogen peroxide is a well-established oxidant that causes oxidative stress via increasing the concentration of cellular ROS (Ayala et al., 2014; Rahal et al., 2014). The strains BY4741 and *sod2*Δ, a known H_2O_2 sensitive strain (Subramaniyan et al., 2019), were incubated overnight at 30°C in 2 mL of SC broth, and then diluted to a 1 mL subculture with a concentration of

approximately 0.128 x 10^7 cells/mL. Cells were grown with and without 1.5 mM H_2O_2 and 1 µg/ml Ech A, with a co-treatment of both with all treatments having a 1% concentration of ethanol. In a 96-well plate (JET BIOFIL®), 95 µL of each treatment was added to the wells in triplicate, followed by the addition of 5 µL of the subculture to give a final volume of 100 µL in each well. The plate was incubated in the dark at 30°C. Absorbance readings were recorded at a wavelength of 590 nm at the start of the experiment as well as the time point where the untreated cells were at mid-log for the control wells for both strains. Absorbance was normalised by subtracting the initial t0 and the residual growth was calculated for each treatment compared to the control wells.

2.2.15 Thin-layer chromatography

Phospholipids were measured using thin-layer chromatography (TLC) as previously described (Knittelfelder & Kohlwein, 2017). Single colonies of yeast cells grown overnight at 30˚C in 2 mL SC broth were used to generate 20 mL subcultures with an OD of 0.25 in SC broth. The subcultures were incubated with agitation at 30˚C until the OD reached 1.0 (approximately 5 hours). 5 OD units of cells were then subcultured in fresh SC broth containing either Ech A or 1% ethanol. Cultures were incubated at 30˚C for 4 hours in the dark, washed twice with ddH_2O and cell pellets were stored at -80˚C overnight. Lipids were extracted using a 150 µL scoop of glass beads (DNature), 600 µL chloroform (Thermo Fisher) and 300 µL methanol (Thermo Fisher) that were added to each sample, vortexed for 1 minute, and incubated at 4˚C with shaking at 1100 rpm for 1 hour. Then 300 µL ice cold chloroform and 300 µL 0.034% manganese chloride (Sigma) were added to each tube and vortexed for 1 minute then centrifuged for 5 min at 7,000 rpm. The bottom layer was extracted using a modified glass pipette (Interlab) and placed in a new tube. A second extraction was then conducted with the addition of 600 µL chloroform that was then vortexed for 1 min, centrifuged for 5 min at 7000

rpm, where the bottom layer was combined with that from the first extraction. Samples were dried using a nitrogen sample concentrator at room temperature (Techne), resuspended in 30 μL chloroform:methanol (2:1), and spotted onto a silica gel TLC sheet (Analtech). The TLC chamber was equilibrated for 1 hour with Whatmann paper (GE Healthcare) in a running solvent consisting of chloroform:ethanol (Pure Science):triethylamine (Thermo Fisher):ddH_2O (28.1:32.8:32.8:6.3). The TLC plate containing the samples was placed in the chamber until the solvent front line was 1 cm from the top. The plate was then air dried for 15 min before being submerged first in 5% sulfuric acid (Thermo Fisher) and then in 5% Vanillin (Sigma). A heat gun was then used to scorch the plate until bands appeared evenly across the plate, that was then imaged using a digital camera (Canon EOS 600D) and the brightness and contrast adjusted till all bands were visible using Fiji (Schindelin et al., 2012).

2.3 Results

2.3.1 Echinochrome A is bioactive in yeast in a dose-dependent manner

Growth inhibition of yeast cells is regularly used to determine the bioactivity of compounds and extracts (Amberg et al., 2005). To assess the bioactivity of Ech A in the yeast model organism, the residual growth of wildtype (BY4741) and the double mutant *pdr1*Δ*pdr3*Δ were measured in a liquid-based growth assay. The *pdr1*Δ*pdr3*Δ mutant has a downregulation of the efflux pumps involved in the pleiotropic drug response, resulting in the cells being unable to pump out drugs from the cells (Coorey et al., 2015). Growth was measured at t0 (time point 0 hrs) and a time point during the exponential growth phase where untreated cells of each strain had reached mid-log (approximately OD_{590nm} = 0.450). Between Ech A concentrations ranging from 0.5-5 µg/ml, both BY4741 and *pdr1*Δ*pdr3*Δ exhibited a reduction in growth, in a dose-dependent manner, with *pdr1*Δ*pdr3*Δ exhibiting a greater inhibition of growth at concentrations between 1.5-4 µg/ml (Figure 2.2). Despite this significant difference in growth inhibition between BY4741 and *pdr*1Δ*pdr3*Δ, I decided to continue using BY4741 as my primary control strain and genetic background for all experiments in this thesis for three main reasons. First, the concentrations for which there was a significant difference between the two strains elicited more than 20% growth inhibition, an amount of inhibition that is required for screening the gene deletion library to identify hypersensitive gene deletion strains. Second, there is not a GFP library in the pdr*1*Δ*pdr3*Δ genetic background to measure protein abundance. Thirdly, we are trying to find potential for human use, therefore using the genetic background that has a functional drug efflux pumps would be the closest comparison to humans.

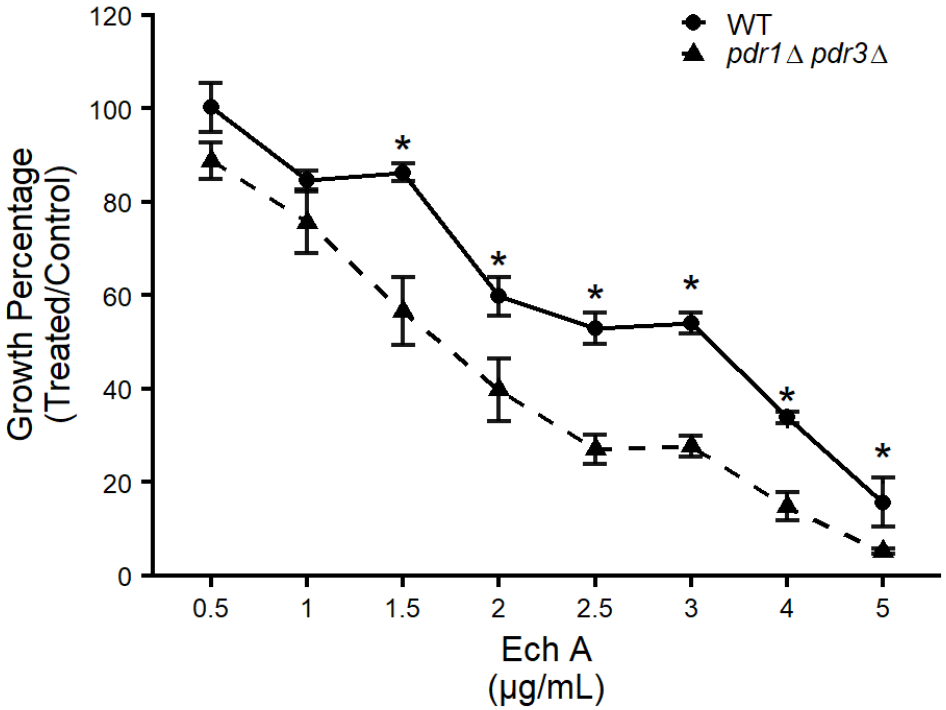

Figure 2.2: **Ech A is bioactive in yeast at a dose-dependent manner.** Growth percentage of wildtype (BY4741) and the mutant *pdr1*Δ*pdr3*Δ in the presence of increasing concentrations of Ech A at mid-log. Data shown as mean of technical triplicates ± SD; *, $p \leq 0.05$, student's t-test comparing mutant *pdr1*Δ*pdr3*Δ to wildtype.

2.3.2 An ethanol:tyloxapol vehicle improves microscopy resolution

During optimization for the high-throughput proteomic screen, it was noted that images taken using ethanol as the vehicle of Ech A showed poor quality images in the treated fields. Both RFP and GFP channels exhibited an overall decrease in fluorescence, meaning these images were unable to be used for analysis. A change in vehicle from ethanol to ethanol:tyloxapol (4:1) improved the quality of images taken, results that were consistent with previous use of this vehicle (Ruggles et al., 2014). To determine whether changing the ethanol:tyloxapol vehicle affected bioactivity of Ech A, a liquid bioactivity assay was performed. Wildtype cells were grown in multiple concentrations of Ech A with a vehicle of either ethanol or ethanol:tyloxapol. Ech A was less inhibitory when the vehicle was

ethanol:tyloxapol (Figure 2.3). At the Ech A concentration of 1 µg/mL, there was 21% growth inhibition in the ethanol:tyloxapol vehicle, while the ethanol vehicle was a lot higher at 70% growth inhibition. A concentration 2 µg/mL in the ethanol:tyloxapol vehicle was selected to be used for the full proteomic screen since this concentration elicited 50% growth inhibition that would provide enough cellular stress to detect changes in the proteome within the 4 hour time frame of the experiment.

There was a difference in the growth percentage at the Ech A concentration 1 µg/ml, 80-90 % in Figure 2.2, compared to 30-40 % seen in Figure 2.3. Throughout my thesis, different aliquots of Ech A batches from different extractions were used at different points of time. It was determined to be the evaporation of ethanol during use and storage (i.e., more ethanol evaporated in the sample that yielded 30-40% residual growth). It became apparent to monitor the growth inhibition of each aliquot before each additional experiment.

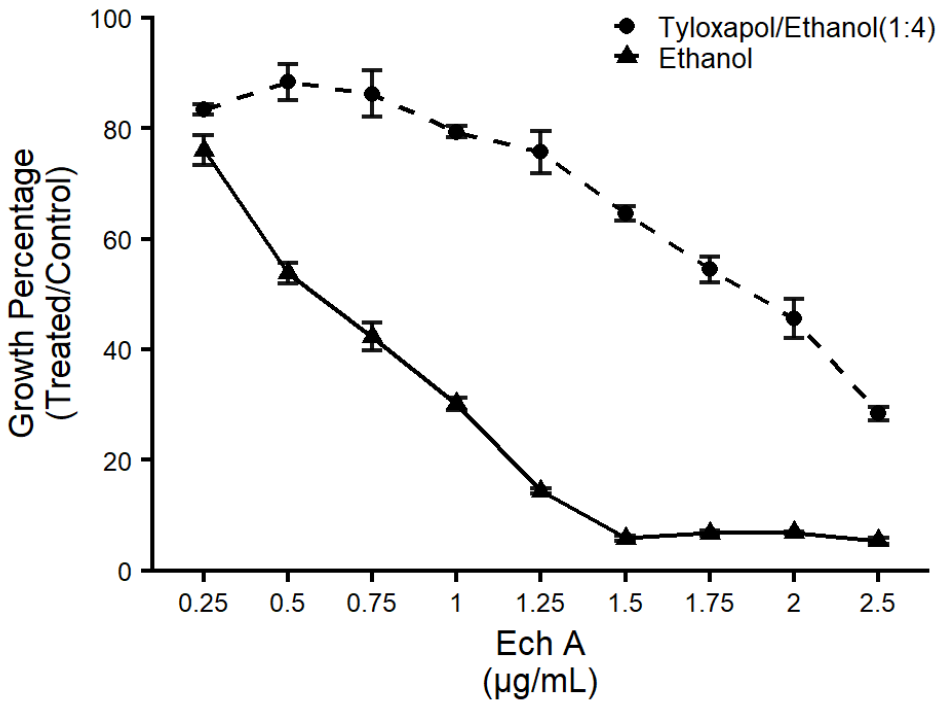

Figure 2.3: **The inhibition concentration of Ech A is altered in the vehicle tyloxapol: ethanol (1:4) compared to the vehicle ethanol**. Percentage growth of wildtype in increasing concentrations of Ech A in either vehicles tyloxapol: ethanol (1:4) or ethanol at mid-log. Data shown as mean of technical triplicates ± SD.

2.3.3 Ech A alters abundance of 341 proteins in a high-throughput analysis

Cells detect and respond to environmental changes in many ways, in order to mediate damage to the cell. An example of this is through regulating the abundance of certain proteins (Kraus et al., 2017; Tkach et al., 2012). A library constructed in my lab has proven to be a useful tool to study protein abundance at a genome-wide level (Bircham et al., 2011). This library consists of ~4,100 strains that have a green fluorescent protein (GFP) fused to a different open reading frame, which allows researchers to analyze proteomic changes in response to drug treatments in a high-throughput manner. The entire library was treated with and without 2 µg/mL Ech A, incubated at 30ºC, and images were captured every 30 minutes over 4 hours using the high-throughput confocal microscope. Every strain had one field of view for both the

control and treated samples. To visualize the cells, samples were excited at 488 nm for the GFP and 561 nm for the red fluorescent protein (RFP). Images had filters applied to correct the exposure contrast using ImageJ Fiji (Schindelin et al., 2012). CellProfiler (McQuin et al., 2018) was used to segment the cells by the nucleus using the RFP Redstar2, which localizes to the nucleus, and then by the cell periphery using the dimmer RFP, mCherry, which localizes to the cytoplasm . GFP intensities were analyzed for the segmented cells and assigned z-scores for each strain compared to the control at every timepoint. As expected, only a subset of the proteins were altered wherein the majority of the strains did not show a significant change in protein abundance over the 4-hour time-lapse (Figure 2.4). Strains that scored a z-score greater than 10 were classified with an increase in protein abundance and z-scores less than -10 were classified with a decrease in protein abundance. A total of 341 strains showed a significant change in protein abundance at any timepoint over the 4 hours. There were more significant changes of protein abundance towards the end of the time-lapse compared to the beginning timepoint (0 min = 5, 30 min = 22, 60 min = 25, 90 min = 28, 120 min = 29, 150 min = 43, 180 min = 52, 210 min = 52, and 240 min = 68). Specifically, 93.2% (n=317) and 6.8% (n=24) of the altered strains exhibited an increase and decrease in protein abundance, respectively (Figure 2.4).

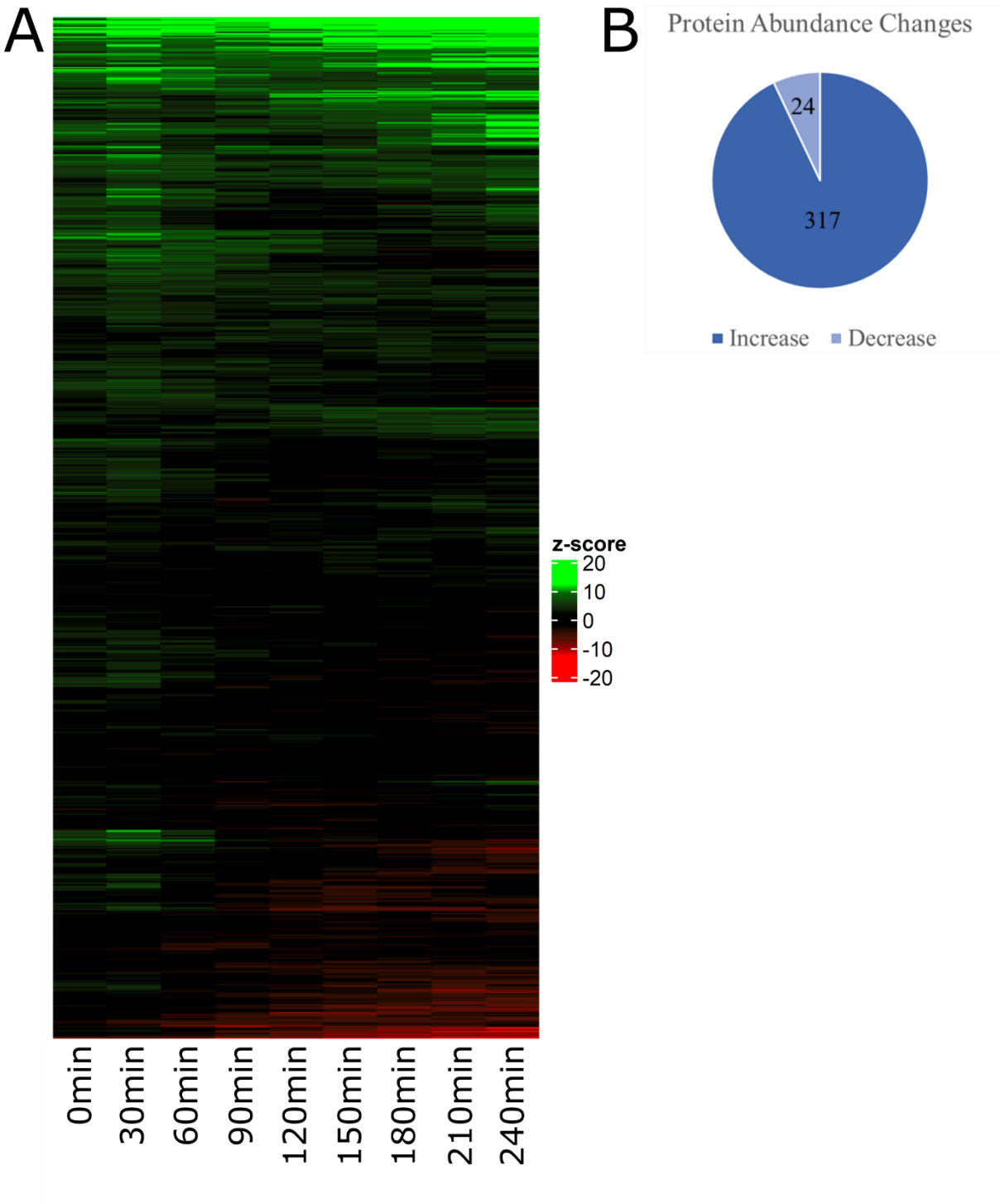

Figure 2.4: **341 strains had a significant change in protein abundance during the 4-hour time-lapse**. **(A)** Heatmap representing the z-score of each strain at every timepoint (30 minutes) over 4 hours. **(B)** Pie chart representing the number of significant changes in protein abundance.

2.3.4 Ech A alters abundance of 92 proteins in a low-throughput analysis

The 341 strains that had a significant change in protein abundance in the high-throughput proteomic analysis were picked for further validation to determine if these changes were reproducible. Validations were performed by using the same microscopy parameters, environmental conditions and growth conditions as the initial screen with one exception where each strain was examined in duplicate (two control and two treated wells). Consistent with the initial screen, there were more strains with an increase in protein abundance; specifically, there were 86 and 6 strains with a significant increase and decrease in protein abundance, respectively (Figure 2.5) (Appendix Tables 3.1 - 3.3). Interestingly, 15 of these strains that showed an increase in protein abundance are either localized to the mitochondria, function in the mitochondria or cause defective mitochondria when mutated (Table 2.3). These results suggest that Ech A bioactivity involves mitochondria, which would align with previous literature in mammalian cells (Jeong, Kim, Song, Lee, et al., 2014; Jeong, Kim, Song, Noh, et al., 2014; Seo et al., 2015) and thus supports the use of yeast as a model to investigate Ech A bioactivity.

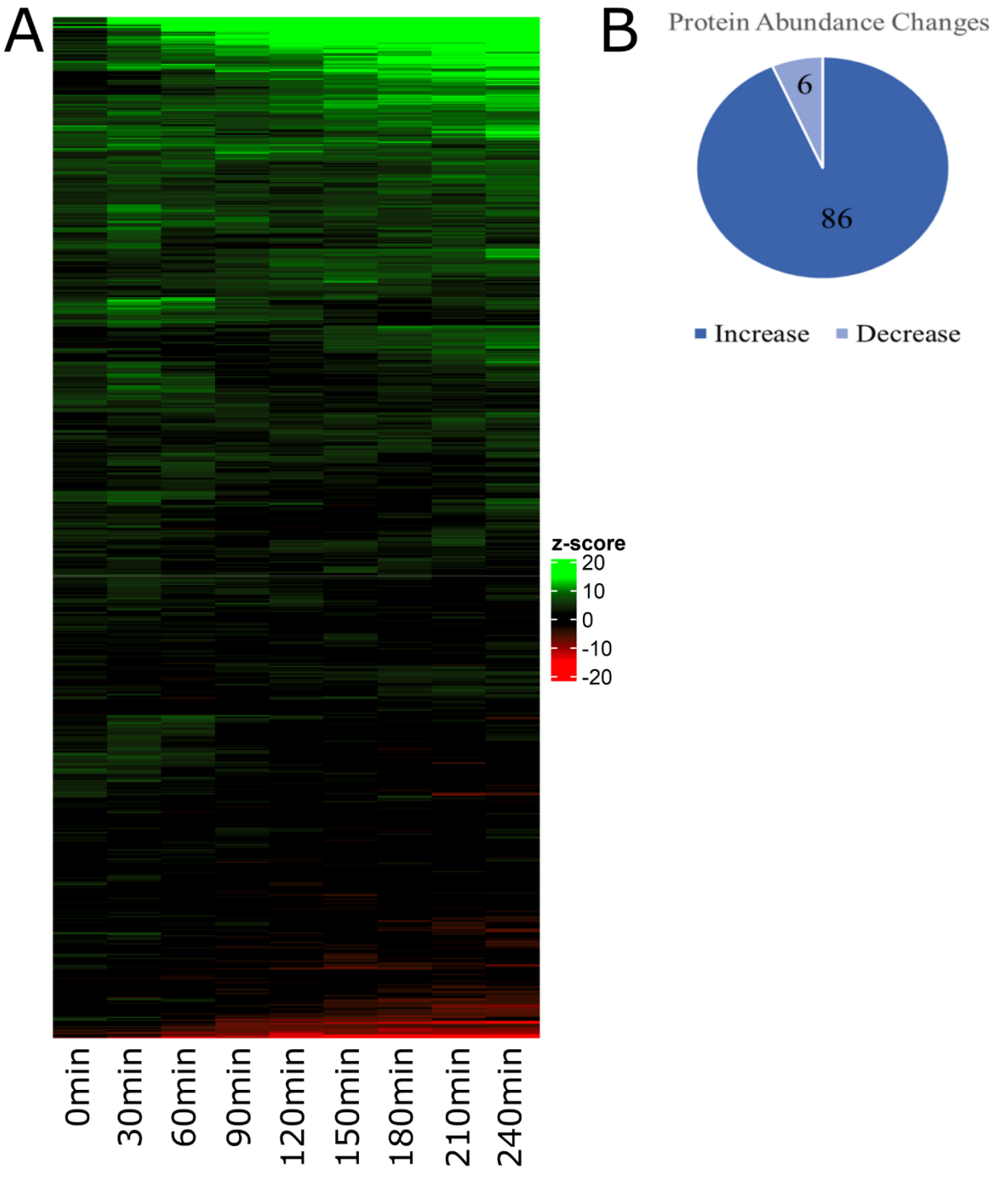

Figure 2.5: **92 strains had a significant change in protein abundance during the 4-hour time-lapse**. **(A)** Heatmap representing the z-score of each strain at every timepoint (30 minutes) over 4 hours. **(B)** Pie chart representing the number of significant changes in protein abundance.

ORF	Gene	Description
YNL305C	*BXI1*	Protein involved in apoptosis; variously described as containing a BCL-2 homology (BH3) domain or as a member of the BAX inhibitor family; reported to promote apoptosis under some conditions and to inhibit it in others; localizes to ER and vacuole; may link the unfolded protein response to apoptosis via regulation of calcium-mediated signalling; translocates to mitochondria under apoptosis-inducing conditions in a process involving Mir1p and Cor1p
YLR346C	*CIS1*	Putative protein of unknown function found in mitochondria; expression is regulated by transcription factors involved in pleiotropic drug resistance, Pdr1p and Yrr1p; YLR346C is not an essential gene
YOR065W	*CYT1*	Cytochrome c1, component of the mitochondrial respiratory chain; expression is regulated by the heme-activated, glucose-repressed Hap2p/3p/4p/5p CCAAT-binding complex
YPL170W	*DAP1*	Heme-binding protein involved in regulation of cytochrome P450 protein Erg11p; damage response protein, related to mammalian membrane progesterone receptors; mutations lead to defects in telomeres, mitochondria, and sterol synthesis
YMR287C	*DSS1*	3'-5' exoribonuclease, component of the mitochondrial degradosome along with the ATP-dependent RNA helicase Suv3p; the degradosome associates with the ribosome and mediates turnover of aberrant or unprocessed RNAs
YGR052W	*FMP48*	Putative protein of unknown function; the authentic, non-tagged protein is detected in highly purified mitochondria in high-throughput studies; induced by treatment with 8-methoxypsoralen and UVA irradiation
YBL013W	*FMT1*	Methionyl-tRNA formyltransferase, catalyzes the formylation of initiator Met-tRNA in mitochondria; potential Cdc28p substrate
YPL135W	*ISU1*	Conserved protein of the mitochondrial matrix, performs a scaffolding function during assembly of iron-sulfur clusters,

		interacts physically and functionally with yeast frataxin (Yfh1p); isu1 isu2 double mutant is inviable
YPL060W	*MFM1*	Mitochondrial inner membrane magnesium transporter, involved in maintenance of mitochondrial magnesium concentrations and membrane potential; indirectly affects splicing of group II introns; functionally and structurally related to Mrs2p
YGR243W	*MPC3*	Putative protein of unknown function; expression regulated by osmotic and alkaline stresses; the authentic, non-tagged protein is detected in highly purified mitochondria in high-throughput studies
YKR052C	*MRS4*	Iron transporter that mediates Fe2+ transport across the inner mitochondrial membrane; mitochondrial carrier family member, similar to and functionally redundant with Mrs3p; active under low-iron conditions; may transport other cations
YGR257C	*MTM1*	Mitochondrial protein of the mitochondrial carrier family, involved in activating mitochondrial Sod2p probably by facilitating insertion of an essential manganese cofactor
YML060W	*OGG1*	Mitochondrial glycosylase/lyase that specifically excises 7,8-dihydro-8-oxoguanine residues located opposite cytosine or thymine residues in DNA, repairs oxidative damage to mitochondrial DNA, contributes to UVA resistance
YDL104C	*QRI7*	Highly conserved mitochondrial protein, essential for t6A modification of mitochondrial tRNAs that decode ANN codons; similar to Kae1p and E. coli YgjD, both of which are also required for tRNA t6A modification
YDL033C	*SLM3*	tRNA-specific 2-thiouridylase, responsible for 2-thiolation of the wobble base of mitochondrial tRNAs; human ortholog is implicated in myoclonus epilepsy associated with ragged red fibers (MERRF)

Table 2.3: **Annotation of mitochondrial genes that had a significant change in protein abundance due to Ech A treatment**. Table contains each open reading frame (ORF), gene name and a brief description of function. Description of function attained from Saccharomyces Genome Database (Cherry et al., 2012).

Representative images of significant changes in 17 proteins over the 4-hour time-lapse are shown in (Figures 2.6 – 2.10). These strains share similarities with each other on functional levels including metabolism of metal ions, multi-drug resistance, autophagy, and proteins with unknown functions.

Eight strains that exhibited statistically significant changes in abundance are involved in metal ion metabolism (Figure 2.6 – 2.7). *DAP1* (YPL170W) is a heme-binding protein involved in the regulation of cytochrome protein Erg11 and acts as a damage response protein (Cherry et al., 2012). Dap1 had a significant increase in protein abundance at every timepoint from 30 minutes onwards. *CYT1* (YOR065C) expression is regulated by the heme-activated protein Hap2 and is a component of the mitochondrial respiratory chain (Cherry et al., 2012). Cyt1 had an increase in protein abundance from 150-240 minutes. *ARN1* (YHL040C) is a transporter protein that is responsible for uptake of bound iron (Cherry et al., 2012). Arn1 had an increase at every timepoint from 60 minutes onwards. *TIS11* (YLR136C) had a significant increase at every timepoint and is a mRNA binding protein that is expressed during iron starvation (Cherry et al., 2012). *MRS4* (YK052C) is an iron ion transporter that transports Fe^{2+} across the inner mitochondrial membrane and is highly active during iron deficiency (Cherry et al., 2012). Mrs4 has a significant increase in protein abundance at every timepoint from 60 minutes onwards. *SMF3* (YLRO34C) is a metal ion transporter that plays a role in iron homeostasis (Cherry et al., 2012). Smf3 had a significant increase in protein abundance at every timepoint from 30 minutes onward. These six described proteins are all integral to the metabolism of iron ions and their increase in protein abundance suggests that there is a lower concentration of metal ions available to the cell, within the cells or in the surrounding environment, for normal function due to the treatment of Ech A. Proteins involved in the metabolism of other metal ions were also observed to be altered in their abundance. *CCC2* (YDR270W) is a transporter of copper ions that had an increase in protein abundance at every timepoint from 60 minutes onwards (Cherry et al., 2012). *COT1* (YOR316C) is a mediator of

zinc transport into the vacuole that had an increase in protein abundance from 150-240 minutes (Cherry et al., 2012). Having an increase in protein abundance in these eight proteins suggests that Ech A is altering the concentration of available metal ions to the cell and the increase in protein abundance is the cell trying to find and use the metal ions that are still available.

Multi-drug resistance is represented with statistically significant changes in abundance in five proteins (Figure 2.8 – 2.9). *SNQ2* (YDR011W) showed the greatest increase in protein abundance over the 4-hour time-lapse, with a z-score of 51.25 at the 4-hour timepoint. *SNQ2* is an ATP-binding cassette multi-drug transporter localized to the plasma membrane of the cell and involved in multi-drug resistance mechanisms (Cherry et al., 2012). Other genes involved in multi-drug resistance that also showed an increase in protein abundance were *YOR1* (YGR281W), *FLR1* (YBR008C), YLR179C, and *CIS1* (YLR346C). Yor1 is a plasma membrane ATP-binding multidrug transporter which had an increase in protein abundance from 90-240 minutes (Cherry et al., 2012). Flr1 is another plasma membrane multidrug transporter that had an increase in protein abundance from 90-240 minutes (Cherry et al., 2012). YLR179C and CIS1 (YLR346C) both have unknown functions however both open reading frames are activated by transcription factors that are part of the cell's multidrug resistance system (Cherry et al., 2012). These results reflect the response of the yeast cells to Ech A via specific changes in the abundance of proteins involved in the multidrug resistance mechanism.

A protein critically involved in autophagy also showed significant decrease in protein abundance (Figure 2.9). *SAM3* is a high-affinity S-adenosylmethionine permease required for the cell to use S-adenosylmethionine as a sulfur source, that when deficient, autophagy is activated (Cherry et al., 2012). *SAM3* abundance decreased with Ech A treatment as time increased, with the lowest overall z-score of -25.78 resulting at 4 hours (240 minutes). This result suggests Ech A bioactivity occurs via a mechanism that includes autophagy.

A few proteins that showed some of the greatest abundance changes have unknown functions (Figure 2.10). These include YDR476C, *APD1* (YBR151W), and YCR087C-A. YCR087C-A had a decrease in abundance at every timepoint except for t0 (0 minutes) and the other two proteins all had increases at every timepoint from 60-240 minutes. Though the function of Apd1 is unknown, it is required for normal tolerance of sodium ions and hydrogen peroxide (H_2O_2) (Cherry et al., 2012). The increase in protein abundance could mean that there was an increased concentration of H_2O_2 caused by Ech A and the cell is trying to get rid of additional H_2O_2. Alternatively, there was a depletion of H_2O_2, and the cell has increased the protein abundance to use the available H_2O_2. Though the functions of these genes are unknown, these changes in protein abundance indicate these proteins and their associated processes in oxidative stress are involved in the metabolism of Ech A.

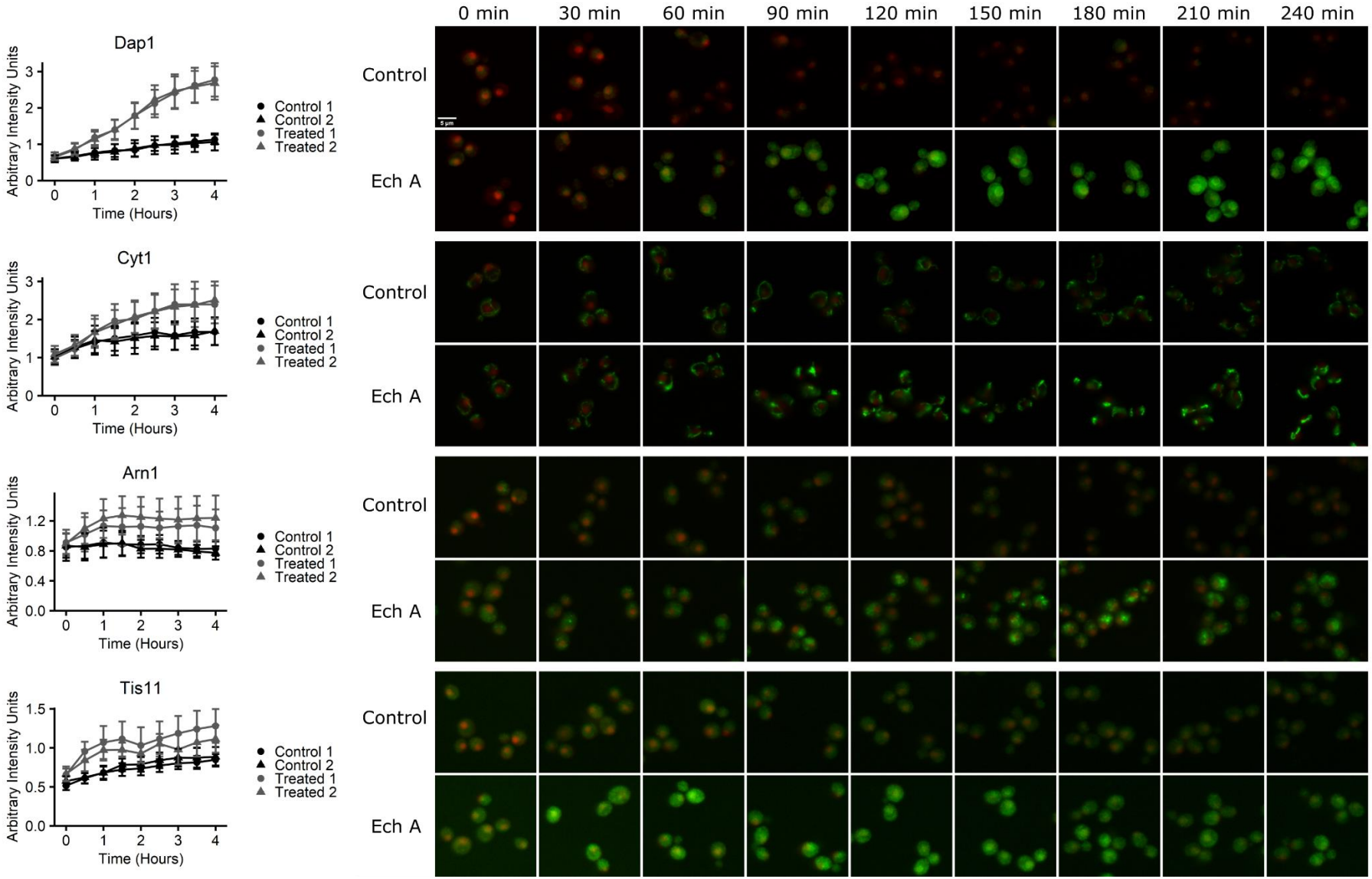

Figure 2.6: **Ech A treatment significantly changes protein abundance of proteins involved in the metabolism of metal ions**. GFP strains were treated with and without 2 µg/mL Ech A and imaged every 30 minutes over 4 hours. Each strain was normalised to the RFP in the control. Line graphs of each strain with the mean arbitrary intensity units (representing GFP fluorescence) of each control and treated replicate over the 4-hour time lapse ± SD.

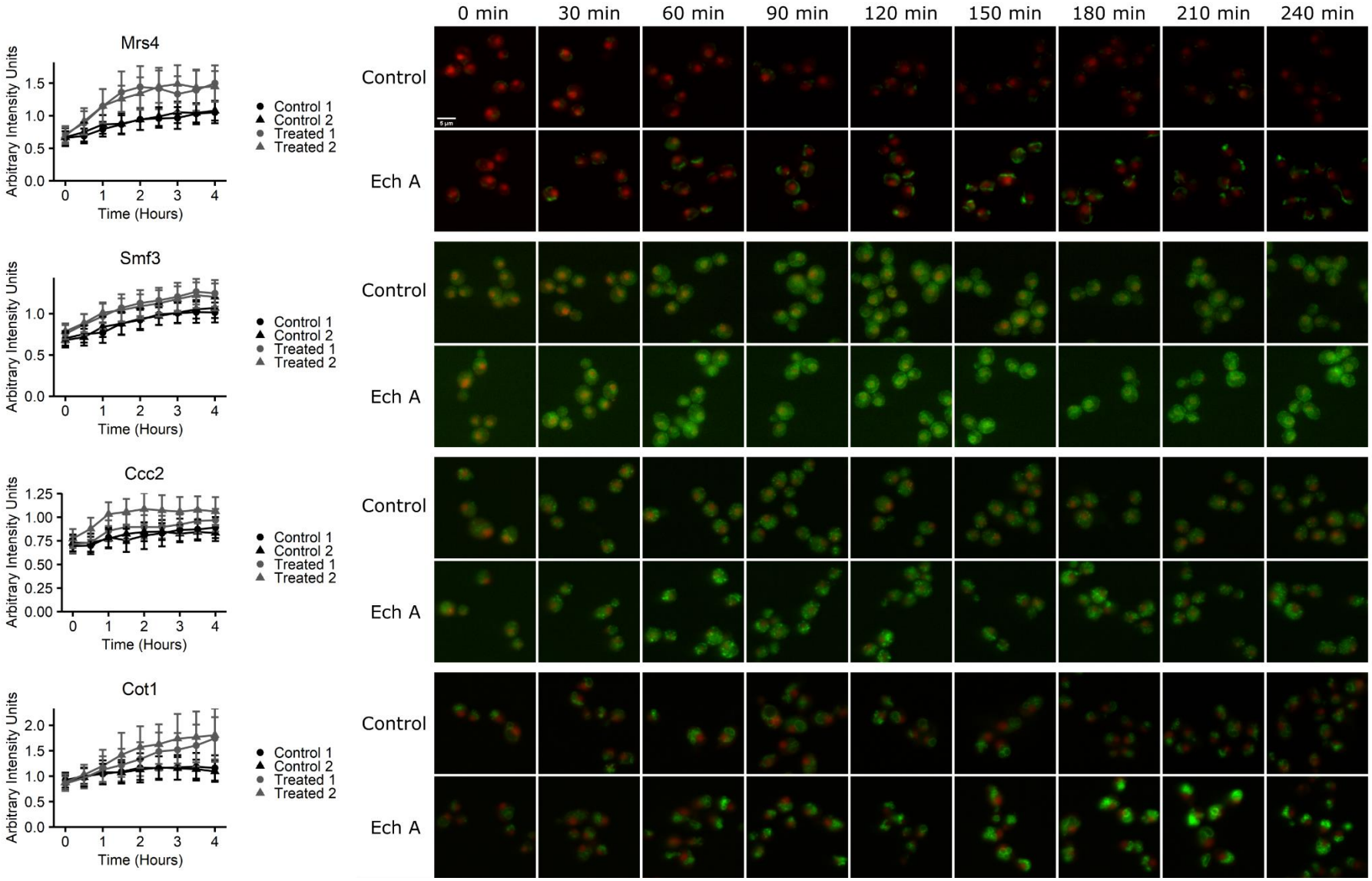

Figure 2.7: **Ech A treatment significantly changes protein abundance of proteins involved in the metabolism of metal ions**. GFP strains were treated with and without 2 µg/mL Ech A and imaged every 30 minutes over 4 hours. Each strain was normalised to the RFP in the control. Line graphs of each strain with the mean arbitrary intensity units (representing GFP fluorescence) of each control and treated replicate over the 4-hour time lapse ± SD.

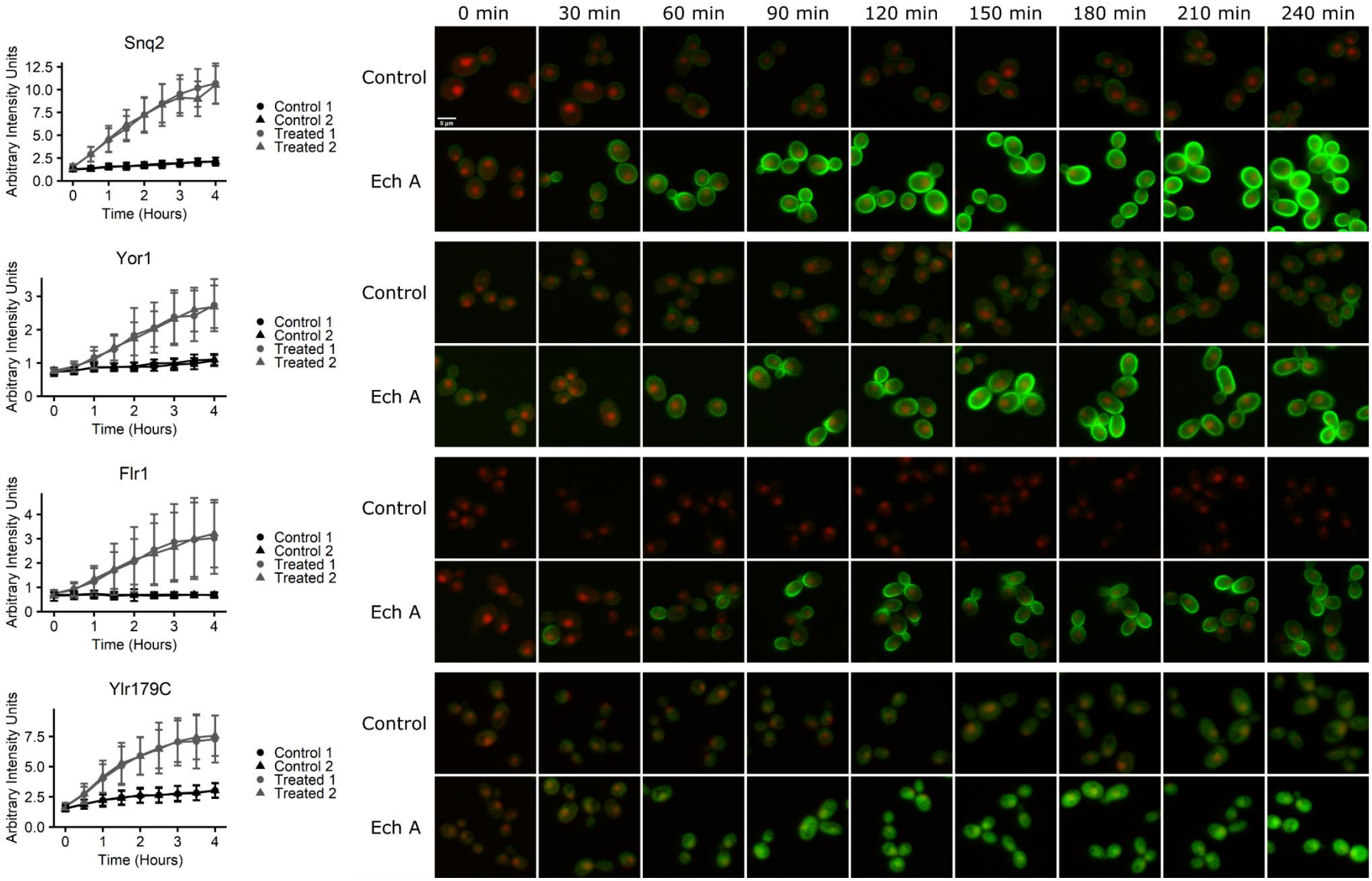

Figure 2.8: **Ech A treatment significantly changes protein abundance of proteins involved in multidrug resistance**. GFP strains were treated with and without 2 µg/mL Ech A and imaged every 30 minutes over 4 hours. Each strain was normalised to the RFP in the control. Line graphs of each strain with the mean arbitrary intensity units (representing GFP fluorescence) of each control and treated replicate over the 4-hour time lapse ± SD.

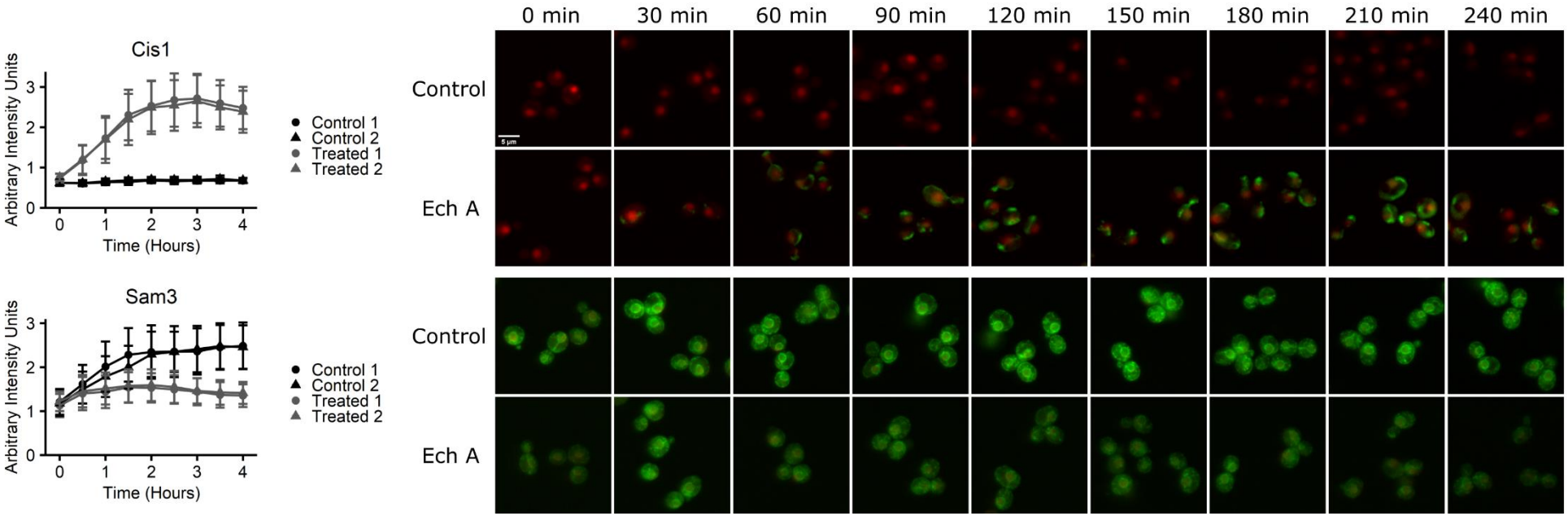

Figure 2.9: Ech A treatment significantly changes protein abundance of proteins involved in multidrug resistance and autophagy. GFP strains were treated with and without 2 µg/mL Ech A and imaged every 30 minutes over 4 hours. Each strain was normalised to the RFP in the control. Line graphs of each strain with the mean arbitrary intensity units (representing GFP fluorescence) of each control and treated replicate over the 4-hour time lapse ± SD.

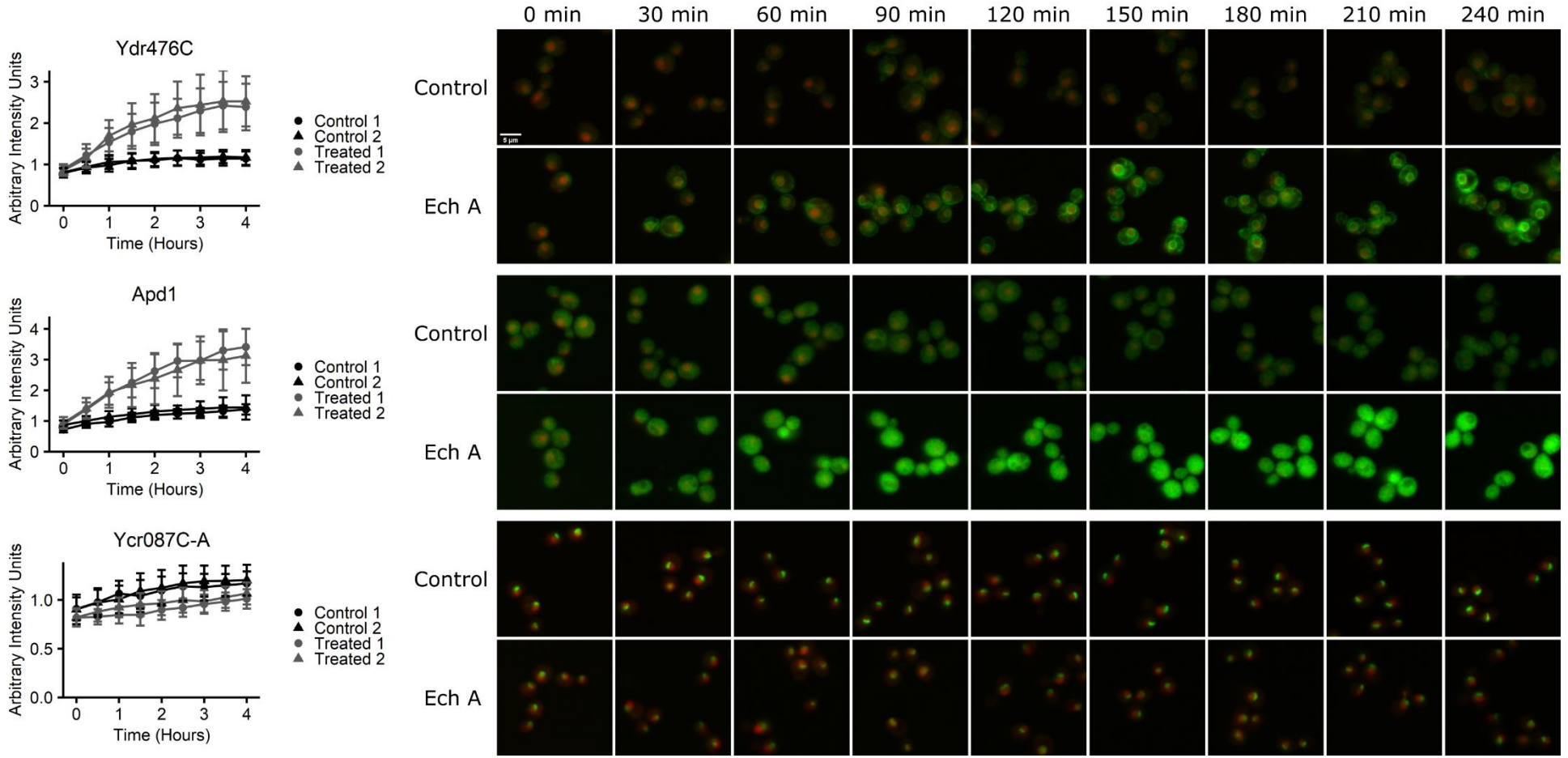

Figure 2.10: Ech A treatment significantly changes protein abundance of proteins with unknown functions. GFP strains were treated with and without 2 µg/mL Ech A and imaged every 30 minutes over 4 hours. Each strain was normalised to the RFP in the control. Line graphs of each strain with the mean arbitrary intensity units (representing GFP fluorescence) of each control and treated replicate over the 4-hour time lapse ± SD.

2.3.5 Over-representation of altered protein abundance in metal ion metabolism

Enrichment analyses provide insight into the over-representation of gene functions within a given gene set (Kuleshov et al., 2016, 2019). We used YeastEnrichr for the analysis of Gene Ontology (GO) terms to provide insight into what biological processes and molecular functions are over-represented among the proteins with altered expression levels. YeastEnrichr provides two algorithms to assign GO enrichments to a gene set list. The first GO enrichment analysis method assessed over-representation of GO terms. The second GO enrichment algorithm, AutoRIF, assessed over-representation of terms based on text-mining in publications in the PubMed database (Kuleshov et al., 2016, 2019). With each algorithm, three scores of significance were used including P-value, z-score and a combined score (z-score multiplied by the negative logarithm of the P-value). Using these two GO enrichment algorithms, the 92 proteins that showed a significant change in protein abundance over the 4-hour time lapse were found to have enrichments at each timepoint and an overall biological process enrichment theme of metabolism of metal ions (Figure 2.11 – 2.12). Both algorithms showed biological process enrichments within the first 30 minutes of treatment for DNA replication and repair, followed by enrichments for iron ion transport and homeostasis as well as transition metal ion transport at every timepoint after 60 minutes. A similar trend was observed for the molecular function enrichments, with functions involved in DNA replication and repair being enriched at 30-minute timepoint and then metabolism of metal ions, specifically iron ions, being enriched at each timepoint from 60-240 minutes.

Using the GO enrichment algorithm for molecular function, significant enrichments were also observed. These included enrichment for multiple transmembrane transporter activity for transition metal ions and inorganic cations as well as kinase activity, which was enriched at seven out of the nine time points (Figure 2.12).

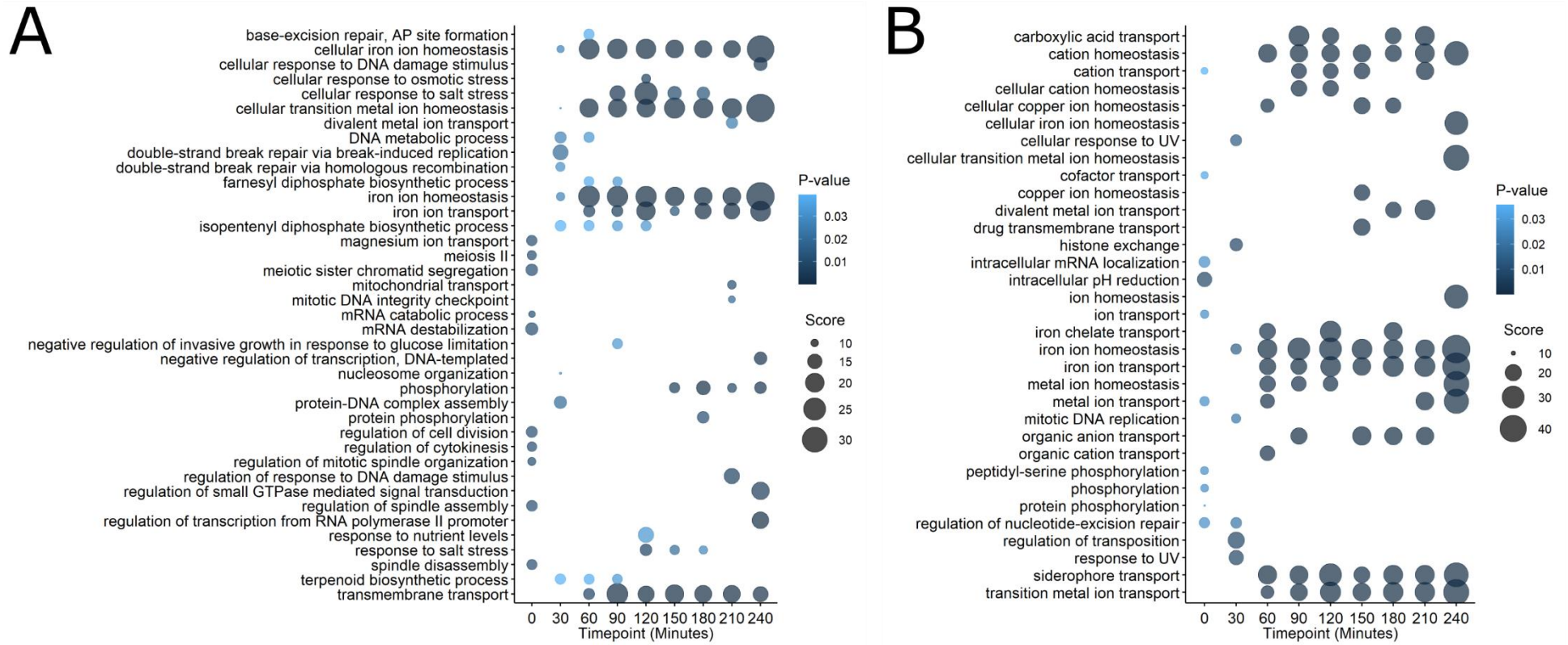

Figure 2.11: **Over-representation of altered protein abundance for biological processes in metal ion metabolism.** Over-representation of biological processes of strains with significant changes in protein abundance at each 30-minute timepoint using YeastEnrichr (Kuleshov et al., 2016, 2019). **(A)** Over-representation using the conventional GO algorithm. **(B)** Over-representation using the text-mining algorithm, AutoRIF. Statistical enrichment is shown with P-value for colour and combined score for size of bubbles.

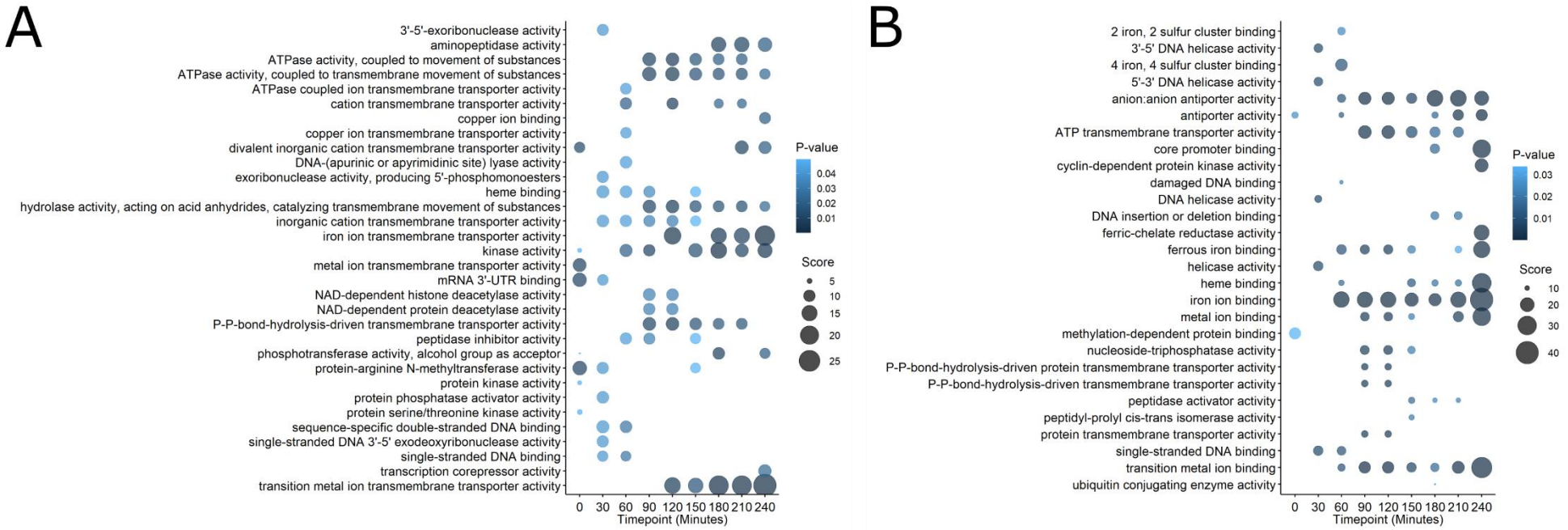

Figure 2.12: **Over-representation of altered protein abundance for molecular function in metal ion metabolism.** Over-representation of molecular function of strains with significant changes in protein abundance at each 30-minute timepoint using YeastEnrichr (Kuleshov et al., 2016, 2019). **(A)** Over-representation using the conventional GO algorithm. **(B)** Over-representation using the text-mining algorithm, AutoRIF. Statistical enrichment is shown with P-value for colour and combined score for size of bubbles.

2.3.6 Exogenous iron supplementation alleviates Ech A bioactivity

Metabolism of iron ions was an enriched biological process and molecular function (Figure 2.11 – 2.12). Therefore, I hypothesized that Ech A affects the transport of iron either into the cell or within the cell. Therefore, I expected supplementation of exogenous iron would reduce the growth defect of wildtype cells when treated with Ech A. To test this hypothesis, four sets of liquid assays were carried out with wildtype cells treated with increasing concentrations of Ech A in normal SC media with supplementation of either 100 μM $FeCl_3$ or 100 μM $FeSO_4$ or in iron-free SC media. The iron concentrations were chosen for optimal yeast growth as previously investigated by (Shakoury-Elizeh et al., 2010), and two different iron sources ensured that both ferrous and ferric forms of the iron ion (Fe^{2+} and Fe^{3+}, respectively) were investigated. Growth inhibition caused by Ech A treatment was alleviated with supplementation of ferrous or ferric ion (Figure 13). Relative to the Ech A alone treatment at the highest concentration (1.5 μg/ml), growth was increased from 21% (no supplementation) to 91% with $FeSO_4$ supplementation and 109% with $FeCl_3$ supplementation. The growth inhibition of wildtype cells in iron-free media was greater than with normal SC media.

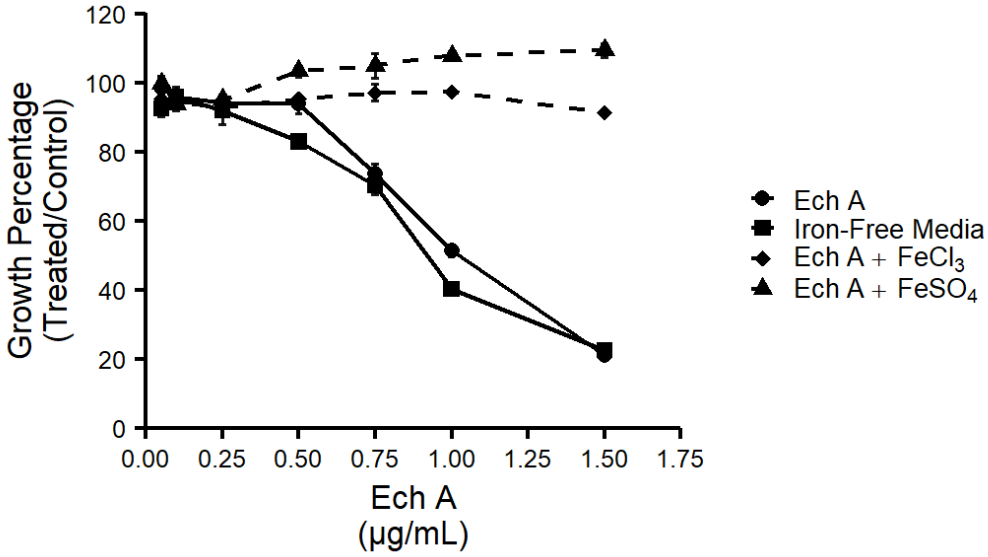

Figure 2.13: **Supplementation of exogenous iron rescued growth from Ech A treatment.** Growth percentage of wildtype cells at mid-log in the presence of increasing concentrations of Ech A, in either normal SC broth or iron-free broth with or without 100 µM of either $FeCl_3$ or $FeSO_4$. Data shown as mean of technical triplicates ± SD.

2.3.7 Ech A chelates iron in a cell-free assay

The GFP strains that increased in abundance with Ech A treatment were enriched in iron transport (Figure 2.11 – 2.12) and iron supplementation restored normal growth in cells treated with Ech A (Figure 2.13). These results suggest that Ech A chelates iron ions and that the up regulation of iron transport proteins is the cell compensating for the lack of free iron available for fundamental metabolism that requires iron. To determine if Ech A chelates iron, a chrome azurol S (CAS) assay was conducted (Alexander & Zuberer, 1991). The CAS assay is a colorimetric assay that uses a solution, that when exposed to an iron chelator, the colour changes from blue to yellow. EDTA is a well-established iron chelator that was used as a

positive control for this assay (Ferrero, 2016). Three concentrations were selected for Ech A and EDTA ranging from 0.5 to 5 µM, and these were compared to untreated controls. A concentration 100 times more concentrated for EDTA was used as a positive control for the CAS assay solution, which can be seen with the colour change from blue to yellow (Figure 2.14). Percentages of each treatment were calculated using the absorbance (630 nm) of each treatment sample divided by the absorbance (630 nm) of the reference solution. Ech A exhibited a greater colour change at each concentration compared to the established iron chelator EDTA, with EDTA having a mild colour change at 1 µM and 5 µM. These results suggest Ech A chelates iron as effectively as EDTA. However, the Ech A stock solution is pale red in colour, thus this colour could be affecting the colorimetric assay. Therefore, I cannot fully confirm that Ech A chelates iron more potently than EDTA.

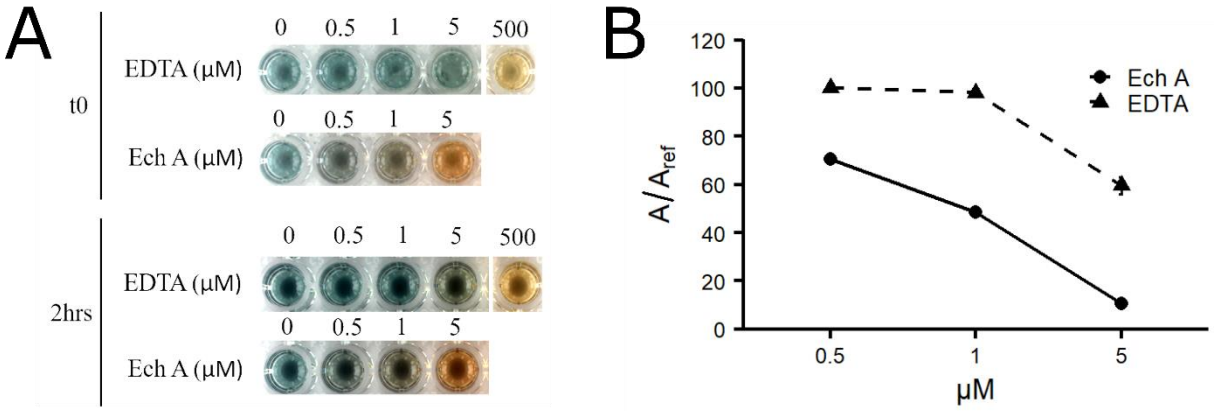

Figure 2.14: **Ech A chelates iron in a cell-free assay**. **(A)** Microtiter well images of CAS assay of EDTA and Ech A at concentrations 0, 0.5, 1, 5 µM at t0 and 2-hour timepoint relative to a positive control of 500 µM EDTA. **(B)** Absorbance (630 nm) after 2 hours of the percentage of A/A_{ref} of EDTA and Ech A. Data shown as mean of technical triplicates ± SD.

2.3.8 Iron, copper and zinc supplementation alleviates Ech A bioactivity

Since iron supplementation rescued Ech A-induced growth inhibition when supplemented with either ferrous (Fe^{2+}) or ferric (Fe^{3+}) forms of iron, I next evaluated the impact of supplementation with other metals (iron sulphate ($FeSO_4$), copper sulphate ($CuSO_4$), zinc sulphate ($ZnSO_4$), magnesium sulphate ($MgSO_4$) and manganese sulphate ($MnSO_4$)) on Ech A bioactivity. Only sulphate salts were selected, and all metals (salts) were treated at a final concentration of 100 µM, the same concentration used in the iron supplementation assay. Metal supplementations that improved the growth percentage to be greater than 60% at the highest concentration of Ech A (1.5 µg/ml) were considered to have shown a supplementation rescue. Iron, copper and zinc significantly improved growth from 31% residual growth to 81, 83 and 63% residual growth, respectively (Figure 2.15). Manganese showed a slight improvement in growth by 8%; however, this improvement fell short of the criterion for rescue (60% growth percentage). In contrast, magnesium was the only metal that worsened growth, whereby residual growth decreased by 5%. These results indicate that supplementation with iron, copper or zinc rescues the growth of cells when co-treated with Ech A, which suggests that Ech A bioactivity impacts homeostasis of these metals.

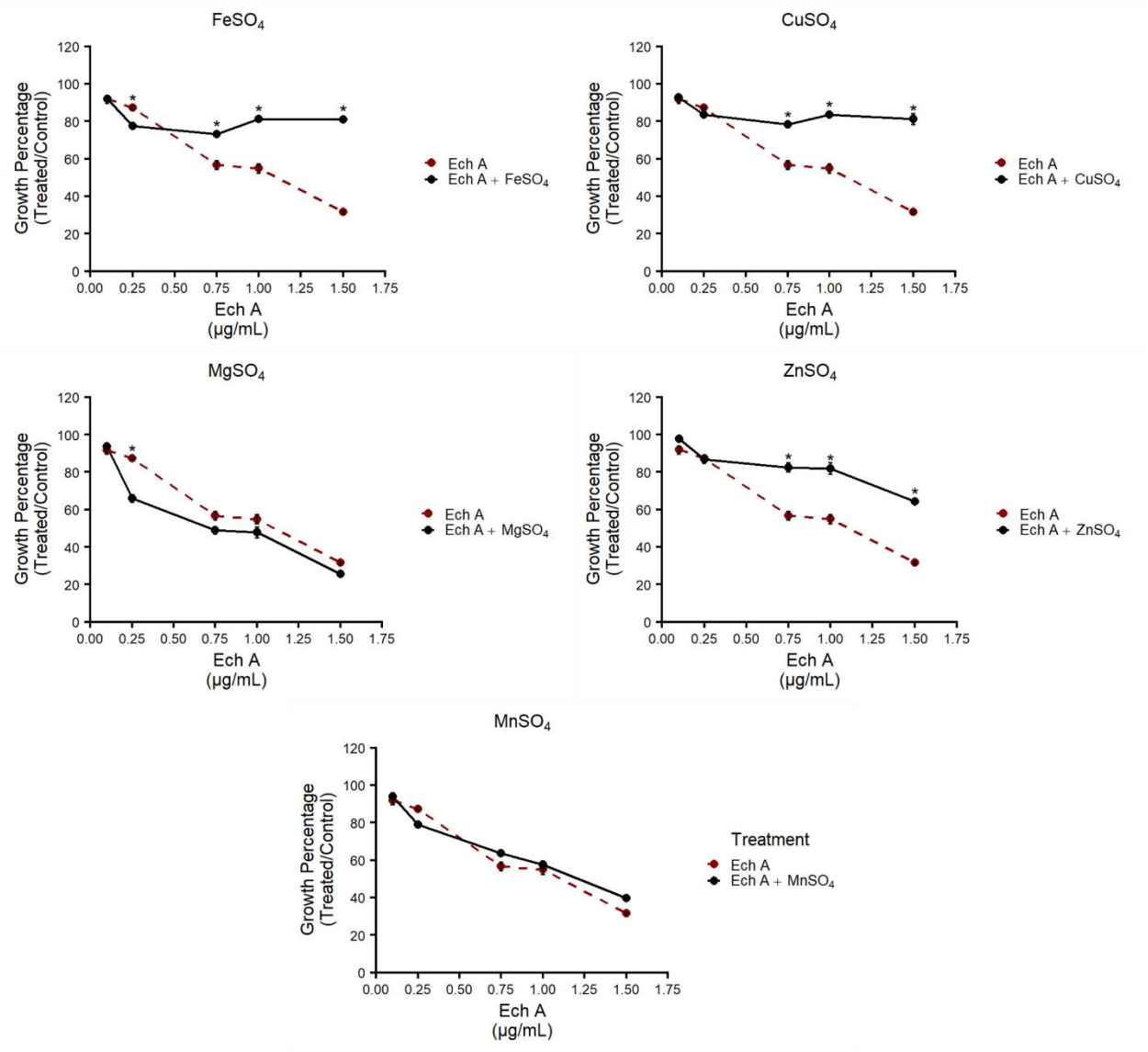

Figure 2.15: **Iron, copper and zinc supplementation recues growth from Ech A treatment.** Growth percentage of wildtype in increasing concentrations of Ech A at mid-log, with supplementation of either 100 µM of either $FeSO_4$, $CuSO_4$, $ZnSO_4$, $MgSO_4$, or $MnSO_4$. Data shown as mean of technical triplicates ± SD: *, $p \leq 0.05$, student's t-test comparing metal supplementation to Ech A treatment.

2.3.9 Echinochrome A is bioactive in agar for genome-wide analysis

A major goal of this thesis was to screen the gene deletion library on agar to distinguish mutants that are hypersensitive to Ech A. To determine if Ech A is bioactive in agar, growth inhibition in various concentrations of Ech A (1 µg/ml, 5 µg/ml, 10 µg/ml, and 25 µg/ml with a 1% ethanol vehicle control) was evaluated in SC agar. Growth was observed at 24 hours of incubation at 30°C (Figure 2.16). Results showed that concentrations above 10 µg/ml had no growth after 24 hours. The desired concentration to use for a genome-wide analysis would have 10-20% growth inhibition compared to the control plates, which would yield a 80-90% window to detect addition growth inhibition due to the gene deletion. The initial assay was conducted in a 24 well plate in order to conserve Ech A and obtain initial insight into bioactivity in agar. The results in the 24 well format indicate that the desired IC_{20} for Ech A would be between 1-10 µg/ml (Figure 2.16).

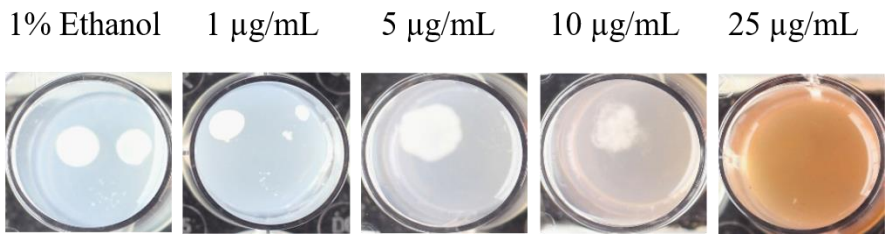

Figure 2.16: **Ech A is bioactive in solid agar.** Wildtype cells were spotted at various cellular concentrations (cells/mL) (1 x 10^8 (top left), 1 x 10^6 (top right) and 1 x 10^4 (bottom)) on agar with or without Ech A (1 µg/mL, 5 µg/mL, 10 µg/mL, or 25 µg/mL). Cells were incubated at 30°C and imaged at 24 hours.

This range of concentrations was further optimized in an agar plate containing 1536 colonies, the same format that was subsequently used for the genome-wide analysis. To determine the optimal IC_{20} concentration to use for the chemical-genomic analysis, growth of Plate 2 of the Deletion Mutant Array (DMA) library was randomly selected and evaluated in the 1536 format with two treatments of Ech A (4 µg/ml, 10 µg/ml) relative to the 1% ethanol vehicle control. Images of the plates were taken after 24 hours of incubation at 30°C. Growth inhibition was calculated using SGA tools that measured and statistically compared the colony sizes on each plate (Wagih et al., 2013). A growth percentage for each treatment plate was calculated using the mean colony size over all 1536 colonies of each treated plate relative to the control plate. Growth inhibition relative to control was 45% with 10 µg/ml, while 4 µg/ml resulted in 20% inhibition. At this point, there was not enough compound to complete a full chemical-genomic screen and I had to wait for more compound to arrive from the Cawthron Institute. Using the next batch of compound, two concentrations were tested, which resulted in 8% inhibition with 4 µg/mL Ech A and 17% inhibition with 7.5 µg/mL Ech A. For the genome-wide analysis, I decided to use 7.5 µg/mL as the inhibition at this concentration was reproducibly within the desired range of 10-20% relative to the control. In addition, this experiment showed that yeast can be pinned in the 1536 format on agar that contains Ech A without any undesired smearing of colonies, which was seen in the agar dose response in the 24 well format.

2.3.10 Genome-wide analysis identifies 36 genes involved in Ech A bioactivity

Genome-wide analysis in the presence and absence of 7.5 µg/mL Ech A was performed to provide insight into possible mechanisms of action of Ech A. Growth of ~ 4,800 strains in 1536 colony format was quantified on treated plates relative to the control plates containing 1% ethanol. The z-score of each deletion strain relative to untreated control was calculated along with the P-value, resulting in 166 deletion strains that had significantly altered growth ($P < 0.05$) with Ech A treatment (Figure 2.17). The majority (n = 137) of these deletion strains exhibited decreased growth and the remaining 29 deletions strains exhibited improved growth compared to the control.

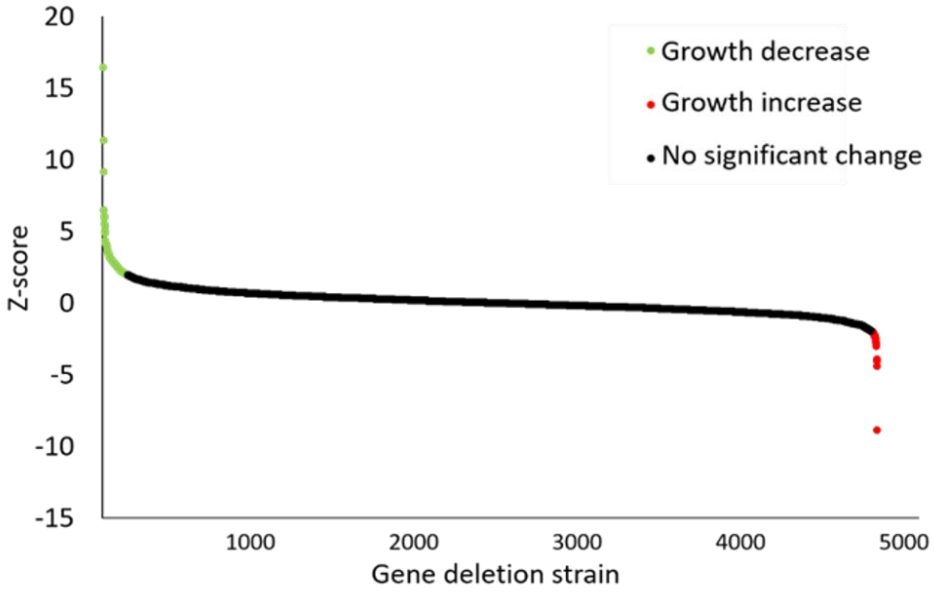

Figure 2.17: **166 gene deletion strains showed significant changes in growth with Ech A treatment.** The haploid deletion mutant library was grown in the presence and absence of 7.5 µg/mL of Ech A in quadruplicate. Z-scores were generated for each mutant by comparing growth of treated and untreated conditions with SGA tools (Wagih et al., 2013). Green data points indicate a significant growth decrease, red data points indicate a significant growth increase and black data points indicate no significant difference in growth.

The 137 gene deletion strains that were sensitive to Ech A were selected for further validation. Serial dilutions of these 137 gene deletions strains were performed at the same Ech A concentration (7.5 µg/mL) as the genome-wide chemical genomic screen. The serial dilutions revealed 36 strains that were sensitive to Ech A based on a minimum of one less spot of growth on treated agar compared to control agar (Figure 2.18). To eliminate any bias selection, images were inspected by multiple individuals. The gene deletions that showed the most sensitivity were *ipk1Δ, gdt1Δ, yrr1Δ, she4Δ, crd1Δ, ume6Δ, rps27bΔ, and vps24Δ.*

The 36 sensitive gene deletion strains had liquid growth assays performed for each strain in the presence and absence of Ech A to further test their sensitivity, but in an independent assay. The liquid growth assays were performed to have statistical evidence to support that these gene deletions strains are sensitive to Ech A. A concentration of 2 µg/mL was selected as it gave 20% growth inhibition in liquid in the wildtype (BY4741) strain (Figure 2.19). Optical density (O.D 590nm) was measured at t0 and mid-log (0.450 O.D) for each strain. The liquid growth assays indicated that 30 gene deletion strains had significantly altered growth compared to wildtype ($p < 0.05$), of which 20 gene deletion strains exhibited more than 40% growth inhibition. The strongest growth inhibition was detected in *yrr1Δ* (0.38% percentage growth)*, ipk1Δ* (0.49% percentage growth)*, hsp12Δ* (4.8% percentage growth)*, ume6Δ* (4.98% percentage growth), *ymr031w-aΔ* (11.03% percentage growth), *crd1Δ* (15.72% percentage growth), *slt2Δ* (23.54% percentage growth), *dbp7Δ* (25.44% percentage growth), and *she4Δ* (26.34% percentage growth). Therefore, 20 genes deletion strains were identified to be highly sensitive to Ech A, suggesting these genes and their associated functions, processes and pathways are required for the normal metabolism of Ech A in yeast (Table 2.4).

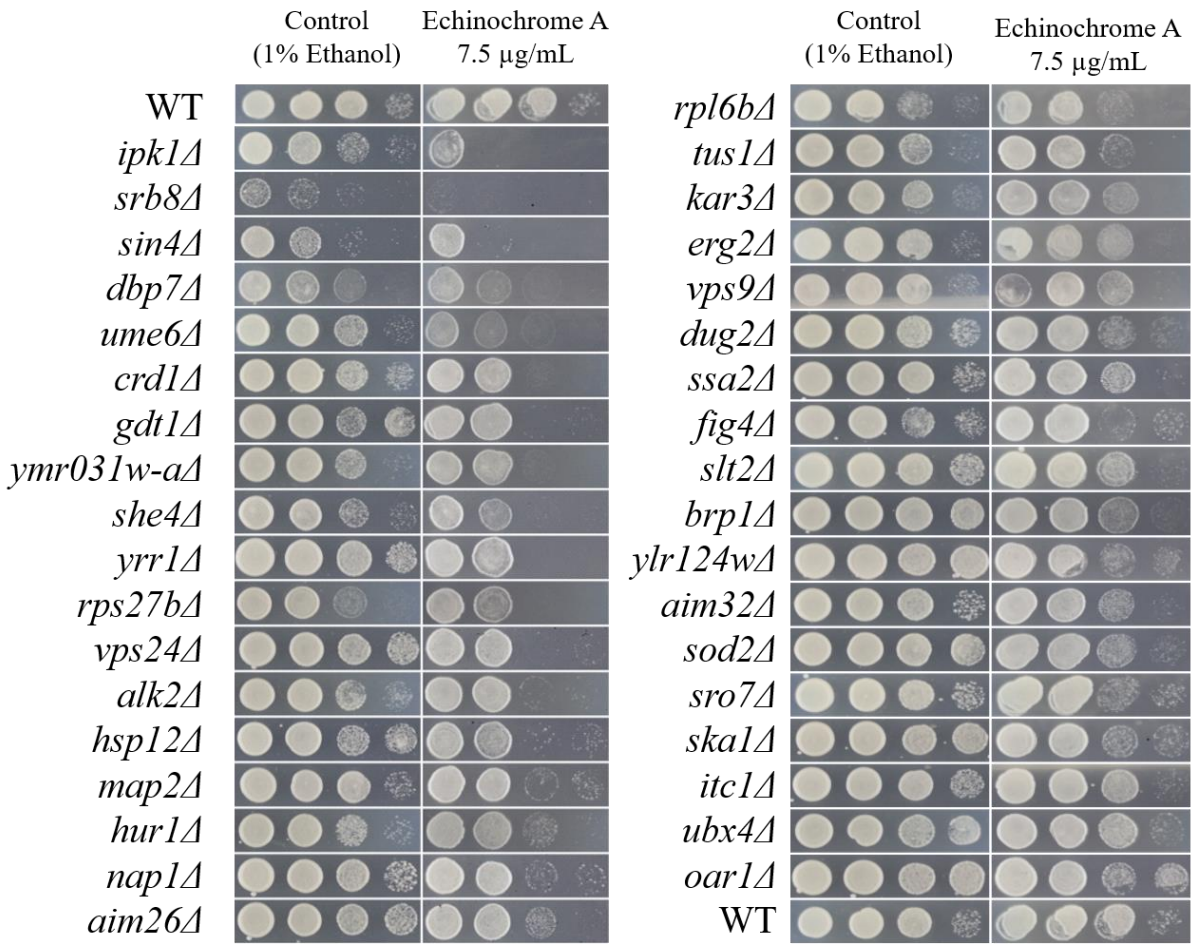

Figure 2.18: **Reproducible sensitivity of 36 gene deletion strains to Ech A on agar.** Five-fold (left to right) spot dilutions of wildtype and gene deletion strains were pinned on SC agar with and without 7.5 µg/mL of Ech A, incubated at 30˚C, and imaged at 24 hours.

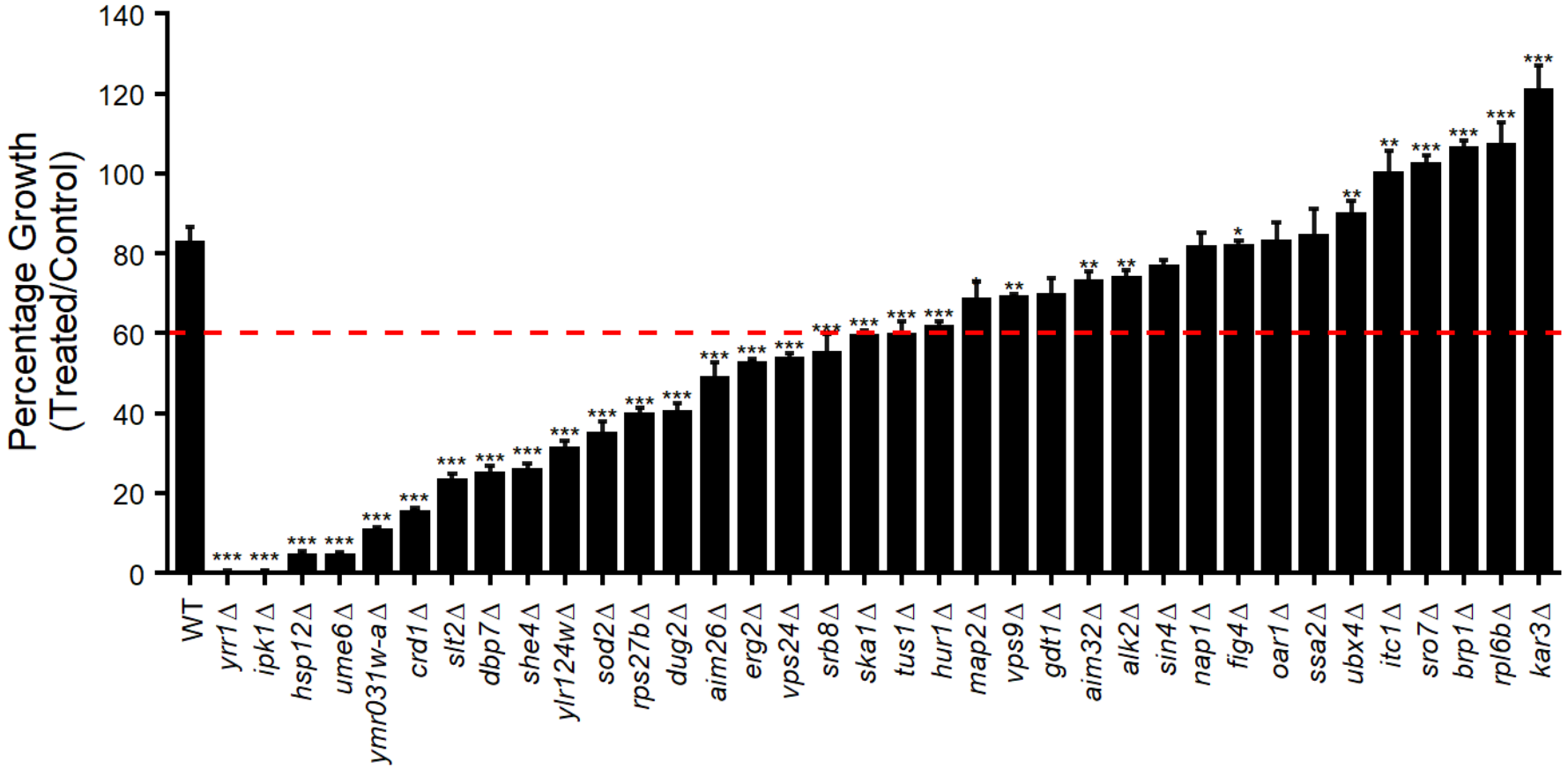

Figure 2.19: **Reproducible sensitivity of 20 gene deletion strains to Ech A in a liquid assay.** Percentage growth of wildtype and validated Ech A sensitive gene deletion strains on agar at mid-log (Abs_{590nm}: 0.450). Cells were grown with and without 2 µg/mL of Ech A. Data shown as mean of technical triplicates ± SD; * $p \leq 0.05$, ** $p \leq 0.01$, *** $p \leq 0.005$, student's t-test compared to wildtype.

ORF	Gene	Function
YBR281C	*DUG2*	Probable di- and tri-peptidase; forms a complex with Dug1p and Dug3p to degrade glutathione (GSH) and other peptides containing a gamma-glu-X bond in an alternative pathway to GSH degradation by gamma-glutamyl transpeptidase (Ecm38p)
YCR081W	*SRB8*	Subunit of the RNA polymerase II mediator complex; associates with core polymerase subunits to form the RNA polymerase II holoenzyme; essential for transcriptional regulation; involved in glucose repression
YDL142C	*CRD1*	Cardiolipin synthase; produces cardiolipin, which is a phospholipid of the mitochondrial inner membrane that is required for normal mitochondrial membrane potential and function; also required for normal vacuolar ion homeostasis
YDR207C	*UME6*	Key transcriptional regulator of early meiotic genes, binds URS1 upstream regulatory sequence, couples metabolic responses to nutritional cues with initiation and progression of meiosis, forms complex with Ime1p, and also with Sin3p-Rpd3p
YDR315C	*IPK1*	Inositol 1,3,4,5,6-pentakisphosphate 2-kinase, nuclear protein required for synthesis of 1,2,3,4,5,6-hexakisphosphate (phytate), which is integral to cell function; has 2 motifs conserved in other fungi; ipk1 gle1 double mutant is inviable
YFL014W	*HSP12*	Plasma membrane protein involved in maintaining membrane organization in stress conditions; induced by heat shock, oxidative stress, osmostress, stationary phase, glucose depletion, oleate and alcohol; regulated by HOG and Ras-Pka pathways
YGL168W	*HUR1*	Protein of unknown function; reported null mutant phenotype of hydroxyurea sensitivity may be due to effects on overlapping PMR1 gene

YHR008C	*SOD2*	Mitochondrial manganese superoxide dismutase, protects cells against oxygen toxicity; phosphorylated
YHR021C	*RPS27B*	Protein component of the small (40S) ribosomal subunit; nearly identical to Rps27Ap and has similarity to rat S27 ribosomal protein
YHR030C	*SLT2*	Serine/threonine MAP kinase; involved in regulating maintenance of cell wall integrity, progression through the cell cycle, and nuclear mRNA retention in heat shock; required for mitophagy and pexophagy; affects recruitment of mitochondria to the phagophore assembly site (PAS); regulated by the PKC1-mediated signalling pathway
YKL023W	*SKA1*	Putative protein of unknown function, predicted by computational methods to be involved in mRNA degradation; green fluorescent protein (GFP)-fusion protein localizes to the cytoplasm
YKL037W	*AIM26*	Putative protein of unknown function; null mutant is viable and displays elevated frequency of mitochondrial genome loss; null mutation confers sensitivity to tunicamycin and DTT
YKL041W	*VPS24*	One of four subunits of the endosomal sorting complex required for transport III (ESCRT-III); forms an ESCRT-III subcomplex with Did4p; involved in the sorting of transmembrane proteins into the multivesicular body (MVB) pathway
YKR024C	*DBP7*	Putative ATP-dependent RNA helicase of the DEAD-box family involved in ribosomal biogenesis; essential for growth under anaerobic conditions
YLR124W	*YLR124W*	Dubious open reading frame unlikely to encode a protein, based on available experimental and comparative sequence data
YLR425W	*TUS1*	Guanine nucleotide exchange factor (GEF) that functions to modulate Rho1p activity as part of the cell integrity

		signalling pathway; multicopy suppressor of tor2 mutation and ypk1 ypk2 double mutation; potential Cdc28p substrate
YMR031W-A	*YMR031W-A*	Dubious open reading frame unlikely to encode a protein, based on available experimental and comparative sequence data; null mutant displays shortened telomeres; partially overlaps the uncharacterized ORF YMR031C
YMR202W	*ERG2*	C-8 sterol isomerase, catalyses the isomerization of the delta-8 double bond to the delta-7 position at an intermediate step in ergosterol biosynthesis
YOR035C	*SHE4*	Protein containing a UCS (UNC-45/CRO1/SHE4) domain, binds to myosin motor domains to regulate myosin function; involved in endocytosis, polarization of the actin cytoskeleton, and asymmetric mRNA localization
YOR162C	*YRR1*	Zn2-Cys6 zinc-finger transcription factor that activates genes involved in multidrug resistance; paralog of Yrm1p, acting on an overlapping set of target genes

Table 2.4: **Annotation of gene deletion strains sensitive to Ech A**. Table contains each open reading frame (ORF), gene name and a brief description of function. Description of function attained from Saccharomyces Genome Database (Cherry et al., 2012).

To verify the identification of the 20 genes, amplicons were produced by PCR that were specific to each ORF. The A and D primers were upstream and downstream of the start and stop codons, respectively, while the B primer was internal within the antibiotic-resistance cassette that replaced each ORF. The A/D and A/B primer pairs were amplified from genomic DNA isolated from WT and the deletion strains. Seventeen of the 20 strains had the expected amplicons for both the wildtype and gene deletion strains (Figure 2.20). Three gene deletions (*slt2Δ*, *ylr124wΔ,* and *ska1Δ*) were not confirmed with the A/D primer pairs because either two bands were present in the mutant strain, meaning the strain could be aneuploidy with two copies or fragments of the same gene in different locations of the genome, or the expected band lengths in the wildtype and mutant strains were too close together to be distinguished apart. The identity of these three gene deletion strains was then confirmed using the A/B primer pair (Figure 2.21). As expected, no amplicon was generated with the A/B primer pair for wildtype. These results confirm the identity of the 20 gene deletion strains sensitive to Ech A.

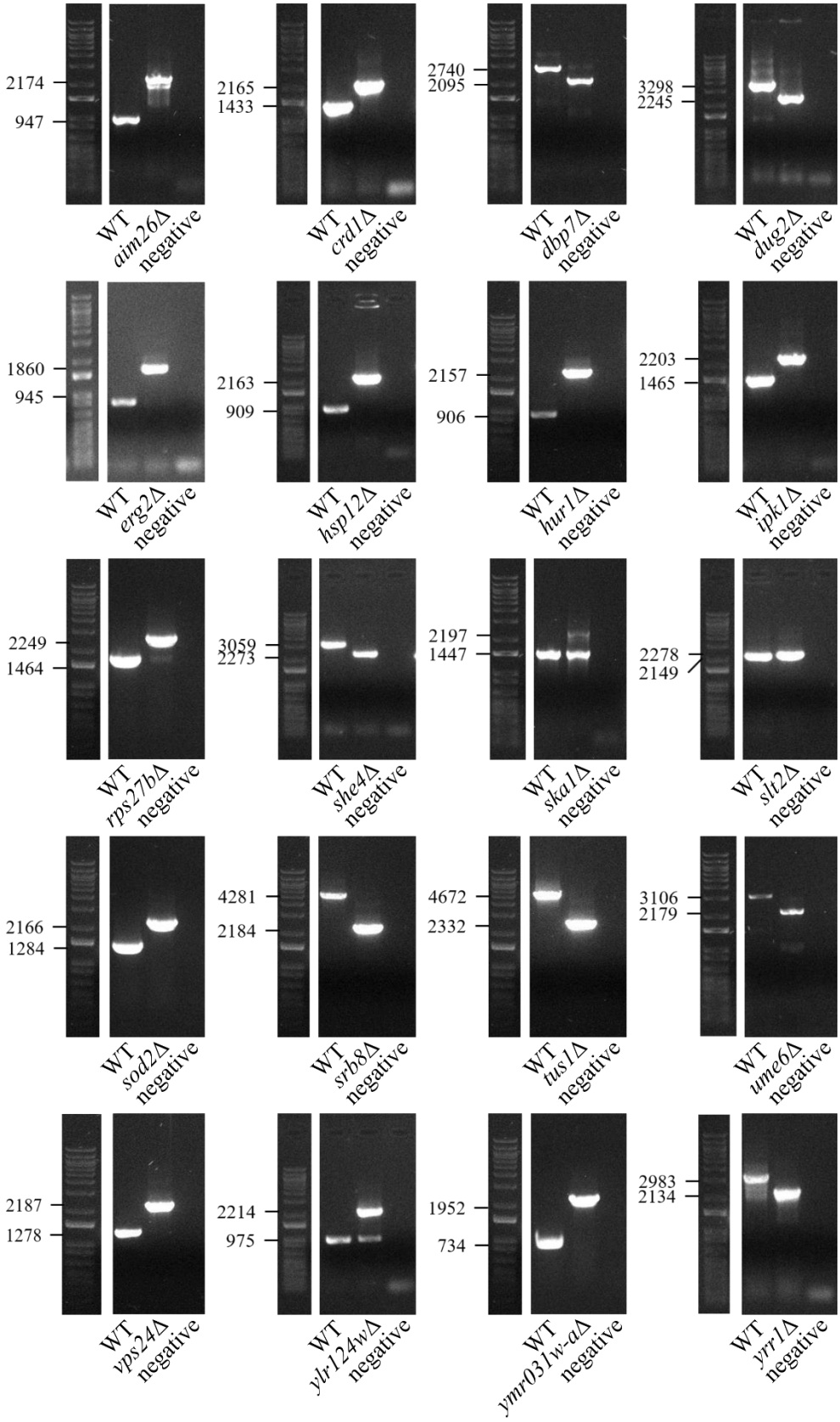

Figure 2.20: **PCR confirmation of identity of the gene deletion strains sensitive to Ech A.** PCRs were performed on wildtype and gene deletion strains with specific confirmation primers for each gene (Table 2.2). Agarose gels labelled with expected product sizes.

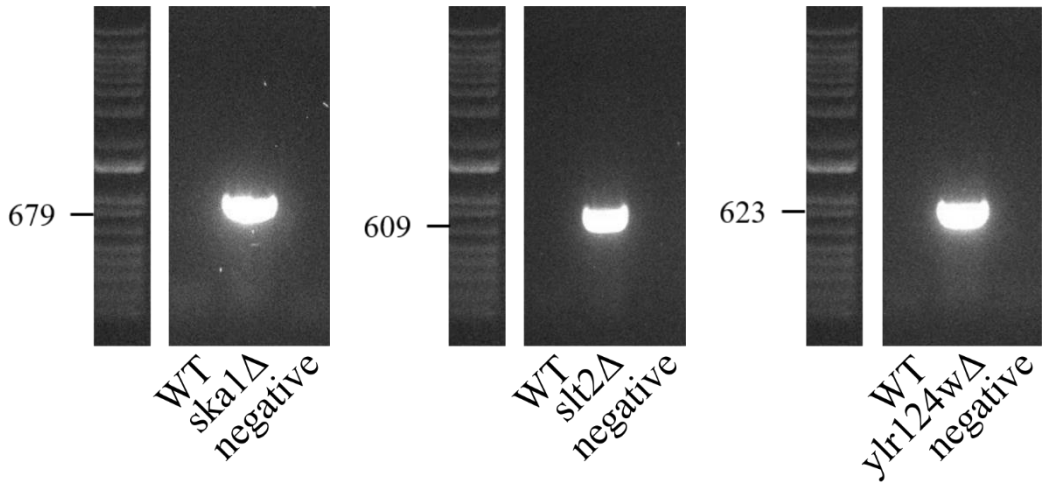

Figure 2.21: **PCR confirmation of identity of the gene deletion strains sensitive to Ech A.** PCRs were performed on wildtype and gene deletion strains with specific A and B confirmation primers for each gene (Table 2.2). Agarose gels labelled with expected product sizes.

2.3.11 Three transcription factors regulate expression of most Ech A-sensitive genes

To understand the regulation of the genes sensitive to Ech A, Yeastract was used to determine transcription factors involved in the regulation of the 20 genes via expression or/and DNA binding (Monteiro et al., 2020). Transcription factors have certain environmental conditions that can upregulate or downregulate the expression of specific genes. It was found that three transcription factors were significantly associated ($P < 0.05$) with 95-100% of the 20 genes sensitive to Ech A (Figure 2.22). These transcription factors were PDR3, YAP1 and RPN4 that regulate at least 19 of the 20 genes. The only gene out of the 20 sensitive genes that YAP1 and RPN4 did not regulate was YLR124W. Interestingly, all three transcription factors are active in a yeast cell upon exposure to a drug/chemical (Monteiro et al., 2020). These results suggest that PDR3 is highly active during drug/chemical stress exposure and is one of the main transcription factors involved in the regulation of genes sensitive to Ech A. YAP1 regulates the genes upon oxidative stress, which is consistent with six of the 20 genes being activated with oxidative stress (SRB8, SOD2, UME6, CRD1, DUG2, HSP12). The RPN4 transcription factor

stimulates expression of proteasome-associated genes and is transcriptionally regulated by various stress responses. Together, these results suggest that the 20 sensitive genes are involved in multiple processes including drug response, oxidative stress and proteasome function.

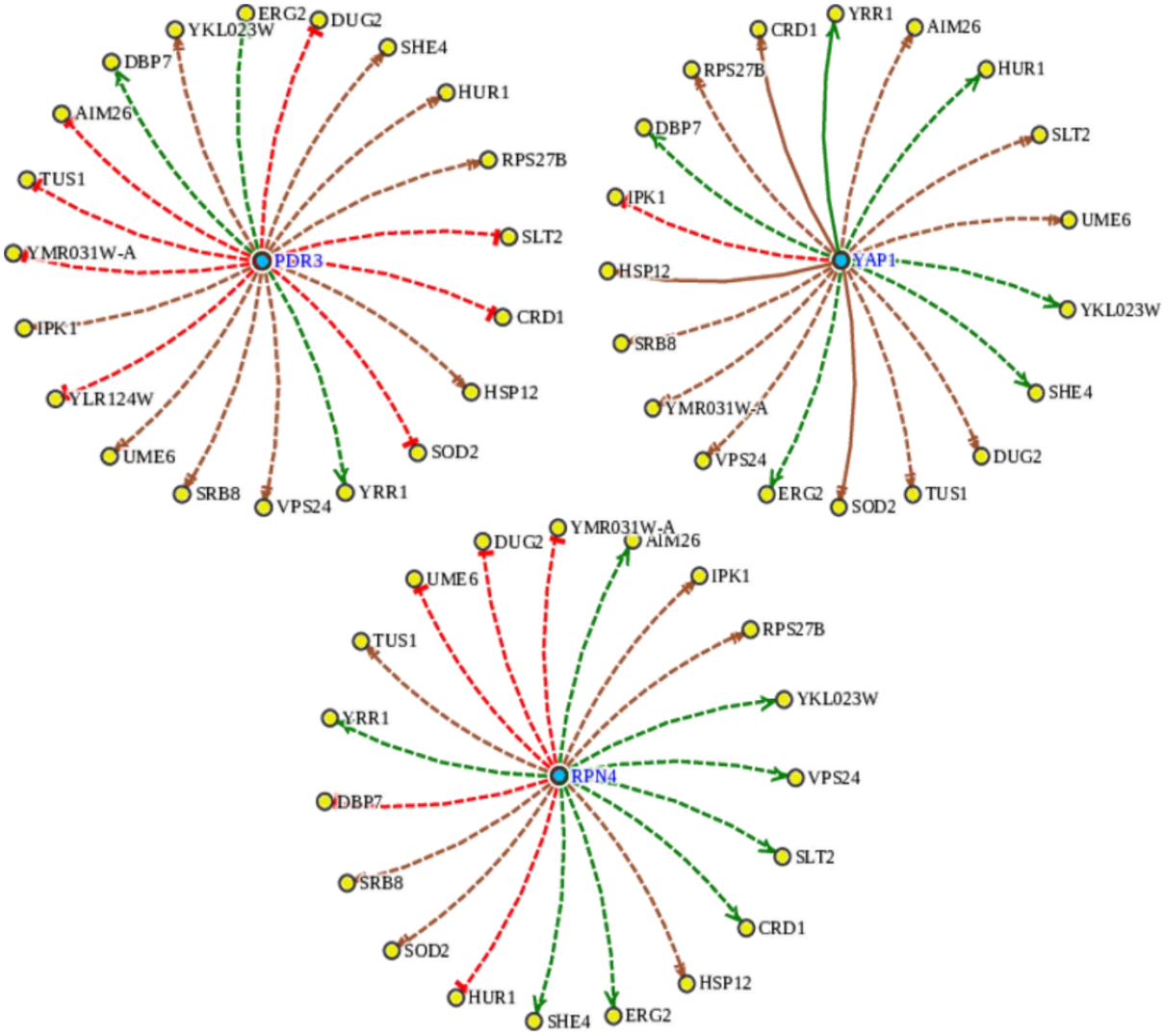

Figure 2.22: **Three transcription factors regulate most of the Ech A-sensitive genes.** Transcription factors association and their regulating genes were generated using Yeastract (Monteiro et al., 2020). Green arrows symbolize positive regulation, red arrows symbolize negative regulation and brown arrows symbolize both positive and negative regulation. Solid arrows symbolize supporting evidence through DNA binding and dashed arrows symbolize supporting evidence through expression only.

2.3.12 Over-representation of Ech A-sensitive gene deletion strains in the oxidative stress response

To determine if there was over-representation for any particular biological process or molecular function among the 20 genes sensitive to Ech A, enrichment analyses were conducted using the conventional algorithm and the text-mining algorithm implemented in YeastEnrichr (Kuleshov et al., 2016, 2019). For biological process, there was an over-representation in genes involved in the response to oxidative stress and response to other stress factors such as heat, salt and acids (Figure 2.23). Different enrichments were observed for molecular function, with over-representation for kinase activity using the text-mining algorithm and over-representation for functions involved in with RNA polymerase, DNA binding and kinase activity using the conventional GO enrichment algorithm.

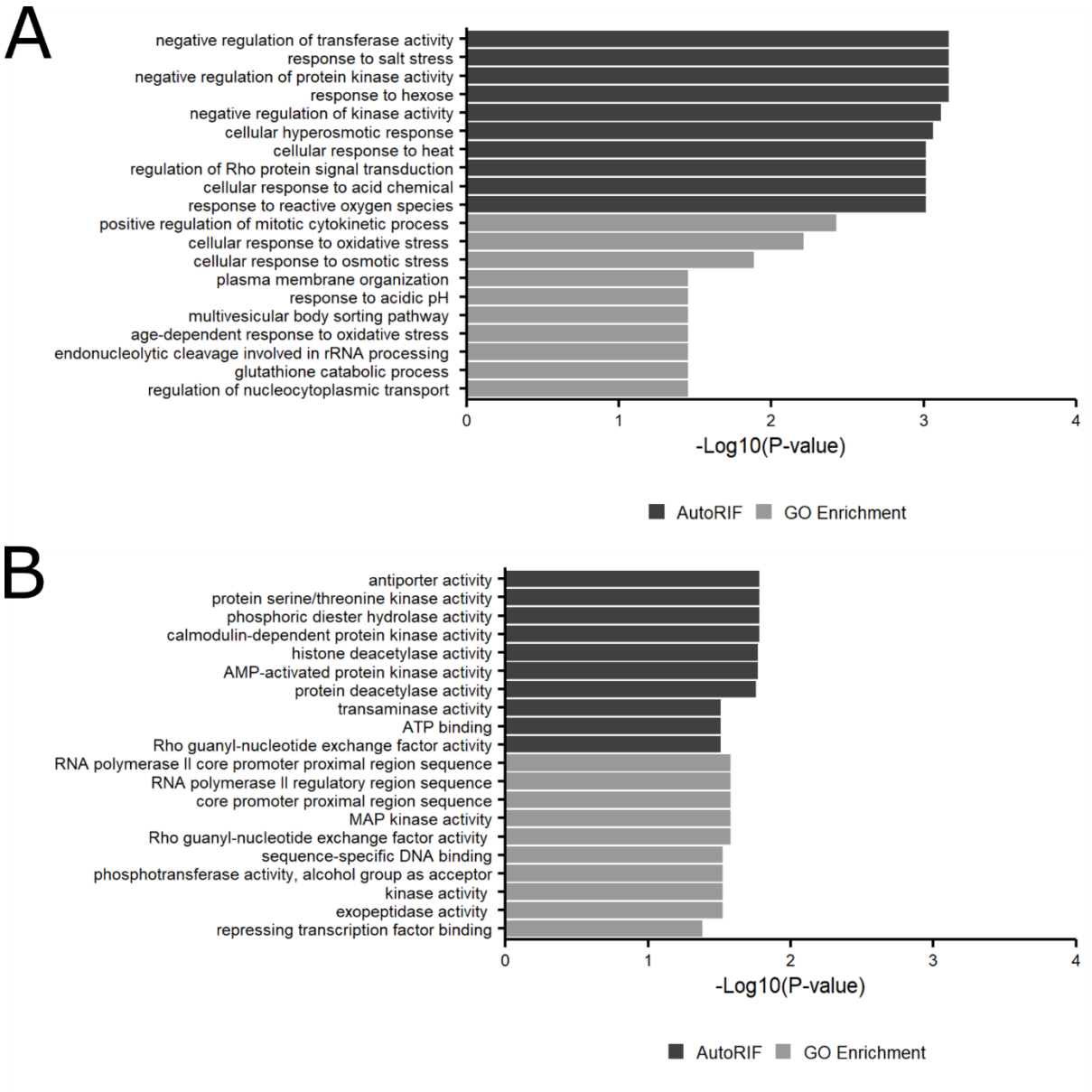

Figure 2.23: **Over-representation analysis of the 20 Ech A-sensitive gene deletion mutants reveals enrichment for oxidative stress.** Over-representation for **(A)** biological processes and **(B)** molecular functions was identified with two algorithms in YeastEnrichr (Kuleshov et al., 2016, 2019) including the conventional GO Enrichment algorithm and the text-mining AutoRIF algorithm. Statistical enrichments shown as a negative logarithm of the adjusted P value.

2.3.13 Ech A exhibits antioxidant activity

To further investigate the enrichment for oxidative stress, growth of Ech A-treated yeast was monitored in the presence and absence of a well-established oxidant (H_2O_2) used to increase the concentration of reactive oxygen species and induce oxidative stress. The wildtype strain (BY4741) was grown in the presence of normal SC media, 1 µg/ml Ech A, 1.5 mM H_2O_2, or co-treatment of Ech A + H_2O_2 with all treatments containing 1% ethanol. Ech A inhibited growth by 30% and H_2O_2 inhibited the growth by 50% (Figure 2.24). Growth was improved by 20% when Ech A and H_2O_2 were co-treated compared to the H_2O_2 treatment alone. These results suggest that Ech A acts as an antioxidant in the yeast model, and also that the gene deletion strains may be sensitive to Ech A via another mechanism.

Since the gene deletion strain *sod2*Δ exhibited sensitivity to Ech A (Figure 2.19) and this strain is known to be sensitive to H_2O_2 (Subramaniyan et al., 2019), we next sought to evaluate a co-treatment of Ech A and H_2O_2 in this strain. The concentrations used were the same concentrations as the wildtype assay with 1 µg/ml Ech A and 1.5 mM H_2O_2. *sod2*Δ was significantly more sensitive to both Ech A and H_2O_2 compared to wildtype ($P < 0.005$), with the Ech A having a growth percentage of 8% and H_2O_2 giving a growth percentage of 31% compared to the untreated control ($P < 0.005$) (Figure 2.24). The co-treatment did not improve the growth of *sod2*Δ compared to H_2O_2 as seen in wildtype, yet it did improve growth compared to the Ech A treatment. These results suggest that Ech A may have a different bioactivity in media with a higher concentration of ROS. Due to the sensitivity of *sod2*Δ to Ech A, a lower concentration of Ech A would need to be tested for antioxidant properties in Ech A-sensitive gene deletion strains such as *sod2*Δ. These results investigating the antioxidant properties of Ech A are preliminary and further experiments were unable to be completed due to time constraints of this thesis.

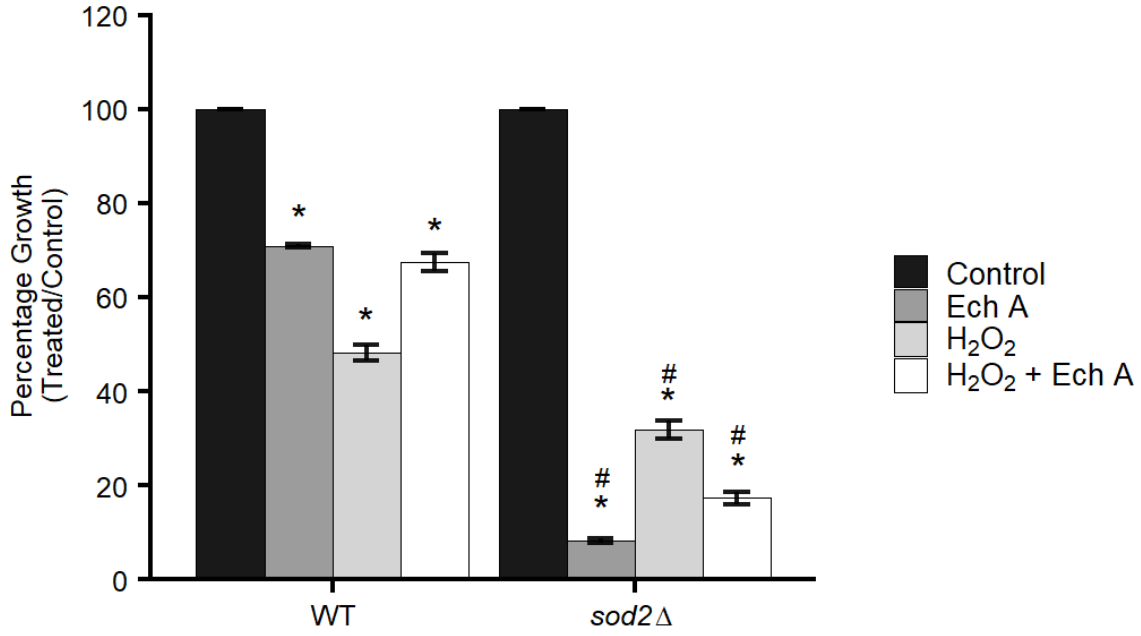

Figure 2.24: **Ech A exhibits antioxidant activity against hydrogen peroxide-induced oxidative stress.** Percentage growth of wildtype and *sod2*Δ grown with and without 1 µg/ml of Ech A and with and without 1.5 mM H_2O_2. Data shown as mean of technical triplicates ± SD; * $p \leq 0.05$ student's t-test comparing treated to the control); # $p \leq 0.05$ student's t-test comparing *sod2*Δ compared to wildtype.

2.3.14 Iron supplementation rescues growth defect in all gene deletion strains sensitive to Ech A

Growth rescue from Ech A treatment was observed with iron supplementation in wildtype. To determine if the iron rescue is exclusive to wildtype or can be seen with all or some of the sensitive gene deletion strains, an iron supplementation assay was performed on the 20 gene deletion strains sensitive to Ech A (Figure 2.25). Each strain was treated with either Ech A, 100 µM iron sulphate ($FeSO_4$) or co-treated with both Ech A and $FeSO_4$. Except for *slt2*Δ, *ume6*Δ, *dbp7*Δ, *dug2*Δ, *erg2*Δ and *hur1*Δ, all strains exhibited a significant increase in growth with iron supplementation. In contrast, *hsp12*Δ exhibited a significant decrease in growth when supplemented with iron. Regardless of how sensitive a gene deletion strain was

to Ech A, the iron supplementation completely rescued the growth of all strains. For example, *yrr1*Δ practically had no growth when treated with Ech A, and this strain had growth in the co-treatment that was not significantly different to the controls. These results indicate that iron depletion may be the contributing mechanism for these gene deletion strains being sensitive to Ech A.

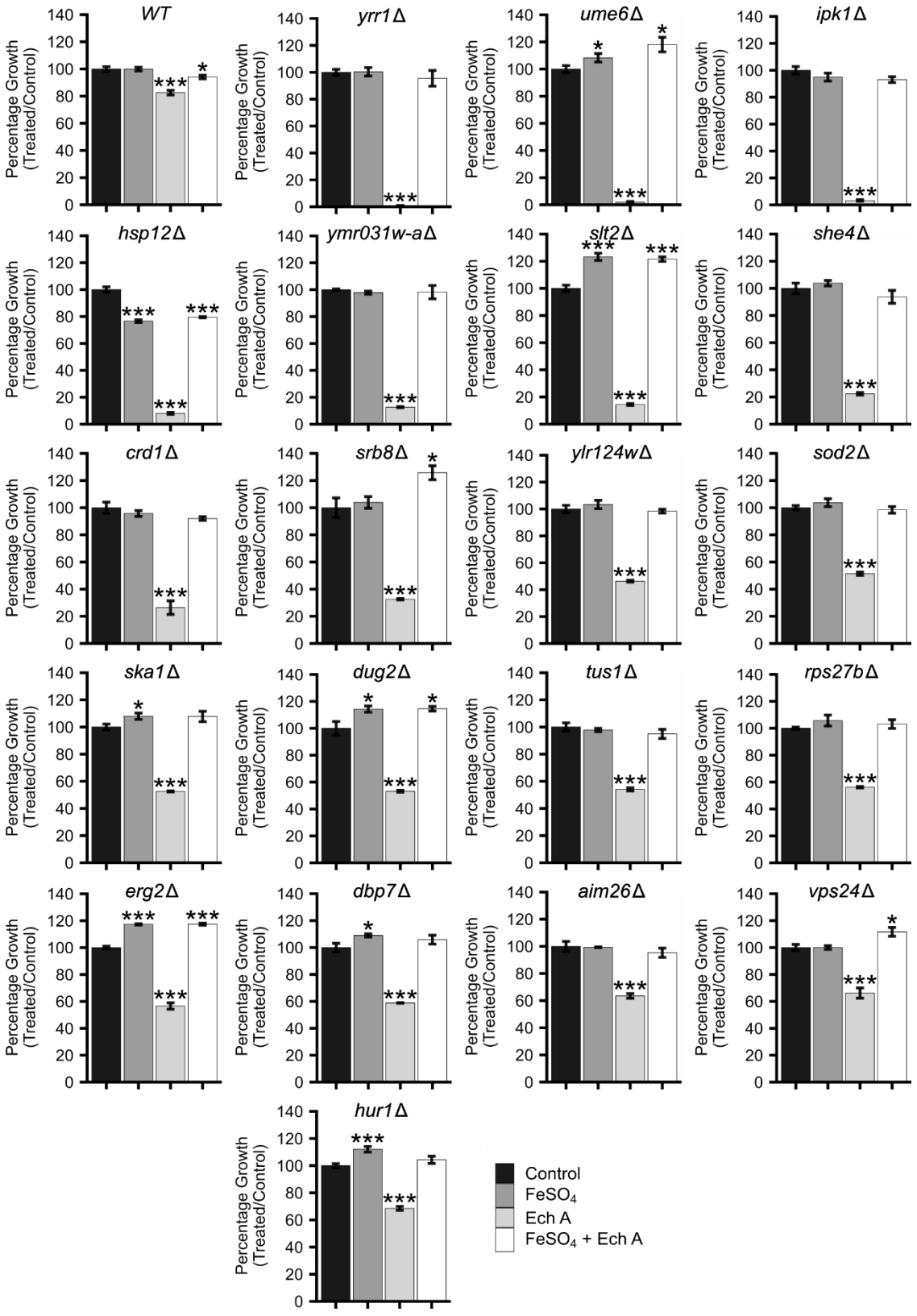

Figure 2.25: **Iron supplementation rescue is observed in every gene deletion strain**. Percentage growth of wildtype and Ech A-senstive gene deletion strains grown with and without 1 µg/ml of Ech A and with and without 100 µM of $FeSO_4$. Data shown as mean of technical triplicates ± SD; * $p \leq 0.05$, ** $p \leq 0.01$, *** $p \leq 0.005$ student's t-test comparing treated to the untreated control).

2.3.15 Deletion of most iron metabolism genes does not result in Ech A sensitivity

Since the proteomic screen revealed bioactivity for Ech A in the metabolism of metal ions, it was surprising that the screen of the gene deletion library did not identify gene deletions involved in the metabolism of metal ions. To determine whether this was an artifact of high-throughput analysis or an authentic result, serial dilutions of 9 gene deletion strains lacking metal ion metabolism genes and 3 gene deletion strains lacking multidrug transporter genes (three of the most significant protein abundance changes) were pinned onto SC media with either 7.5 µg/ml Ech A or 1% ethanol (Figure 2.26). Interestingly, only three gene deletion strains (*smf3*Δ, *tis11*Δ, and *snq2*Δ) showed greater sensitivity to Ech A compared to wildtype. *SMF3* is a metal ion transporter involved in iron homeostasis and *TIS11* is a mRNA-binding protein which is expressed during iron starvation (Cherry et al., 2012). *SNQ2* is a multidrug transporter located on the plasma membrane (Cherry et al., 2012). It can be concluded that these three genes are required for normal metabolism of Ech A.

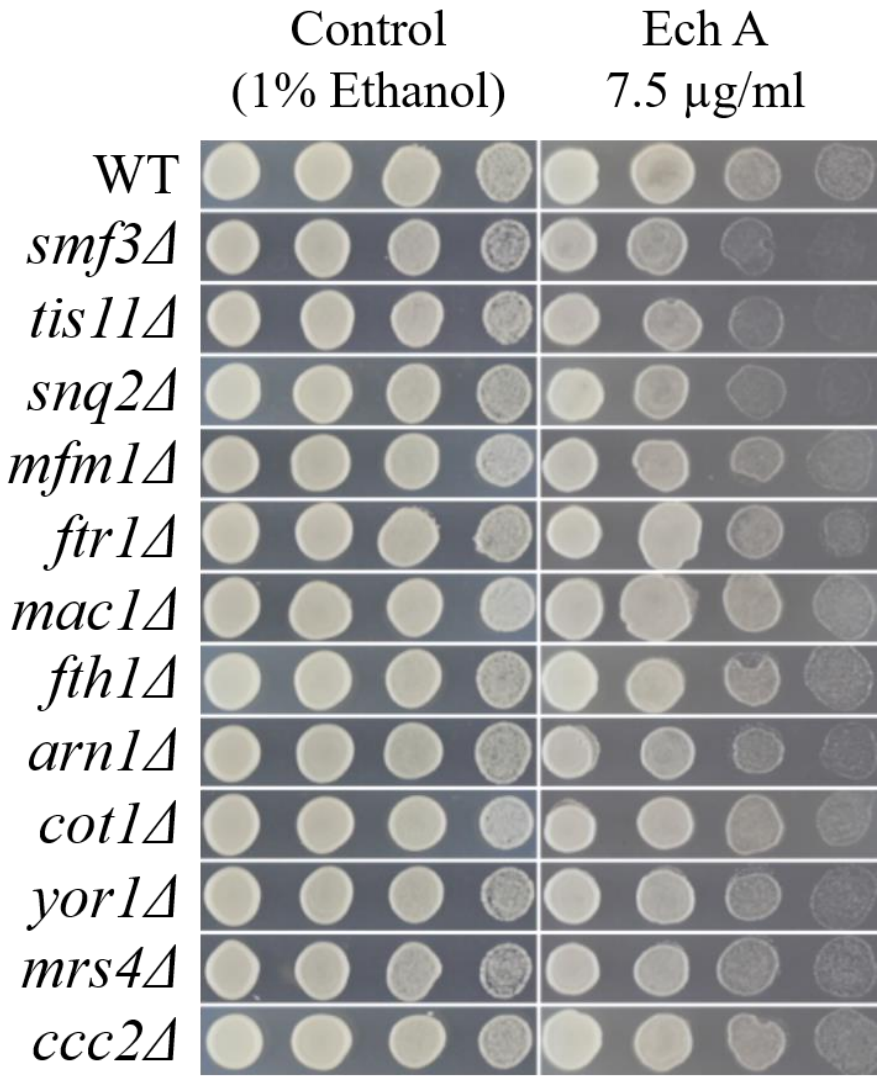

Figure 2.26: **Deletions of three genes that had a significant increase in protein abundance show growth sensitivity to Ech A.** Five-fold (left to right) spot dilutions of wildtype and gene deletion strains were pinned on SC agar with and without 7.5 µg/mL of Ech A, incubated at 30˚C, and imaged at 24 hours.

2.3.16 Thin-layer chromatography analysis to monitor cardiolipin metabolism in response to Ech A treatment

In the GFP proteomic screen, multiple proteins that had significant changes in protein abundance were localized in the mitochondria or were involved in mitochondrial functions (*e.g.*, the iron transporter MRS4 that transports Fe^{2+} across the inner mitochondrial membrane) (Figure 2.7). Likewise, one of the gene deletion strains that showed high sensitivity to Ech A was *crd1*Δ*;* CRD1 is a cardiolipin synthase required for the biosynthesis of cardiolipins that are an essential component of mitochondrial membranes critical for normal mitochondrial membrane potential and mitochondrial function (Cherry et al., 2012). To further investigate the connection of Ech A with cardiolipin, thin-layer chromatography (TLC) was conducted to isolate and evaluate the abundance of cardiolipin and other phospholipids (Figure 2.27). There was no visual difference in any phospholipid except cardiolipin. In Ech A-treated cells, there was an obvious band just above the cardiolipin standard and this increased in abundance with increasing concentration of Ech A. Unfortunately, the band overlapped with cardiolipin and was not possible to distinguish from cardiolipin. Due to the increasing abundance of the band as Ech A concentration increased, it is plausible that this band is either Ech A itself or a combination of Ech A binding to cardiolipin. I next performed a small, cell-free TLC where Ech A and the cardiolipin standard were examined (Figure 2.27). Ech A alone migrated just above the cardiolipin standard. Therefore, the enigmatic band in the TLC could be increasing amounts of Ech A still present in the extracted lipid solution. Unfortunately, this method was not suitable to measure cardiolipin metabolism in response to Ech A treatment.

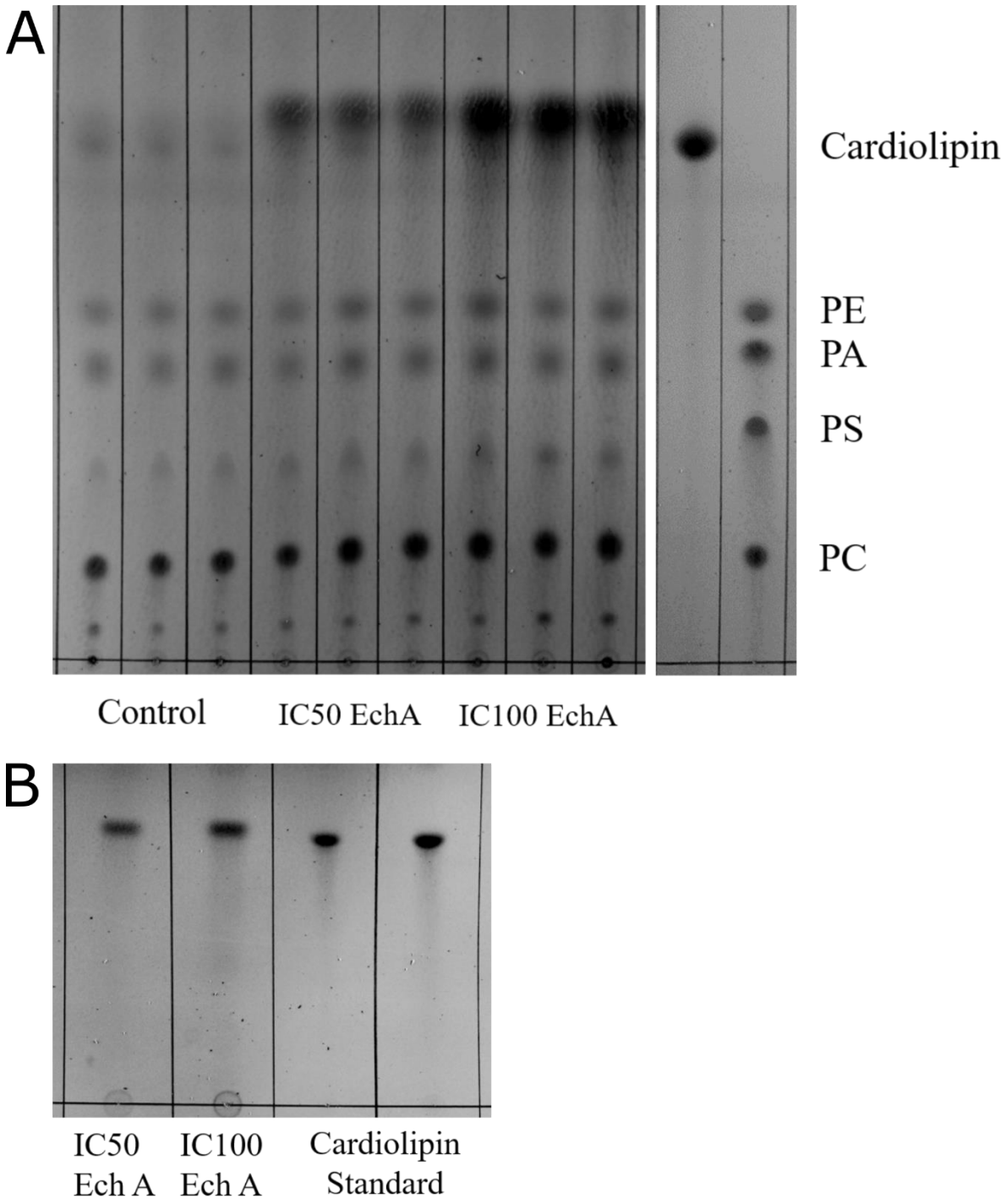

Figure 2.27: **Thin-layer chromatography analysis of cardiolipin and other phospholipids. (A)** Cellular phospholipids extracted from cells grown in the presence and absence of Ech A were spotted and run on a TLC sheet to separate cardiolipin, phosphatidylethanolamine (PE), phosphatidic acid (PA), phosphatidylserine (PS) and phosphatidylcholine (PC). Biological triplicates of each condition are shown. **(B)** Cell free phospholipid TLC with two concentrations of Ech A and a cardiolipin standard.

2.4 Discussion

2.4.1 Summary

Using *Saccharomyces cerevisiae*, unbiased genome wide genomic and proteomic level analysis tools provided further insight into the mode of action of Echinochrome A (Ech A); a compound extracted from the shells of New Zealand East Coast Kina. It was identified that 92 proteins had significant changes in protein abundance caused by Ech A treatment with an overall enrichment theme of specific changes in DNA replication, repair and RNA binding at 30 minutes, followed by metabolism of metal ions (specifically iron and copper) from 60-240 minutes. Further analysis indicated that Ech A chelates iron ions, and that supplementation with iron can negate the growth inhibition caused by Ech A in both wildtype and Ech A-sensitive gene deletion strains. Additionally, it was identified that 20 single gene deletion strains showed high sensitivity to Ech A, which were enriched in genes involved in the cell response to oxidative stress. However, when wildtype cells under oxidative stress (induced by H_2O_2) were treated with Ech A, there was a rescue of growth - suggesting that antioxidant properties were present in the yeast model. Further, similar to past literature investigating Ech A in mammalian models, there were a number of mitochondrial genes and proteins involved in the metabolism of Ech A. With the mitochondrial proteins having significant changes in protein abundance and the mitochondrial gene deletion strains such as *crd1Δ,* showed high sensitivity to Ech A.

2.4.2 Metal ion chelation

Iron is an essential metal that is involved in many important pathways that are required for regular cell function (Romero et al., 2020). Genes that showed a significant change in protein abundance caused by the treatment of Ech A were enriched in functions and processes involved in the metabolism of iron ions (Figure 2.11 – 2.12). These genes involved in the metabolism of iron ions had an up regulation of protein abundance and suggests that Ech A

alters iron ion availability to the cell. My results in protein abundance are consistent with previous gene expression data of yeast cells during iron deficiency (Romero et al., 2019). Supporting the hypothesis that Ech A is decreasing the availability of iron ions, resulting in an increase of protein abundance for genes involved in iron ion homeostasis. A rescue in growth was observed when exogenous iron was supplemented during Ech A treatment, further indicating that Ech A is altering the cellular iron levels available to cells by directly binding to iron ions and/or targeting iron metabolism genes (Figure 2.13). To analyze the potential of iron chelation properties, an iron chelation assay was performed; results suggested that Ech A can chelate iron at high levels, even more so than the well-established iron chelator, EDTA (Figure 2.14). This is seen at 5 µM where Ech A had a greater colour change compared to EDTA. However, the change of color may be due to the pale red color of Ech A, meaning this could be a false positive result. Nonetheless, past literature supports that Ech A chelates iron ions and has a high affinity to iron (Lebedev et al., 2005, 2008).

The spectrophotometric spectrum of Ech A is altered when ferrous iron is added, indicating that a formation of an iron-Ech A complex is possible - although the addition of EDTA did not restore the UV-visible spectrum of Ech A to the original state (Lebedev et al., 2005). This result further supports that Ech A can effectively bind iron and does so at a higher intensity than the positive control, EDTA. Iron is evenly distributed between Ech A and EDTA when ferrous iron is added to a mixture of the two compounds at molar ratio of 40:100 (Lebedev et al., 2005). These results suggest that a lower concentration of Ech A is needed to bind to the same amount of iron ions as EDTA.

The ability of iron chelation of Fe^{3+} and Fe^{2+} means Ech A can effectively inhibit the activity of the Haber-Weiss reaction, whereby superoxides ($O2^{\cdot-}$) convert Fe^{3+} to Fe^{2+}, and inhibit the Fenton reaction catalyzed by the iron ion Fe^{2+} converting H_2O_2 into hydroxyl radicals (•OH) (Ayala et al., 2014). Inhibiting these reactions results in a reduction of hydroxyl

radicals being produced and therefore can protect cells from lipid peroxidation. Lipid peroxidation is caused during oxidative stress where the free radicals such as hydroxyl radicals attack unsaturated lipids such as cardiolipins, resulting in oxidative damage due to loss of normal function to organelles such as the mitochondria, culminating in cell/tissue death (Ayala et al., 2014). Preventing lipid peroxidation via iron chelation has been investigated in livers of rats after ischemic stress (Omar et al., 1989). The presence of iron is a key catalyst for lipid peroxidation and deactivating the iron with the iron chelator deferoxamine significantly reduced lipid peroxidation. Treatments of the iron chelator occurred either before the induction of ischemia or before reperfusion, with both reducing the damage caused by lipid peroxidation (Omar et al., 1989). In humans, lipid peroxidation occurs during a cardiopulmonary bypass (CPB) where cells under ischemic stress become sources of free radicals once reoxygenated. The iron chelator, deferoxamine, inhibited the production of hydroxyl radicals, reduced lipid peroxidation and in turn protected cells against post ischemic reperfusion that otherwise damages the heart, lung, kidney and brain tissues (Menasché et al., 1990). This implies that Ech A could be a potential treatment as an iron chelator to reduce lipid peroxidation in humans during ischemic stress.

The deficiency of cellular iron triggers global changes in translation as organisms are dependent on iron as an essential redox co-factor in fundamental cellular processes such as DNA replication and repair, mRNA translation, cellular respiration, and oxygen transport (Romero et al., 2020). This may be the reason why protein abundance changes at the 30-minute timepoint involved DNA binding, replication and repair and mRNA binding, suggesting that these global changes in translation may occur during the first 30 minutes of Ech A treatment (Figure 2.11 – 2.12). This may mean that these proteins and their orthologues could be primary responders to iron deficiency in yeast and mammalian cells. Tis11 and Rad57 are the only two proteins that had a change in protein abundance which have a reported connection with iron

and with one of the enrichments at the 30-minute time point. *TIS11* is a mRNA-binding protein that is expressed during iron starvation, so having an increase of the Tis11 protein is expected if Ech A alters the concentration of available iron ions (Cherry et al., 2012). *RAD57* stabilizes the binding of Rad51 to single-stranded DNA and is involved in the recombinational repair of double-strand breaks of DNA during vegetative growth and meiosis (Cherry et al., 2012). Having an increase in the Rad57 protein was less expected. Interestingly, the gene deletion mutant *rad57*Δ has shown increased sensitivity to iron sulphate (Jo et al., 2008). Six other genes that resulted in the DNA replication/repair and RNA binding enrichments at the 30-minute timepoint, include the subunit of DNA polymerase delta, *POL32*, a component of the chromatin assembly complex, *CAC2*, the RNA exonuclease, *REX3*, the single-stranded DNA binding and annealing protein, *SLD2*, the gene essential for the modification of mitochondrial tRNAs, *QRI7*, and a kinetochore protein, *CNN1* (Cherry et al., 2012). The connection of these genes and iron homeostasis have not yet been reported which may suggest that they are novel links between DNA replication/repair and iron homeostasis.

No genes involved in the metabolism of iron ions that had an increase in protein abundance were Ech A-sensitive when the gene was deleted (Table 2.4). The only gene that is involved in iron homeostasis that showed Ech A-sensitivity but did not show a protein abundance change is the MAP kinase, *SLT2*, which is involved in the regulation of the transcription factor, *AFT1*, a gene responsible for the utilization and homeostasis of iron. The activation of *AFT1* is in response to changes in the iron availability (Pujol-Carrion et al., 2021). This result suggests that iron chelation is not the only mechanism of Ech A and other factors may play a role in Ech A-sensitivity in gene deletion strains. The naturally derived iron chelator tannic acid shows rescued growth of wildtype and tannic acid-sensitive mutant strains when treated cells are supplemented with iron (Pilc et al., 2021). The same trend was observed with every Ech A-sensitive gene deletion strains had a full rescue in growth percentage when iron

supplementation is performed (Figure 2.25). This result suggests the depletion of accessible iron maybe a causative factor for the Ech A-sensitivity in the gene deletion mutants.

The level of rescued growth observed with copper sulphate ($CuSO_4$) supplementation of Ech A-treated cells was similar to iron sulphate ($FeSO_4$) supplementation (Figure 2.15), suggesting involvement of both copper and iron in Ech A bioactivity. This link is strengthened with increased abundance of Ccc2, a transporter protein of iron and copper, in response to Ech A treatment. In fact, increased levels of Ccc2 were among the most dramatic changes with Ech A treatment (Figure 2.7) (Appendix Tables 3.1 – 3.3). These results suggest that Ech A interferes with copper metabolism as well as iron metabolism, and potentially binds to copper. This is supported by Kuzuya and colleagues, who investigated the relationship between Ech A and copper, and observed that the addition of copper resulted in an ultra-violet spectrum change consistent with binding copper (Kuzuya et al., 1973). Like iron, copper ions can also part take in the Fenton reaction, producing hydroxyl free radicals from H_2O_2. The family of superoxide dismutase proteins (SOD) plays an important role in the protection of cells against oxidative stress. Two distinct forms of SOD proteins are usually found in eukaryotes (Luk et al., 2005). SOD1 is a copper-dependent enzyme that is located in the cytosol and the intermembrane space of mitochondria, while SOD2 is a manganese-dependent enzyme that is only located in the mitochondrial matrix (Cherry et al., 2012; Luk et al., 2005). Interestingly, the deletion of SOD2 resulted in high sensitivity to Ech A compared to the wildtype (Figure 2.19). This sensitivity may be due to Ech A interfering with the concentration of copper ions, which in turn may cause a down regulation of the copper-dependent enzyme SOD1 activity. In essence, there may be a dramatic deficiency in superoxide dismutase activity with reduced SOD1 levels in the *sod2Δ* strain. The *sod1Δ* strain was not examined in this thesis as this strain is not part of the deletion mutant array library, hence further investigation into the sensitivity of this strain to Ech A will be needed to understand this mechanism. Overall, further investigation into the chelation of

copper ions is needed to determine if Ech A has a similar affinity to copper ions as it does with iron ions.

2.4.3 Antioxidant properties

Ech A has been previously established as an antioxidant in free radical scavenging assays in both *in vitro* and *in vivo* mammalian models (Jeong, Kim, Song, Noh, et al., 2014; Lebedev et al., 2005). Interestingly, yeast gene deletion strains and their regulating transcription factors that showed high sensitivity to Ech A were enriched for genes involved in the oxidative stress response (Figure 2.22 – 2.23). To further investigate the antioxidant properties of Ech A in yeast, cells were treated with H_2O_2 to increase the concentration of reactive oxygen species and treated with or without Ech A. In wildtype, a significant increase in percentage growth was observed in the co-treatment compared to H_2O_2 alone (Figure 2.24). These results suggest that similarly to mammalian models, Ech A exhibits antioxidant properties in the yeast model. However, a rescue was not observed in the Ech A-sensitive *sod2Δ* strain (Figure 2.24). Co-treatment showed an improved growth percentage compared to the Ech A treatment, but this growth improvement was still lower than the growth percentage of the H_2O_2 treatment. Due to the sensitivity of *sod2Δ* to Ech A, a lower concentration of Ech A may be needed to test for antioxidant properties in Ech A-sensitive gene deletion strains such as *sod2Δ*. Intriguingly, the natural polyphenol, magnolol, shows the opposite result when *sod2Δ* cells have been co-treated with H_2O_2 and magnolol. Magnolol significantly rescued the *sod2Δ* strain under oxidative stress (Subramaniyan et al., 2019). However, direct comparisons of the magnolol experiment in agar and my Ech A experiment in liquid cannot be made, as concentrations of H_2O_2 as well as growth medium were not the same.

Likewise, Ech A elicited antioxidant activity in pulmonary fibroblasts derived from rats when cells were treated with H_2O_2 (Sazonova et al., 2020). The negative effects specifically caused by oxidative stress, such as a decrease in DNA synthesis and ribosomal RNA synthesis, were corrected by the treatment of Ech A. However in the absence of H_2O_2, there was a decrease in levels of intracellular calcium ions due the decreased activity of calcium channels caused by Ech A treatment (Sazonova et al., 2020). This suggests that Ech A has different mechanisms depending on the environmental conditions (*e.g.*, with or without oxidative stress). This may have been observed in the Ech A-sensitive gene *sod2Δ* where there was an improvement in growth with co-treatment of Ech A and H_2O_2, compared to the Ech A alone. Although the mechanism by which Ech A exhibits antioxidant activity in yeast was not resolved in this thesis, future research could include a genome-wide analysis of the gene deletion library and/or a proteome-wide analysis of the GFP library, where in both cases the additional condition of oxidative stress is implemented.

Two antioxidant mechanisms, notably iron chelation and free radical scavenging have been reported to describe how Ech A protects cells from oxidative stress (Lebedev et al., 2005). Impressively, Ech A scavenged free radicals more potently than established antioxidants such as α-Tocopherol (Lebedev et al., 2005, 2008). More specifically, the ability to scavenge free radical species that are formed during oxidative stress protects cells from lipid peroxidation, thus it is plausible that Ech A could neutralize the hydroxyl radicals that are present with H_2O_2 treatment. This is seen with the anthraquinone derivatives isolated from the plant *Pediomelum cuspidatum*, where the antioxidant properties of these derivatives protected rat heart mitochondria from hydroxyl radicals produced by the iron-catalyzed Fenton reaction, resulting in the reduction lipid peroxidation (Huang et al., 1995). Hence it is plausible that Ech A may protect cells from free radicals that are already present in the cells, or alternatively, inhibit the production of new free radicals by chelating the iron ions that would normally catalyze the

Fenton reaction. This combination of free radical scavenging and iron chelation potentially make Ech A a better antioxidant than current established antioxidants.

It is thus understandable why Ech A is a key component of the therapeutic drug Histochrome that is currently approved in Russia. Histochrome has been used to treat patients who have suffered ischemic heart disease or a heart attack where there is an increase in free radical species that cause oxidative damage via lipid peroxidation (Mishchenko et al., 2003). Ischemic heart disease patients treated with Histochrome showed a decrease in concentration of the lipid peroxidation product, malonic dialdehyde, in serum compared to the control group (Mishchenko et al., 2003). Likewise, patients that have suffered from a heart attack that were treated with Histochrome showed a rapid reduction in tissue death by 55% relative to the control group (Mishchenko et al., 2003). My results investigating the antioxidant properties of Ech A in the yeast model are preliminary and further work is needed to determine the mechanisms behind the proposed antioxidant properties of Ech A.

2.4.4 Mitochondria and Ech A

A common theme throughout this thesis was the involvement of mitochondria in the metabolism of Ech A. This was seen in both the genome-wide chemical assays at the genetic level and the proteome-wide GFP assay at the protein level. Proteins involved in mitochondrial function or located in the mitochondria were increased in abundance when treated with Ech A and some gene deletion mutants that showed high sensitivity to Ech A were mitochondrial genes (Table 2.3 - 2.4). This theme aligns with previous literature showing Ech A increased mitochondrial function and mitochondrial mass (Jeong, Kim, Song, Noh, et al., 2014; Seo et al., 2015). Expression levels of mitochondrial biogenesis genes were upregulated in rat cardio myoblast cells treated with Ech A. Although the orthologous yeast proteins were not

upregulated in this thesis that measured protein abundance, it is clear the general mechanism of mitochondrial function is integral to Ech A bioactivity in yeast (i.e., same pathway, different genes/proteins).

The mitochondrial proteins in yeast that did show a significant change in abundance are involved in metal ion metabolism (specifically iron ions), tRNA wobble and oxidative stress (Table 2.3). This result may be exclusive to the yeast model, albeit it is also possible that other studies have not examined all of these functions in one publication. In addition to altered abundance of mitochondrial proteins, deletion of mitochondrial genes resulted in high sensitivity to Ech A. Notably, the most sensitive mitochondrial gene was the cardiolipin synthase (*CRD1*). *CRD1* is integral to the synthesis of cardiolipins, required for mitochondrial membrane function and mitochondrial membrane potential, and is a key phospholipid species in the mitochondrial membrane (Cherry et al., 2012; Malina et al., 2018). Reactive oxygen species are harmful to unsaturated lipids such as cardiolipin, resulting in lipid peroxidation and decreasing the mitochondrial membrane potential. This damage was reversed with Ech A treatment in rat cardio myoblast cells via reduced ROS levels and recovery of the mitochondrial membrane potential (Jeong, Kim, Song, Noh, et al., 2014). Our results pinpointing cardiolipin to Ech A bioactivity in yeast suggest cardiolipin may be a part of the therapeutic mechanism already observed in mammalian cells.

As the role for cardiolipin in Ech A bioactivity was not known prior to this thesis, I attempted to characterize this mechanism by monitoring cardiolipin levels in response to Ech A treatment. Thin-layer chromatography analysis of cardiolipin resulted in an enigmatic finding where a band that migrates to the region of the cardiolipin standard increased in size as Ech A concentration increased (Figure 2.27). However, this band was also present in a cell-free assay, revealing that Ech A migrates just above cardiolipin (Figure 2.27). Therefore, the band increasing in size was likely Ech A; and thin-layer chromatography was not a suitable

method of measuring cardiolipin abundance in response to Ech A treatment. As this thesis determined CRD1 to be an important gene for buffering Ech A bioactivity (based on sensitivity of the *crd1Δ* strain), it would be interesting to measure the importance of other cardiolipin synthase genes to Ech A bioactivity. PGS1 is a rate-limiting step of cardiolipin biosynthesis upstream of CRD1 and the catalyst in the conversion of CDP-diacylglycerol to phosphatidylglycerolphosphate (Malina et al., 2018). TAZ1 catalyses the acylation of monolysocardiolipin with unsaturated fatty acids downstream of CRD1 (Malina et al., 2018). Unfortunately, the *pgs1Δ* strain is not included in the gene deletion library. Interestingly, the *taz1Δ* strain was sensitive to Ech A in the initial genome-wide analysis, but this sensitivity did not repeat during the validation spot dilutions on agar. As liquid growth assays can be more sensitive than agar growth assays, future investigation of *taz1Δ* sensitivity to Ech A in liquid will provide a better understanding of this mechanism and the effects of Ech A on cardiolipin metabolism.

The Ech A-treated *ipk1Δ* strain showed one of the highest sensitivities of the 4,800 deletion strains with practically no growth compared to untreated cells (Figure 2.19). *IPK1* is an inositol 1,3,4,5,6-pentakisphosphate 2-kinase, that is required for the synthesis of phytate that is integral to cell function (Cherry et al., 2012; Zhu et al., 2020). Interestingly, phytate is a natural metal ion chelator and binds to zinc, iron and calcium. Phytate is generally found in high concentrations in lower-income plant based diets, resulting in a deficiency of zinc, iron and calcium (Gibson et al., 2010). The deletion of *IPK1* causes dysfunction to the mitochondria via compromised mitochondrial respiratory chain complexes, depolarization of mitochondrial membrane potential, reduced ATP synthesis and mitochondrial structural abnormalities (Zhu et al., 2020). These changes may be the reasons why we see dramatic sensitivity of the *ipk1Δ* strain to Ech A, as the loss of normal mitochondrial function renders the cells more susceptible to stress. Further assays to measure mitochondrial membrane potential and the abundance of

cardiolipin will be needed to investigate these phenotypes and provide further insight into the importance of IPK1 and CRD1 in the metabolism of Ech A.

2.5 Future directions

2.5.1 Changes in protein localization mediating Ech A bioactivity

Protein abundance changes mediating Ech A bioactivity were investigated in this thesis and now using the same images from the high-throughput time-lapse microscopy, machine learning can be used to assign localizations to proteins in treated and untreated cells at each time point. The Res18 convolutional neural network (CNN) will be used as it has been reported to have the best results for training and accurately assigning localization of yeast proteins (Xiao et al., 2019). The machine learning system will be trained with thousands of individual cell images that will be manually assigned into 18 different localizations. Proteins with altered localization will likely be fundamental to Ech A bioactivity and provide insight in addition to that already determined in this thesis.

2.5.2 Investigating potential binding of multiple metals

My thesis identified that Ech A interacts with metal ions (specifically iron and copper), as proteins involved in the metabolism of metal ions increased in abundance in the presence of Ech A, and in addition, metal supplementation rescued growth defects from Ech A treatment. Understanding the affinity of metal ions to Ech A (specifically iron and copper) is essential to understand the effect of Ech A on cellular functions. Using electrospray-based metabolomics (Aron et al., 2019), it will be possible to identify which metal ions bind to Ech A and quantify the binding of each metal ion to Ech A to determine which metal has the greatest affinity to Ech A.

2.5.3 Antioxidant ROS staining via flow cytometry and imaging

This thesis demonstrated the potential for Ech A to reduce levels of reactive oxygen species (ROS) in yeast, although this was not directly measured in this thesis. The stain 2′,7′-dichlorofluorescin diacetate (DCFDA) is cleaved by ROS to produce a green fluorescence (Eruslanov & Kusmartsev, 2010; Subhaswaraj et al., 2017). Using flow cytometry to quantify ROS levels, we can accurately quantify ROS levels increased with H_2O_2 and potentially reduced with Ech A. In addition, yeast genes identified in this thesis that are predicted to be involved in antioxidant activity can be evaluated using gene deletion strains. These results will provide insight the molecular basis of antioxidant properties that have been observed in my thesis in yeast and reported in the literature in mammalian cells.

2.5.4 Mitochondrial analysis

To investigate the relationship of Ech A and mitochondria in yeast, it would be worth investigating the effect that Ech A has on the mitochondria and the mitochondrial membrane potential. By using the green fluorescent stain rhodamine 123, we can visualize changes in mitochondrial membrane potential and mitochondrial respiratory function (Kwolek-Mirek & Zadrag-Tecza, 2014; Ludovico et al., 2001). Using wildtype, and the gene deletions mutants *crd1Δ, taz1Δ* and *pgs1Δ* this assay would provide insight into the importance of cardiolipins in the metabolism of Ech A. To investigate the effect Ech A has on mitochondria, the stain MitoTracker-Red can be used (Oxelmark et al., 2000). MitoTracker-Red is a fluorescent dye that stains mitochondria and will provide insight into the number of mitochondria and determine if the phenotype with an increase in mitochondria biogenesis in mammalian models will be observed in yeast.

2.5.5 Pleiotropic drug response-deficient (*pdr1Δpdr3Δ*) library

The Ech A-sensitive gene deletion strains were regulated by the transcription factors PDR3, YAP1 and RPN4, which are all active during various stress responses. Also, there were a number of proteins increased in abundance that were involved in the cell's drug response. The deletion of the transcription factors PDR1 and PDR3 results in compromised drug efflux pumps involved in the pleiotropic drug response, whereby cells are unable to pump out drugs that enter (Coorey et al., 2015). Using a gene deletion library in the *pdr1Δpdr3Δ* genetic background (Coorey et al., 2015), sensitive genes and their associated pathways will be identified to provide further insight into the molecular basis of Ech A bioactivity.

2.6 Conclusion

To conclude, this thesis provided further insight into the molecular mechanisms of Ech A using the proteomic and genomic tools available to *S. cerevisiae* (yeast). 92 proteins were identified to have significant changes in abundance due to Ech A treatment, with an overall enrichment theme of specific changes in DNA replication, repair and RNA binding at 30 minutes, followed by metabolism of metal ions (specifically iron and copper) from 60-240 minutes. Further investigation identified iron chelation as a key causative factor for Ech A-sensitivity. Ech A was also identified to exhibit antioxidant properties in the yeast cells under oxidative stress. This combination of iron chelation and antioxidant properties of Ech A suggest it could be a highly efficient drug to treat lipid peroxidation which occurs during ischemic heart disease and heart attacks. Mitochondrial genes and proteins were also identified throughout my thesis, which specifically contribute an additional level of detail to help explain previous literature reporting mitochondria are involved in the metabolism of Ech A.

2.6 References

Alexander, D. B., & Zuberer, D. A. (1991). Use of chrome azurol S reagents to evaluate siderophore production by rhizosphere bacteria. *Biology and Fertility of Soils*, *12*(1), 39–45. https://doi.org/10.1007/BF00369386

Amberg, D. C., Burke, D. J., Burke, D., & Strathern, J. N. (2005). *Methods in Yeast Genetics: A Cold Spring Harbor Laboratory Course Manual*. https://books.google.com.au/books?id=47zspjkKkCwC&printsec=frontcover&dq=Amberg,+DC.;+Burke,+DJ.+and+Strathern,+JN.+(2005).+Methods+in+Yeast+Genetics&hl=en&sa=X&ved=0ahUKEwiD377SoOXiAhXy63MBHYaKDrAQ6AEIRjAG#v=onepage&q&f=false

Aron, A., Petras, D., Schmid, R., Gauglitz, J. M., Büttel, I., Antelo, L., Zhi, H., Saak, C. C., Malarney, K. P., Thines, E., Dutton, R. J., Raffatellu, M., & Dorrestein, P. C. (2019). Native electrospray-based metabolomics enables the detection of metal-binding compounds. In *bioRxiv* (p. 824888). bioRxiv. https://doi.org/10.1101/824888

Ayala, A., Muñoz, M. F., & Argüelles, S. (2014). Lipid peroxidation: Production, metabolism, and signaling mechanisms of malondialdehyde and 4-hydroxy-2-nonenal. In *Oxidative Medicine and Cellular Longevity* (Vol. 2014). Landes Bioscience. https://doi.org/10.1155/2014/360438

Bircham, P. W., Maass, D. R., Roberts, C. A., Kiew, P. Y., Low, Y. S., Yegambaram, M., Matthews, J., Jack, C. A., & Atkinson, P. H. (2011). Secretory pathway genes assessed by high-throughput microscopy and synthetic genetic array analysis. *Molecular BioSystems*, *7*(9), 2589–2598. https://doi.org/10.1039/c1mb05175j

Blunt, J. W., Copp, B. R., Keyzers, R. A., Munro, M. H. G., & Prinsep, M. R. (2016). Marine natural products. In *Natural Product Reports* (Vol. 33, Issue 3, pp. 382–431). Royal Society of Chemistry. https://doi.org/10.1039/c5np00156k

Boone, C., Bussey, H., & Andrews, B. J. (2007). Exploring genetic interactions and networks with yeast. In *Nature Reviews Genetics* (Vol. 8, Issue 6, pp. 437–449). Nature Publishing Group. https://doi.org/10.1038/nrg2085

Botstein, D., & Fink, G. R. (2011). Yeast: An Experimental Organism for 21st Century Biology. *Genetics*, *189*(3), 695–704. https://doi.org/10.1534/genetics.111.130765

Carroll, A. R., Copp, B. R., Davis, R. A., Keyzers, R. A., & Prinsep, M. R. (2019). Marine natural products. In *Natural Product Reports* (Vol. 36, Issue 1, pp. 122–173). Royal Society of Chemistry. https://doi.org/10.1039/c8np00092a

Cherry, J. M., Hong, E. L., Amundsen, C., Balakrishnan, R., Binkley, G., Chan, E. T., Christie, K. R., Costanzo, M. C., Dwight, S. S., Engel, S. R., Fisk, D. G., Hirschman, J. E., Hitz, B. C., Karra, K., Krieger, C. J., Miyasato, S. R., Nash, R. S., Park, J., Skrzypek, M. S., … Wong, E. D. (2012). Saccharomyces Genome Database: the genomics resource of budding yeast. *Nucleic Acids Research*, *40*(D1), D700–D705. https://doi.org/10.1093/nar/gkr1029

Chong, Y. T., Koh, J. L. Y., Friesen, H., Duffy, K., Cox, M. J., Moses, A., Moffat, J., Boone, C., & Andrews, B. J. (2015). Yeast proteome dynamics from single cell imaging and automated analysis. *Cell*, *161*(6), 1413–1424. https://doi.org/10.1016/j.cell.2015.04.051

Coorey, N. V. C., Matthews, J. H., Bellows, D. S., & Atkinson, P. H. (2015). Pleiotropic

drug-resistance attenuated genomic library improves elucidation of drug mechanisms. *Molecular BioSystems*, *11*(11), 3129–3136. https://doi.org/10.1039/c5mb00406c

Dias, D. A., Urban, S., & Roessner, U. (2012). A Historical overview of natural products in drug discovery. In *Metabolites* (Vol. 2, Issue 2, pp. 303–336). MDPI AG. https://doi.org/10.3390/metabo2020303

El-Demerdash, A., Atanasov, A. G., Horbanczuk, O. K., Tammam, M. A., Abdel-Mogib, M., Hooper, J. N. A., Sekeroglu, N., Al-Mourabit, A., & Kijjoa, A. (2019). Chemical diversity and biological activities of marine sponges of the genus Suberea: A systematic review. In *Marine Drugs* (Vol. 17, Issue 2). MDPI AG. https://doi.org/10.3390/md17020115

Eruslanov, E., & Kusmartsev, S. (2010). Identification of ROS using oxidized DCFDA and flow-cytometry. *Methods in Molecular Biology*, *594*, 57–72. https://doi.org/10.1007/978-1-60761-411-1_4

Ferrero, M. E. (2016). Rationale for the Successful Management of EDTA Chelation Therapy in Human Burden by Toxic Metals. In *BioMed Research International* (Vol. 2016). Hindawi Limited. https://doi.org/10.1155/2016/8274504

Foury, F. (1997). Human genetic diseases: a cross-talk between man and yeast. *Gene*, *195*(1), 1–10. http://www.ncbi.nlm.nih.gov/pubmed/9300813

Giaever, G., Chu, A. M., Ni, L., Connelly, C., Riles, L., Véronneau, S., Dow, S., Lucau-Danila, A., Anderson, K., André, B., Arkin, A. P., Astromoff, A., El Bakkoury, M., Bangham, R., Benito, R., Brachat, S., Campanaro, S., Curtiss, M., Davis, K., … Johnston, M. (2002). Functional profiling of the Saccharomyces cerevisiae genome. *Nature*, *418*(6896), 387–391. https://doi.org/10.1038/nature00935

Giaever, G., Flaherty, P., Kumm, J., Proctor, M., Nislow, C., Jaramillo, D. F., Chu, A. M., Jordan, M. I., Arkin, A. P., & Davis, R. W. (2004). Chemogenomic profiling: Identifying the functional interactions of small molecules in yeast. *Proceedings of the National Academy of Sciences of the United States of America*, *101*(3), 793–798. https://doi.org/10.1073/pnas.0307490100

Gibson, R. S., Bailey, K. B., Gibbs, M., & Ferguson, E. L. (2010). A review of phytate, iron, zinc, and calcium concentrations in plant-based complementary foods used in low-income countries and implications for bioavailability. In *Food and Nutrition Bulletin* (Vol. 31, Issue 2 SUPPL.). United Nations University Press. https://doi.org/10.1177/15648265100312s206

Goffeau, A., Barrell, B. G., Bussey, H., Davis, R. W., Dujon, B., Feldmann, H., Galibert, F., Hoheisel, J. D., Jacq, C., Johnston, M., Louis, E. J., Mewes, H. W., Murakami, Y., Philippsen, P., Tettelin, H., & Oliver, S. G. (1996). Life with 6000 genes. *Science (New York, N.Y.)*, *274*(5287), 546, 563–567. http://www.ncbi.nlm.nih.gov/pubmed/8849441

Haefner, B. (2003). Drugs from the deep: Marine natural products as drug candidates. In *Drug Discovery Today* (Vol. 8, Issue 12, pp. 536–544). Drug Discov Today. https://doi.org/10.1016/S1359-6446(03)02713-2

Harrison, R. K. (2016). Phase II and phase III failures: 2013–2015. *Nature Reviews Drug Discovery*, *15*(12), 817–818. https://doi.org/10.1038/nrd.2016.184

Hillenmeyer, M. E., Ericson, E., Davis, R. W., Nislow, C., Koller, D., & Giaever, G. (2010).

Systematic analysis of genome-wide fitness data in yeast reveals novel gene function and drug action. *Genome Biology*, *11*(3), R30. https://doi.org/10.1186/gb-2010-11-3-r30

Hoffman, C. S., & Winston, F. (1987). A ten-minute DNA preparation from yeast efficiently releases autonomous plasmids for transformaion of Escherichia coli. *Gene*, *57*(2–3), 267–272. https://doi.org/10.1016/0378-1119(87)90131-4

Hou, Y., Vasileva, E. A., Mishchenko, N. P., Carne, A., McConnell, M., & Bekhit, A. E. D. A. (2019). Extraction, structural characterization and stability of polyhydroxylated naphthoquinones from shell and spine of New Zealand sea urchin (Evechinus chloroticus). *Food Chemistry*, *272*, 379–387. https://doi.org/10.1016/j.foodchem.2018.08.046

Huang, S. S., Yeh, S. F., & Hong, C. Y. (1995). Effect of anthraquinone derivatives on lipid peroxidation in rat heart mitochondria: Structure-activity relationship. *Journal of Natural Products*, *58*(9), 1365–1371. https://doi.org/10.1021/np50123a005

Hughes, J. P., Rees, S. S., Kalindjian, S. B., & Philpott, K. L. (2011). Principles of early drug discovery. In *British Journal of Pharmacology* (Vol. 162, Issue 6, pp. 1239–1249). Br J Pharmacol. https://doi.org/10.1111/j.1476-5381.2010.01127.x

Huh, W. K., Falvo, J. V., Gerke, L. C., Carroll, A. S., Howson, R. W., Weissman, J. S., & O'Shea, E. K. (2003). Global analysis of protein localization in budding yeast. *Nature*, *425*(6959), 686–691. https://doi.org/10.1038/nature02026

Jeong, S. H., Kim, H. K., Song, I. S., Lee, S. J., Ko, K. S., Rhee, B. D., Kim, N., Mishchenko, N. P., Fedoryev, S. A., Stonik, V. A., & Han, J. (2014). Echinochrome a protects mitochondrial function in cardiomyocytes against cardiotoxic drugs. *Marine Drugs*, *12*(5), 2922–2936. https://doi.org/10.3390/md12052922

Jeong, S. H., Kim, H. K., Song, I. S., Noh, S. J., Marquez, J., Ko, K. S., Rhee, B. D., Kim, N., Mishchenko, N. P., Fedoreyev, S. A., Stonik, V. A., & Han, J. (2014). Echinochrome a increases mitochondrial mass and function by modulating mitochondrial biogenesis regulatory genes. *Marine Drugs*, *12*(8), 4602–4615. https://doi.org/10.3390/md12084602

Jo, W. J., Loguinov, A., Chang, M., Wintz, H., Nislow, C., Arkin, A. P., Giaever, G., & Vulpe, C. D. (2008). Identification of Genes Involved in the Toxic Response of Saccharomyces cerevisiae against Iron and Copper Overload by Parallel Analysis of Deletion Mutants. *Toxicological Sciences*, *101*(1), 140–151. https://doi.org/10.1093/toxsci/kfm226

Kim, S., Chen, J., Cheng, T., Gindulyte, A., He, J., He, S., Li, Q., Shoemaker, B. A., Thiessen, P. A., Yu, B., Zaslavsky, L., Zhang, J., & Bolton, E. E. (2021). PubChem in 2021: new data content and improved web interfaces. *Nucleic Acids Research*, *49*. https://doi.org/10.1093/nar/gkaa971

Knittelfelder, O. L., & Kohlwein, S. D. (2017). Thin-layer chromatography to separate phospholipids and neutral lipids from yeast. *Cold Spring Harbor Protocols*, *2017*(5), 412–415. https://doi.org/10.1101/pdb.prot085456

Koehn, F. E., & Carter, G. T. (2005). The evolving role of natural products in drug discovery. In *Nature Reviews Drug Discovery* (Vol. 4, Issue 3, pp. 206–220). Nature Publishing Group. https://doi.org/10.1038/nrd1657

Kraus, O. Z., Grys, B. T., Ba, J., Chong, Y., Frey, B. J., Boone, C., & Andrews, B. J. (2017). Automated analysis of high-content microscopy data with deep learning. *Molecular Systems Biology*, *13*(4), 924. https://doi.org/10.15252/msb.20177551

Kuleshov, M. V., Diaz, J. E. L., Flamholz, Z. N., Keenan, A. B., Lachmann, A., Wojciechowicz, M. L., Cagan, R. L., & Ma'ayan, A. (2019). ModEnrichr: A suite of gene set enrichment analysis tools for model organisms. *Nucleic Acids Research*, *47*(W1), W183–W190. https://doi.org/10.1093/nar/gkz347

Kuleshov, M. V., Jones, M. R., Rouillard, A. D., Fernandez, N. F., Duan, Q., Wang, Z., Koplev, S., Jenkins, S. L., Jagodnik, K. M., Lachmann, A., McDermott, M. G., Monteiro, C. D., Gundersen, G. W., & Ma'ayan, A. (2016). Enrichr: a comprehensive gene set enrichment analysis web server 2016 update. *Nucleic Acids Research*, *44*(W1), W90–W97. https://doi.org/10.1093/nar/gkw377

Kuzuya, H., Ikuta, K., & Nagatsu, T. (1973). Inhibition of dopamine-β-hydroxylase by spinochrome A and echinochrome A, naphthoquinone pigments of echinoids. *Biochemical Pharmacology*, *22*(21), 2772–2774. https://doi.org/10.1016/0006-2952(73)90140-8

Kwolek-Mirek, M., & Zadrag-Tecza, R. (2014). Comparison of methods used for assessing the viability and vitality of yeast cells. *FEMS Yeast Research*, *14*(7), 1068–1079. https://doi.org/10.1111/1567-1364.12202

Lebedev, A. V., Ivanova, M. V., & Levitsky, D. O. (2005). Echinochrome, a naturally occurring iron chelator and free radical scavenger in artificial and natural membrane systems. *Life Sciences*, *76*(8), 863–875. https://doi.org/10.1016/j.lfs.2004.10.007

Lebedev, A. V., Ivanova, M. V., & Levitsky, D. O. (2008). Iron chelators and free radical scavengers in naturally occurring polyhydroxylated 1,4-naphthoquinones. *Hemoglobin*, *32*(1–2), 165–179. https://doi.org/10.1080/03630260701700017

Lopez, A., Parsons, A. B., Nislow, C., Giaever, G., & Boone, C. (2008). Chemical-genetic approaches for exploring the mode of action of natural products. In *Progress in Drug Research* (Vol. 66, pp. 237–271). Birkhauser Verlag Basel. https://doi.org/10.1007/978-3-7643-8595-8_5

Ludovico, P., Sansonetty, F., & Côrte-Real, M. (2001). Assessment of mitochondrial membrane potential in yeast cell populations by flow cytometry. *Microbiology*, *147*(12), 3335–3343. https://doi.org/10.1099/00221287-147-12-3335

Luk, E., Yang, M., Jensen, L. T., Bourbonnais, Y., & Culotta, V. C. (2005). Manganese activation of superoxide dismutase 2 in the mitochondria of Saccharomyces cerevisiae. *Journal of Biological Chemistry*, *280*(24), 22715–22720. https://doi.org/10.1074/jbc.M504257200

Lum, P. Y., Armour, C. D., Stepaniants, S. B., Cavet, G., Wolf, M. K., Butler, J. S., Hinshaw, J. C., Garnier, P., Prestwich, G. D., Leonardson, A., Garrett-Engele, P., Rush, C. M., Bard, M., Schimmack, G., Phillips, J. W., Roberts, C. J., & Shoemaker, D. D. (2004). Discovering Modes of Action for Therapeutic Compounds Using a Genome-Wide Screen of Yeast Heterozygotes. *Cell*, *116*(1), 121–137. https://doi.org/10.1016/S0092-8674(03)01035-3

Malina, C., Larsson, C., & Nielsen, J. (2018). Yeast mitochondria: An overview of mitochondrial biology and the potential of mitochondrial systems biology. In *FEMS*

Yeast Research (Vol. 18, Issue 5, p. 40). Oxford University Press. https://doi.org/10.1093/femsyr/foy040

Malve, H. (2016). Exploring the ocean for new drug developments: Marine pharmacology. *Journal of Pharmacy and Bioallied Sciences*, *8*(2), 83. https://doi.org/10.4103/0975-7406.171700

Martins, A., Vieira, H., Gaspar, H., & Santos, S. (2014). Marketed marine natural products in the pharmaceutical and cosmeceutical industries: Tips for success. In *Marine Drugs* (Vol. 12, Issue 2, pp. 1066–1101). MDPI AG. https://doi.org/10.3390/md12021066

McQuin, C., Goodman, A., Chernyshev, V., Kamentsky, L., Cimini, B. A., Karhohs, K. W., Doan, M., Ding, L., Rafelski, S. M., Thirstrup, D., Wiegraebe, W., Singh, S., Becker, T., Caicedo, J. C., & Carpenter, A. E. (2018). CellProfiler 3.0: Next-generation image processing for biology. *PLOS Biology*, *16*(7), e2005970. https://doi.org/10.1371/journal.pbio.2005970

Menasché, P., Antébi, H., Alcindor, L., Teiger, E., Perez, G., Giudicelli, Y., Nordmann, R., & Piwnica, A. (1990). Iron chelation by deferoxamine inhibits lipid peroxidation during cardiopulmonary bypass in humans. *Undefined*.

Miller, S. L., & Abraham, E. R. (2011). *Characterisation of New Zealand kina fisheries*.

Mishchenko, N. P., Fedoreev, S. A., & Bagirova, V. L. (2003). Histochrome: A new original domestic drug. *Pharmaceutical Chemistry Journal*, *37*(1), 48–52. https://doi.org/10.1023/A:1023659331010

Monteiro, P. T., Oliveira, J., Pais, P., Antunes, M., Palma, M., Cavalheiro, M., Galocha, M., Godinho, C. P., Martins, L. C., Bourbon, N., Mota, M. N., Ribeiro, R. A., Viana, R., Sá-Correia, I., & Teixeira, M. C. (2020). YEASTRACT+: A portal for cross-species comparative genomics of transcription regulation in yeasts. *Nucleic Acids Research*, *48*(D1), D642–D649. https://doi.org/10.1093/nar/gkz859

Munro, M. H. G., Blunt, J. W., Dumdei, E. J., Hickford, S. J. H., Lill, R. E., Li, S., Battershill, C. N., & Duckworth, A. R. (1999). The discovery and development of marine compounds with pharmaceutical potential. *Journal of Biotechnology*, *70*(1–3), 15–25. https://doi.org/10.1016/S0168-1656(99)00052-8

Newman, D. J., & Cragg, G. M. (2020). Natural Products as Sources of New Drugs over the Nearly Four Decades from 01/1981 to 09/2019. In *Journal of Natural Products* (Vol. 83, Issue 3, pp. 770–803). American Chemical Society. https://doi.org/10.1021/acs.jnatprod.9b01285

Nijman, S. M. B. (2011). Synthetic lethality: General principles, utility and detection using genetic screens in human cells. *FEBS Letters*, *585*(1), 1–6. https://doi.org/10.1016/j.febslet.2010.11.024

Omar, R., Nomikos, I., Piccorelli, G., Savino, J., & Agarwal, N. (1989). Prevention of postischaemic lipid peroxidation and liver cell injury by iron chelation. *Gut*, *30*(4), 510–514. https://doi.org/10.1136/gut.30.4.510

Oxelmark, E., Marchini, A., Malanchi, I., Magherini, F., Jaquet, L., Hajibagheri, M. A. N., Blight, K. J., Jauniaux, J.-C., & Tommasino, M. (2000). Mmf1p, a Novel Yeast Mitochondrial Protein Conserved throughout Evolution and Involved in Maintenance of the Mitochondrial Genome. *Molecular and Cellular Biology*, *20*(20), 7784–7797.

https://doi.org/10.1128/mcb.20.20.7784-7797.2000

Park, J. H., Lee, N. K., Lim, H. J., Mazumder, S., Rethineswaran, V. K., Kim, Y. J., Jang, W. B., Ji, S. T., Kang, S., Kim, D. Y., Van, L. T. H., Giang, L. T. T., Kim, D. H., Ha, J. S., Yun, J., Kim, H., Han, J., Mishchenko, N. P., Fedoreyev, S. A., … Baek, S. H. (2019). Therapeutic cell protective role of histochrome under oxidative stress in human cardiac progenitor cells. *Marine Drugs*, *17*(6). https://doi.org/10.3390/md17060368

Parsons, A. B., Brost, R. L., Ding, H., Li, Z., Zhang, C., Sheikh, B., Brown, G. W., Kane, P. M., Hughes, T. R., & Boone, C. (2004). Integration of chemical-genetic and genetic interaction data links bioactive compounds to cellular target pathways. *Nature Biotechnology*, *22*(1), 62–69. https://doi.org/10.1038/nbt919

Parsons, A. B., Lopez, A., Givoni, I. E., Williams, D. E., Gray, C. A., Porter, J., Chua, G., Sopko, R., Brost, R. L., Ho, C. H., Wang, J., Ketela, T., Brenner, C., Brill, J. A., Fernandez, G. E., Lorenz, T. C., Payne, G. S., Ishihara, S., Ohya, Y., … Boone, C. (2006). Exploring the Mode-of-Action of Bioactive Compounds by Chemical-Genetic Profiling in Yeast. *Cell*, *126*(3), 611–625. https://doi.org/10.1016/j.cell.2006.06.040

Patridge, E., Gareiss, P., Kinch, M. S., & Hoyer, D. (2016). An analysis of FDA-approved drugs: Natural products and their derivatives. In *Drug Discovery Today* (Vol. 21, Issue 2, pp. 204–207). Elsevier Ltd. https://doi.org/10.1016/j.drudis.2015.01.009

Petrovska, B. (2012). Historical review of medicinal plants′ usage. *Pharmacognosy Reviews*, *6*(11), 1. https://doi.org/10.4103/0973-7847.95849

Pilc, E. M., Ganesh, S., & Kerscher, O. (2021). A genome-wide screen in Saccharomyces cerevisiae identifies Tannic Acid-sensitive mutants. *MicroPublication Biology*, *2021*. https://doi.org/10.17912/micropub.biology.000358

Pujol-Carrion, N., Pavón-Vergés, M., Arroyo, J., & de la Torre-Ruiz, M. A. (2021). The MAPK Slt2/Mpk1 plays a role in iron homeostasis through direct regulation of the transcription factor Aft1. *Biochimica et Biophysica Acta - Molecular Cell Research*, *1868*(5), 118974. https://doi.org/10.1016/j.bbamcr.2021.118974

Rahal, A., Kumar, A., Singh, V., Yadav, B., Tiwari, R., Chakraborty, S., & Dhama, K. (2014). Oxidative stress, prooxidants, and antioxidants: The interplay. In *BioMed Research International* (Vol. 2014). Hindawi Limited. https://doi.org/10.1155/2014/761264

Rangel, M., & Falkenberg, M. (2015). An overview of the marine natural products in clinical trials and on the market. *Journal of Coastal Life Medicine*, *3*(6), 421–428. https://doi.org/10.12980/jclm.3.2015jclm-2015-0018

Reid, R. J. D., Sunjevaric, I., Kedacche, M., & Rothstein, R. (2002). Efficient PCR-based gene disruption in Saccharomyces strains using intergenic primers. *Yeast*, *19*(4), 319–328. https://doi.org/10.1002/yea.817

Romero, A. M., Ramos-Alonso, L., Alepuz, P., Puig, S., & Martínez-Pastor, M. T. (2020). Global translational repression induced by iron deficiency in yeast depends on the Gcn2/eIF2α pathway. *Scientific Reports*, *10*(1), 1–11. https://doi.org/10.1038/s41598-019-57132-0

Romero, A. M., Ramos-Alonso, L., Montellá-Manuel, S., García-Martínez, J., de la Torre-Ruiz, M. Á., Pérez-Ortín, J. E., Martínez-Pastor, M. T., & Puig, S. (2019). A genome-

wide transcriptional study reveals that iron deficiency inhibits the yeast TORC1 pathway. *Biochimica et Biophysica Acta - Gene Regulatory Mechanisms*, *1862*(9). https://doi.org/10.1016/j.bbagrm.2019.194414

Ruggles, K. V., Garbarino, J., Liu, Y., Moon, J., Schneider, K., Henneberry, A., Billheimer, J., Millar, J. S., Marchadier, D., Valasek, M. A., Joblin-Mills, A., Gulati, S., Munkacsi, A. B., Repa, J. J., Rader, D., & Sturley, S. L. (2014). A functional, genome-wide evaluation of liposensitive yeast identifies the ARE2 required for viability (ARV1) gene product as a major component of eukaryotic fatty acid resistance. *Journal of Biological Chemistry*, *289*(7), 4417–4431. https://doi.org/10.1074/jbc.M113.515197

Sayed, D. A., Soliman, A. M., & Fahmy, S. R. (2018). Echinochrome pigment as novel therapeutic agent against experimentally - induced gastric ulcer in rats. *Biomedicine and Pharmacotherapy*, *107*, 90–95. https://doi.org/10.1016/j.biopha.2018.07.173

Sazonova, E. N., Kuznetsova, M. S., Vasileva, E. A., Mishchenko, N. P., Tsimbalist, N. A., & Lebed'ko. (2020). Cytoprotective Effect of Echinochrome A in Primary Culture of Pulmonary Fibroblasts from Albino Rats under Conditions of Oxidative Stress. *Bulletin of Experimental Biology and Medicine*, *169*(4), 582–585. https://doi.org/10.1007/s10517-020-04933-3

Schindelin, J., Arganda-Carreras, I., Frise, E., Kaynig, V., Longair, M., Pietzsch, T., Preibisch, S., Rueden, C., Saalfeld, S., Schmid, B., Tinevez, J. Y., White, D. J., Hartenstein, V., Eliceiri, K., Tomancak, P., & Cardona, A. (2012). Fiji: An open-source platform for biological-image analysis. In *Nature Methods* (Vol. 9, Issue 7, pp. 676–682). Nature Publishing Group. https://doi.org/10.1038/nmeth.2019

Seo, D. Y., McGregor, R. A., Noh, S. J., Choi, S. J., Mishchenko, N. P., Fedoreyev, S. A., Stonik, V. A., & Han, J. (2015). Echinochrome a improves exercise capacity during short-term endurance training in rats. *Marine Drugs*, *13*(9), 5722–5731. https://doi.org/10.3390/md13095722

Shakoury-Elizeh, M., Protchenko, O., Berger, A., Cox, J., Gable, K., Dunn, T. M., Prinz, W. A., Bard, M., & Philpott, C. C. (2010). Metabolic Response to Iron Deficiency in Saccharomyces cerevisiae. *Journal of Biological Chemistry*, *285*(19), 14823–14833. https://doi.org/10.1074/jbc.M109.091710

Subhaswaraj, P., Sowmya, M., Bhavana, V., Dyavaiah, M., & Siddhardha, B. (2017). Determination of antioxidant activity of Hibiscus sabdariffa and Croton caudatus in Saccharomyces cerevisiae model system. *Journal of Food Science and Technology*, *54*(9), 2728–2736. https://doi.org/10.1007/s13197-017-2709-2

Subramaniyan, S., Alugoju, P., Sudharshan, S. J., Veerabhadrappa, B., & Dyavaiah, M. (2019). Magnolol protects Saccharomyces cerevisiae antioxidant-deficient mutants from oxidative stress and extends yeast chronological life span. *FEMS Microbiology Letters*, *366*(8). https://doi.org/10.1093/femsle/fnz065

Tkach, J. M., Yimit, A., Lee, A. Y., Riffle, M., Costanzo, M., Jaschob, D., Hendry, J. A., Ou, J., Moffat, J., Boone, C., Davis, T. N., Nislow, C., & Brown, G. W. (2012). Dissecting DNA damage response pathways by analysing protein localization and abundance changes during DNA replication stress. *Nature Cell Biology*, *14*(9), 966–976. https://doi.org/10.1038/ncb2549

Tong, A. H. Y., Evangelista, M., Parsons, A. B., Xu, H., Bader, G. D., Pagé, N., Robinson,

M., Raghibizadeh, S., Hogue, C. W. V., Bussey, H., Andrews, B., Tyers, M., & Boone, C. (2001). Systematic genetic analysis with ordered arrays of yeast deletion mutants. *Science*, *294*(5550), 2364–2368. https://doi.org/10.1126/science.1065810

Ventola, C. L. (2015). The antibiotic resistance crisis: part 1: causes and threats. *P & T : A Peer-Reviewed Journal for Formulary Management*, *40*(4), 277–283. http://www.ncbi.nlm.nih.gov/pubmed/25859123

Vignesh, S., Raja, A., & Arthur Jam, R. (2011). Marine Drugs: Implication and Future Studies. *International Journal of Pharmacology*, *7*(1), 22–30. https://doi.org/10.3923/ijp.2011.22.30

Wagih, O., Usaj, M., Baryshnikova, A., VanderSluis, B., Kuzmin, E., Costanzo, M., Myers, C. L., Andrews, B. J., Boone, C. M., & Parts, L. (2013). SGAtools: one-stop analysis and visualization of array-based genetic interaction screens. *Nucleic Acids Research*, *41*(W1), W591–W596. https://doi.org/10.1093/nar/gkt400

Winzeler, E. A., Shoemaker, D. D., Astromoff, A., Liang, H., Anderson, K., Andre, B., Bangham, R., Benito, R., Boeke, J. D., Bussey, H., Chu, A. M., Connelly, C., Davis, K., Dietrich, F., Dow, S. W., El Bakkoury, M., Foury, F., Friend, S. H., Gentalen, E., … Davis, R. W. (1999). Functional characterization of the S. cerevisiae genome by gene deletion and parallel analysis. *Science (New York, N.Y.)*, *285*(5429), 901–906. http://www.ncbi.nlm.nih.gov/pubmed/10436161

Xiao, M., Shen, X., & Pan, W. (2019). Application of deep convolutional neural networks in classification of protein subcellular localization with microscopy images. *Genetic Epidemiology*, *43*(3), 330–341. https://doi.org/10.1002/gepi.22182

Zhang, F., Zhao, M., Braun, D. R., Ericksen, S. S., Piotrowski, J. S., Nelson, J., Peng, J., Ananiev, G. E., Chanana, S., Barns, K., Fossen, J., Sanchez, H., Chevrette, M. G., Guzei, I. A., Zhao, C., Guo, L., Tang, W., Currie, C. R., Rajski, S. R., … Bugni, T. S. (2020). A marine microbiome antifungal targets urgent-threat drug-resistant fungi. *Science*, *370*(6519), 974–978. https://doi.org/10.1126/science.abd6919

Zhu, H., Zhu, N., Peng, L., Zhang, B., Yu, Q., & Li, M. (2020). The inositol polyphosphate kinase Ipk1 transcriptionally regulates mitochondrial functions in Candida albicans. *FEMS Yeast Research*, *20*(6). https://doi.org/10.1093/femsyr/foaa050

3 Appendix

ORF	Gene	Time (minutes)	Function
YAL015C	*NTG1*	60	DNA N-glycosylase and apurinic/apyrimidinic (AP) lyase involved in base excision repair; acts in both nucleus and mitochondrion; creates a double-strand break at mtDNA origins that stimulates replication in response to oxidative stress
YBL013W	*FMT1*	90, 120, 150, 180, 210, 240	Methionyl-tRNA formyltransferase, catalyzes the formylation of initiator Met-tRNA in mitochondria; potential Cdc28p substrate
YBL080C	*PET112*	150, 240	Subunit of the trimeric GatFAB AmidoTransferase(AdT) complex; involved in the formation of Q-tRNAQ; mutation is functionally complemented by the bacterial GatB ortholog
YBR008C	*FLR1*	90, 150, 180, 210, 240	Plasma membrane multidrug transporter of the major facilitator superfamily, involved in efflux of fluconazole, diazaborine, benomyl, methotrexate, and other drugs; expression induced in cells treated with the mycotoxin patulin
YBR093C	*PHO5*	240	Repressible acid phosphatase (1 of 3) that also mediates extracellular nucleotide-derived phosphate hydrolysis; secretory pathway derived cell surface glycoprotein; induced by phosphate starvation and coordinately regulated by PHO4 and PHO2
YBR138C	*YBR138C*	120, 180, 210, 240	Cytoplasmic protein of unknown function, potentially phosphorylated by Cdc28p; YBR138C is not an essential gene
YBR151W	*APD1*	0, 60, 90, 120, 150, 180, 210, 240	Protein of unknown function, required for normal localization of actin patches and for normal tolerance of sodium ions and hydrogen peroxide; localizes to both cytoplasm and nucleus
YBR207W	*FTH1*	120, 180, 210, 240	Putative high affinity iron transporter involved in transport of intravacuolar stores of iron; forms complex with Fet5p; expression is regulated by iron; proposed to play indirect role in endocytosis

YBR272C	*HSM3*	60	Proteasome-interacting protein involved in the assembly of the base subcomplex of the 19S proteasomal regulatory particle (RP); involved in DNA mismatch repair during slow growth; weak similarity to Msh1p; related to human 19S subunit S5b
YDL033C	*SLM3*	210, 240	tRNA-specific 2-thiouridylase, responsible for 2-thiolation of the wobble base of mitochondrial tRNAs; human ortholog is implicated in myoclonus epilepsy associated with ragged red fibers (MERRF)
YDL104C	*QRI7*	30	Highly conserved mitochondrial protein, essential for t6A modification of mitochondrial tRNAs that decode ANN codons; similar to Kae1p and E. coli YgjD, both of which are also required for tRNA t6A modification
YDL105W	*NSE4*	210, 240	Nuclear protein that plays a role in the function of the Smc5p-Rhc18p complex
YDL108W	*KIN28*	240	Serine/threonine protein kinase, subunit of the transcription factor TFIIH; involved in transcription initiation at RNA polymerase II promoters
YDR004W	*RAD57*	30, 60	Protein that stimulates strand exchange by stabilizing the binding of Rad51p to single-stranded DNA; involved in the recombinational repair of double-strand breaks in DNA during vegetative growth and meiosis; forms heterodimer with Rad55p
YDR011W	*SNQ2*	30, 60, 90, 120, 150, 180, 210, 240	Plasma membrane ATP-binding cassette (ABC) transporter, multidrug transporter involved in multidrug resistance and resistance to singlet oxygen species
YDR043C	*NRG1*	90, 120	Transcriptional repressor that recruits the Cyc8p-Tup1p complex to promoters; mediates glucose repression and negatively regulates a variety of processes including filamentous growth and alkaline pH response
YDR105C	*TMS1*	210	Vacuolar membrane protein of unknown function that is conserved in mammals; predicted to contain eleven transmembrane helices; interacts with Pdr5p, a protein involved in multidrug resistance

YDR132C	*YDR132C*	60, 180, 210, 240	Putative protein of unknown function
YDR191W	*HST4*	90, 120, 150, 210, 240	Member of the Sir2 family of NAD(+)-dependent protein deacetylases; involved along with Hst3p in silencing at telomeres, cell cycle progression, radiation resistance, genomic stability and short-chain fatty acid metabolism
YDR270W	*CCC2*	60, 90, 120, 150, 180, 210, 240	Cu(+2)-transporting P-type ATPase, required for export of copper from the cytosol into an extracytosolic compartment; has similarity to human proteins involved in Menkes and Wilsons diseases
YDR460W	*TFB3*	180, 240	Subunit of TFIIH and nucleotide excision repair factor 3 complexes, involved in transcription initiation, required for nucleotide excision repair; ring finger protein similar to mammalian CAK and TFIIH subunit
YDR476C	*YDR476C*	60, 90, 120, 150, 180, 210, 240	Putative protein of unknown function; green fluorescent protein (GFP)-fusion protein localizes to the endoplasmic reticulum; YDR476C is not an essential gene
YDR520C	*URC2*	90	Putative Zn(II)2Cys6 motif containing transcription factor; non-essential gene identified in a screen for mutants with increased levels of rDNA transcription; similar to S. kluyveri Urc2p involved in uracil catabolism
YEL029C	*BUD16*	60, 90, 120, 150, 180, 210, 240	Putative pyridoxal kinase, a key enzyme involved in pyridoxal 5'-phosphate synthesis, the active form of vitamin B6; required for genome integrity; involved in bud-site selection; similarity to yeast BUD17 and human pyridoxal kinase (PDXK)
YER054C	*GIP2*	60, 150, 180, 210, 240	Putative regulatory subunit of the protein phosphatase Glc7p, involved in glycogen metabolism; contains a conserved motif (GVNK motif) that is also found in Gac1p, Pig1p, and Pig2p
YER145C	*FTR1*	240	High affinity iron permease involved in the transport of iron across the plasma membrane; forms complex with Fet3p; expression is regulated by iron

YFL027C	*GYP8*	30, 60, 90, 120, 150, 180, 210, 240	GTPase-activating protein for yeast Rab family members; Ypt1p is the preferred in vitro substrate but also acts on Sec4p, Ypt31p and Ypt32p; involved in the regulation of ER to Golgi vesicle transport
YFR046C	*CNN1*	30, 60, 120, 240	Kinetochore protein of unknown function; associated with the essential kinetochore proteins Nnf1p and Spc24p; phosphorylated by both Clb5-Cdk1 and, to a lesser extent, Clb2-Cdk1.
YGL209W	*MIG2*	240	Protein containing zinc fingers, involved in repression, along with Mig1p, of SUC2 (invertase) expression by high levels of glucose; binds to Mig1p-binding sites in SUC2 promoter
YGR017W	*YGR017W*	180	Putative protein of unknown function; green fluorescent protein (GFP)-fusion protein localizes to both the nucleus and the cytoplasm
YGR052W	*FMP48*	30, 60, 90, 120, 150, 180, 210, 240	Putative protein of unknown function; the authentic, non-tagged protein is detected in highly purified mitochondria in high-throughput studies; induced by treatment with 8-methoxypsoralen and UVA irradiation
YGR161C	*RTS3*	150, 180, 210, 240	Putative component of the protein phosphatase type 2A complex
YGR243W	*MPC3*	180, 210, 240	Putative protein of unknown function; expression regulated by osmotic and alkaline stresses; the authentic, non-tagged protein is detected in highly purified mitochondria in high-throughput studies
YGR257C	*MTM1*	240	Mitochondrial protein of the mitochondrial carrier family, involved in activating mitochondrial Sod2p probably by facilitating insertion of an essential manganese cofactor
YGR281W	*YOR1*	90, 120, 150, 180, 210, 240	Plasma membrane ATP-binding cassette (ABC) transporter, multidrug transporter mediates export of many different organic anions including oligomycin; similar to human cystic fibrosis transmembrane receptor (CFTR)
YHL020C	*OPI1*	180, 210, 240	Transcriptional regulator of a variety of genes; phosphorylation by protein kinase A stimulates Opi1p function in negative regulation of phospholipid biosynthetic genes; involved in telomere maintenance

YHL040C	*ARN1*	60, 90, 120, 150, 180, 210, 240	Transporter, member of the ARN family of transporters that specifically recognize siderophore-iron chelates; responsible for uptake of iron bound to ferrirubin, ferrirhodin, and related siderophores
YHR140W	*YHR140W*	150, 180, 210, 240	Putative integral membrane protein of unknown function
YIL104C	*SHQ1*	150, 180, 210, 240	Chaperone protein required for the assembly of box H/ACA snoRNPs and thus for pre-rRNA processing, forms a complex with Naf1p and interacts with H/ACA snoRNP components Nhp2p and Cbf5p; homology with known Hsp90p cochaperones
YIL160C	*POT1*	210, 240	3-ketoacyl-CoA thiolase with broad chain length specificity, cleaves 3-ketoacyl-CoA into acyl-CoA and acetyl-CoA during beta-oxidation of fatty acids
YJR043C	*POL32*	30	Third subunit of DNA polymerase delta, involved in chromosomal DNA replication; required for error-prone DNA synthesis in the presence of DNA damage and processivity; interacts with Hys2p, PCNA (Pol30p), and Pol1p
YJR053W	*BFA1*	240	Component of the GTPase-activating Bfa1p-Bub2p complex involved in multiple cell cycle checkpoint pathways that control exit from mitosis
YJR136C	*TTI2*	120, 150, 180, 240	Putative protein of unknown function; subunit of the ASTRA complex which is part of the chromatin remodeling machinery; similar to S. pombe Tti2p; may interact with Rsm23p; GFP-fusion protein localizes to the cytoplasm
YJR148W	*BAT2*	240	Cytosolic branched-chain amino acid (BCAA) aminotransferase, preferentially involved in BCAA catabolism; homolog of murine ECA39; highly expressed during stationary phase and repressed during logarithmic phase
YKL103C	*APE1*	180, 210, 240	Vacuolar aminopeptidase yscI; zinc metalloproteinase that belongs to the peptidase family M18; often used as a marker protein in studies of autophagy and cytosol to vacuole targeting (CVT) pathway

YKL108W	*SLD2*	30, 60, 150, 180, 210, 240	Single-stranded DNA origin-binding and annealing protein; required for the initiation of DNA replication; phosphorylated in S phase by cyclin-dependent kinases (Cdks), promoting origin binding, DNA replication and Dpb11p complex formation; component of the preloading complex; required for the S phase checkpoint
YKL162C	*YKL162C*	0, 30, 90, 120, 150, 180, 210, 240	Putative protein of unknown function; green fluorescent protein (GFP)-fusion protein localizes to the mitochondrion
YKR011C	*YKR011C*	150	Putative protein of unknown function; green fluorescent protein (GFP)-fusion protein localizes to the nucleus
YKR052C	*MRS4*	60, 90, 120, 150, 180, 210, 240	Iron transporter that mediates Fe2+ transport across the inner mitochondrial membrane; mitochondrial carrier family member, similar to and functionally redundant with Mrs3p; active under low-iron conditions; may transport other cations
YLR034C	*SMF3*	30, 60, 90, 120, 150, 180, 210, 240	Putative divalent metal ion transporter involved in iron homeostasis; transcriptionally regulated by metal ions; member of the Nramp family of metal transport proteins
YLR085C	*ARP6*	0, 150, 210, 240	Actin-related protein that binds nucleosomes; a component of the SWR1 complex, which exchanges histone variant H2AZ (Htz1p) for chromatin-bound histone H2A
YLR105C	*SEN2*	180	Subunit of the tRNA splicing endonuclease, which is composed of Sen2p, Sen15p, Sen34p, and Sen54p; Sen2p contains the active site for tRNA 5' splice site cleavage and has similarity to Sen34p and to Archaeal tRNA splicing endonuclease
YLR107W	*REX3*	30	RNA exonuclease; required for maturation of the RNA component of RNase MRP; functions redundantly with Rnh70p and Rex2p in processing of U5 snRNA and RNase P RNA; member of RNase D family of exonucleases
YLR136C	*TIS11*	0, 30, 60, 90, 120, 150, 180, 210, 240	mRNA-binding protein expressed during iron starvation; binds to a sequence element in the 3'-untranslated regions of specific mRNAs to

			mediate their degradation; involved in iron homeostasis
YLR179C	*YLR179C*	60, 90, 120, 150, 180, 210, 240	Protein of unknown function with similarity to Tfs1p; transcription is activated by paralogous proteins Yrm1p and Yrr1p along with proteins involved in multidrug resistance; GFP-tagged protein localizes to the cytoplasm and nucleus
YLR265C	*NEJ1*	150, 180, 210, 240	Protein involved in regulation of nonhomologous end joining; interacts with DNA ligase IV components Dnl4p and Lif1p; repressed by MAT heterozygosity; regulates cellular distribution of Lif1p
YLR346C	*CIS1*	30, 60, 120, 150, 180, 210, 240	Putative protein of unknown function found in mitochondria; expression is regulated by transcription factors involved in pleiotropic drug resistance, Pdr1p and Yrr1p; YLR346C is not an essential gene
YLR405W	*DUS4*	210, 240	Dihydrouridine synthase, member of a widespread family of conserved proteins including Smm1p, Dus1p, and Dus3p
YML038C	*YMD8*	60, 90, 120, 150, 180, 210, 240	Putative nucleotide sugar transporter, has similarity to Vrg4p
YML060W	*OGG1*	240	Mitochondrial glycosylase/lyase that specifically excises 7,8-dihydro-8-oxoguanine residues located opposite cytosine or thymine residues in DNA, repairs oxidative damage to mitochondrial DNA, contributes to UVA resistance
YML102W	*CAC2*	30	Component of the chromatin assembly complex (with Rlf2p and Msi1p) that assembles newly synthesized histones onto recently replicated DNA, required for building functional kinetochores, conserved from yeast to humans
YMR021C	*MAC1*	240	Copper-sensing transcription factor involved in regulation of genes required for high affinity copper transport
YMR067C	*UBX4*	150	UBX (ubiquitin regulatory X) domain-containing protein that interacts with Cdc48p
YMR102C	*YMR102C*	240	Protein of unknown function; transcription is activated by paralogous transcription factors Yrm1p and Yrr1p along with genes involved in multidrug resistance; mutant shows increased

			resistance to azoles; YMR102C is not an essential gene
YMR171C	*EAR1*	150	Specificity factor required for Rsp5p-dependent ubiquitination and sorting of specific cargo proteins at the multivesicular body; mRNA is targeted to the bud via the mRNA transport system involving She2p
YMR220W	*ERG8*	60, 90, 120, 150, 180, 210, 240	Phosphomevalonate kinase, an essential cytosolic enzyme that acts in the biosynthesis of isoprenoids and sterols, including ergosterol, from mevalonate
YMR253C	*YMR253C*	90, 150, 180, 210, 240	Putative protein of unknown function; green fluorescent protein (GFP)-fusion protein localizes to the cytoplasm in a punctate pattern; YMR253C is not an essential gene
YMR287C	*DSS1*	180, 240	3'-5' exoribonuclease, component of the mitochondrial degradosome along with the ATP-dependent RNA helicase Suv3p; the degradosome associates with the ribosome and mediates turnover of aberrant or unprocessed RNAs
YNL164C	*IBD2*	30	Component of the BUB2-dependent spindle checkpoint pathway, interacts with Bfa1p and functions upstream of Bub2p and Bfa1p
YNL217W	*PPN2*	210	Putative protein of unknown function; weak sequence similarity to bis (5'-nucleotidyl)-tetraphosphatases; (GFP)-fusion protein localizes to the vacuole; null mutant is highly sensitive to azaserine and resistant to sodium-O-vandate
YNL239W	*LAP3*	150, 180, 210, 240	Cysteine aminopeptidase with homocysteine-thiolactonase activity; protects cells against homocysteine toxicity; has bleomycin hydrolase activity in vitro; transcription is regulated by galactose via Gal4p; orthologous to human BLMH
YNL254C	*RTC4*	240	Protein of unknown function; null mutation suppresses cdc13-1 temperature sensitivity; (GFP)-fusion protein localizes to both the cytoplasm and the nucleus
YNL305C	*BXI1*	180	Protein involved in apoptosis; variously described as containing a BCL-2 homology (BH3) domain or as a member of the BAX

			inhibitor family; reported to promote apoptosis under some conditions and to inhibit it in others; localizes to ER and vacuole; may link the unfolded protein response to apoptosis via regulation of calcium-mediated signaling; translocates to mitochondria under apoptosis-inducing conditions in a process involving Mir1p and Cor1p
YOL049W	*GSH2*	150, 180, 210, 240	Glutathione synthetase, catalyzes the ATP-dependent synthesis of glutathione (GSH) from gamma-glutamylcysteine and glycine; induced by oxidative stress and heat shock
YOL082W	*ATG19*	30	Receptor protein specific for the cytoplasm-to-vacuole targeting (Cvt) pathway; delivers cargo proteins aminopeptidase I (Lap4p) and alpha-mannosidase (Ams1p) to the phagophore assembly site for packaging into Cvt vesicles
YOR059C	*LPL1*	90, 120, 150, 180, 210, 240	Lipid particle protein of unknown function; contains a putative lipase serine active site; induced by transcription factor RPN4
YOR065W	*CYT1*	150, 180, 210, 240	Cytochrome c1, component of the mitochondrial respiratory chain; expression is regulated by the heme-activated, glucose-repressed Hap2p/3p/4p/5p CCAAT-binding complex
YOR316C	*COT1*	150, 180, 210, 240	Vacuolar transporter that mediates zinc transport into the vacuole; overexpression confers resistance to cobalt and rhodium
YOR324C	*FRT1*	90, 120, 150, 180, 210	Tail-anchored ER membrane protein that is a substrate of the phosphatase calcineurin; interacts with homolog Frt2p; promotes cell growth in stress conditions, possibly via a role in posttranslational translocation
YPL026C	*SKS1*	180	Putative serine/threonine protein kinase; involved in the adaptation to low concentrations of glucose independent of the SNF3 regulated pathway
YPL060W	*MFM1*	0, 210, 240	Mitochondrial inner membrane magnesium transporter, involved in maintenance of mitochondrial magnesium concentrations and membrane potential; indirectly affects splicing of group II introns; functionally and structurally related to Mrs2p

YPL135W	*ISU1*	240	Conserved protein of the mitochondrial matrix, performs a scaffolding function during assembly of iron-sulfur clusters, interacts physically and functionally with yeast frataxin (Yfh1p); isu1 isu2 double mutant is inviable
YPL139C	*UME1*	60, 240	Negative regulator of meiosis, required for repression of a subset of meiotic genes during vegetative growth, binding of histone deacetylase Rpd3p required for activity, contains a NEE box and a WD repeat motif; homologous with Wtm1p, Wtm2p
YPL152W	*RRD2*	30	Activator of the phosphotyrosyl phosphatase activity of PP2A,peptidyl-prolyl cis/trans-isomerase; regulates G1 phase progression, the osmoresponse, microtubule dynamics; subunit of the Tap42p-Pph21p-Rrd2p complex
YPL170W	*DAP1*	30, 60, 90, 120, 150, 180, 210, 240	Heme-binding protein involved in regulation of cytochrome P450 protein Erg11p; damage response protein, related to mammalian membrane progesterone receptors; mutations lead to defects in telomeres, mitochondria, and sterol synthesis
YPL209C	*IPL1*	0, 150, 180, 210, 240	Aurora kinase subunit of the conserved chromosomal passenger complex (CPC; Ipl1p-Sli15p-Bir1p-Nbl1p), involved in regulating kinetochore-microtubule attachments; helps maintain condensed chromosomes during anaphase and early telophase

Table 3.1: Annotation of proteins that had a significant increase in protein abundance due to Ech A treatment. Table contains each open reading frame (ORF), gene name, time points when significant increase occurred, and a brief description of function. Description of function attained from Saccharomyces Genome Database (Cherry et al., 2012).

ORF	Gene	Time (minutes)	Function
YCR087C-A	*YCR087C-A*	30, 60, 90, 120,150, 180, 210, 240	Putative protein of unknown function; green fluorescent protein (GFP)-fusion protein localizes to the nucleolus; YCR087C-A is not an essential gene
YDL104C	*QRI7*	180	Highly conserved mitochondrial protein, essential for t6A modification of mitochondrial tRNAs that decode ANN codons; similar to Kae1p and E. coli YgjD, both of which are also required for tRNA t6A modification
YGR138C	*TPO2*	210, 240	Polyamine transport protein specific for spermine; localizes to the plasma membrane; transcription of TPO2 is regulated by Haa1p; member of the major facilitator superfamily
YGR280C	*PXR1*	120	Essential protein involved in rRNA and snoRNA maturation; competes with TLC1 RNA for binding to Est2p, suggesting a role in negative regulation of telomerase; human homolog inhibits telomerase; contains a G-patch RNA interacting domain
YNL065W	*AQR1*	150, 180, 210, 240	Plasma membrane multidrug transporter of the major facilitator superfamily, confers resistance to short-chain monocarboxylic acids and quinidine; involved in the excretion of excess amino acids
YPL274W	*SAM3*	90, 120,150, 180, 210, 240	High-affinity S-adenosylmethionine permease, required for utilization of S-adenosylmethionine as a sulfur source; has similarity to S-methylmethionine permease Mmp1p

Table 3.2: Annotation of proteins that had a significant decrease in protein abundance due to Ech A treatment. Table contains each open reading frame (ORF), gene name, time points when significant decrease occurred, and a brief description of function. Description of function attained from Saccharomyces Genome Database (Cherry et al., 2012).

	Timepoints (Minutes)								
ORF	0	30	60	90	120	150	180	210	240
Increased protein abundance									
YAL015C	-	-	10.10	-	-	-	-	-	-
YBL013W	-	-	-	11.50	12.08	13.73	15.21	14.17	15.53
YBL080C	-	-	-	-	-	11.35	-	-	10.80
YBR008C	-	-	-	10.82	-	14.15	14.63	15.11	20.49
YBR093C	-	-	-	-	-	-	-	-	12.44
YBR138C	-	-	-	-	10.806	-	12.18	12.71	12.49
YBR151W	10.23	17.16	22.12	22.82	24.02	31.31	27.33	33.13	35.54
YBR207W	-	-	-	-	11.49	-	10.47	12.60	10.14
YBR272C	-	-	12.36	-	-	-	-	-	-
YDL033C	-	-	-	-	-	-	-	10.67	11.63
YDL104C	-	10.58	-	-	-	-	-10.29	-	-
YDL105W	-	-	-	-	-	-	-	10.89	15.17
YDL108W	-	-	-	-	-	-	-	-	11.11
YDR004W	-	13.35	11.50	-	-	-	-	-	-
YDR011W	-	16.74	21.15	29.99	31.45	33.80	43.21	50.21	51.25
YDR043C	-	-	-	10.68	11.83	-	-	-	-
YDR105C	-	-	-	-	-	-	-	10.48	-
YDR132C	-	-	10.25	-	-	-	10.40	12.71	12.08
YDR191W	-	-	-	11.48	10.09	-	12.06	13.77	16.82
YDR270W	-	-	17.20	15.42	14.41	14.19	16.51	18.54	20.60
YDR460W	-	-	-	-	-	-	10.23	-	10.64
YDR476C	-	-	14.62	15.53	16.60	20.21	23.94	23.06	26.96
YDR520C	-	-	-	12.12	-	-	-	-	-
YEL029C	-	-	10.92	10.28	14.03	12.83	15.76	17.41	18.13
YER054C	-	-	10.12	-	-	12.99	12.74	12.93	15.54
YER145C	-	-	-	-	-	-	-	-	10.54
YFL027C	-	11.55	10.83	13.66	14.476	13.44	16.95	18.57	19.20
YFR046C	-	11.11	10.14	-	11.18	-	-	-	11.83
YGL209W	-	-	-	-	-	-	-	-	10.88
YGR017W	-	-	-	-	-	-	11.14	-	-
YGR052W	-	10.19	10.16	10.57	-	11.46	10.94	11.29	11.51
YGR161C	-	-	-	-	-	11.29	12.92	12.91	11.88

YGR243W	-	-	-	-	-	-	10.18	10.60	15.78
YGR257C	-	-	-	-	-	-	-	-	11.09
YGR281W	-	-	-	12.77	14.97	17.52	17.59	22.64	27.68
YHL020C	-	-	-	-	-	-	10.24	11.68	14.16
YHL040C	-	-	11.91	13.56	15.626	16.39	15.02	19.45	21.48
YHR140W	-	-	-	-	-	12.44	14.91	18.19	18.95
YIL104C	-	-	-	-	-	11.48	18.05	16.18	17.87
YIL160C	-	-	-	-	-	-	-	13.26	14.06
YJR043C	-	11.25	-	-	-	-	-	-	-
YJR053W	-	-	-	-	-	-	-	-	10.41
YJR136C	-	-	-	-	10.65	11.85	10.68	-	11.68
YJR148W	-	-	-	-	-	-	-	-	10.96
YKL103C	-	-	-	-	-	-	11.26	11.25	12.69
YKL108W	-	10.63	15.95	-	-	10.37	11.34	12.22	18.94
YKL162C	10.87	10.21	-	10.41	14.710	13.81	10.46	-	11.06
YKR011C	-	-	-	-	-	10.46	-	-	-
YKR052C	-	-	12.07	14.26	13.63	14.50	12.31	12.21	18.15
YLR034C	-	12.32	11.07	10.35	13.04	10.62	16.69	16.69	16.87
YLR085C	-	11.12	-	-	-	10.11	-	10.47	10.53
YLR105C	-	-	-	-	-	-	12.24	-	-
YLR107W	-	11.04	-	-	-	-	-	-	-
YLR136C	15.46	25.52	17.95	18.81	14.14	17.16	22.24	25.14	28.71
YLR179C	-	-	14.04	15.65	19.04	23.70	24.30	23.38	28.74
YLR265C	-	-	-	-	-	10.65	12.63	11.70	11.25
YLR346C	-	14.47	20.66	29.04	33.58	39.58	40.43	44.76	49.16
YLR405W	-	-	-	-	-	-	-	11.35	15.56
YML038C	-	-	10.79	12.38	19.29	19.81	17.49	18.63	20.96
YML060W	-	-	-	-	-	-	-	-	12.77
YML102W	-	11.05	-	-	-	-	-	-	-
YMR021C	-	-	-	-	-	-	-	-	12.73
YMR067C	-	-	-	-	-	11.19	-	-	-
YMR102C	-	-	-	-	-	-	-	-	10.95
YMR171C	-	-	-	-	-	11.22	-	-	-
YMR220W	-	10.60	13.67	14.27	16.64	15.78	18.45	18.22	21.11
YMR253C	-	-	-	13.05	-	13.71	12.97	10.90	13.85

YMR287C	-	-	-	-	-	-	10.87	-	10.18
YNL164C	-	10.31	-	-	-	-	-	-	-
YNL217W	-	-	-	-	-	-	-	10.00	-
YNL239W	-	-	-	-	-	10.95	10.24	10.84	12.17
YNL254C	-	-	-	-	-	-	-	-	11.52
YNL305C	-	-	-	-	-	-	10.13	-	-
YOL049W	-	-	-	-	-	10.58	12.59	11.32	13.02
YOL082W	-	10.25	-	-	-	-	-	-	-
YOR059C	-	-	-	12.84	13.82	17.52	15.09	18.07	14.18
YOR065W	-	-	-	-	-	10.88	13.00	15.57	15.08
YOR316C	-	-	-	-	-	10.58	11.69	13.81	14.43
YOR324C	-	-	-	10.41	12.38	14.13	11.08	13.66	-
YPL026C	-	-	-	-	-	-	10.67	-	-
YPL060W	11.75	-	-	-	-	-	-	10.78	11.85
YPL135W	-	-	-	-	-	-	-	-	10.15
YPL139C	-	-	10.70	-	-	-	-	-	12.28
YPL152W	-	10.76	-	-	-	-	-	-	-
YPL170W	-	11.79	13.75	19.59	23.30	30.03	33.16	39.98	40.18
YPL209C	10.44	-	-	-	-	13.30	18.07	13.61	15.01
Decreased protein abundance									
YCR087C-A	-	-10.40	-14.91	-11.50	-15.90	-18.85	-15.66	-17.99	-16.52
YDL104C	-	10.58	-	-	-	-	-10.29	-	-
YGR138C	-	-	-	-	-	-	-	-10.79	-13.34
YGR280C	-	-	-	-	-	-	-11.96	-	-
YNL065W	-	-	-	-	-	-11.43	-13.35	-14.06	-15.00
YPL274W	-	-	-	-11.00	- 13.069	-16.45	-19.49	-23.48	-25.73

Table 3.3: **Z-scores for all the strains that had a significant change in protein abundance due to Ech A treatment.** A breakdown of the significant increases and decreases of protein abundance for each validated strain at every 30-minute timepoint.